6-7-2023

THE USE OF POINT CLOUD DATA TO SUPPORT CONCRETE BRIDGE DECK CONDITION ASSESSMENT

Issa Nidal Al Shaini
Rowan University

THE USE OF POINT CLOUD DATA TO SUPPORT CONCRETE BRIDGE DECK CONDITION ASSESSMENT

By

Issa Nidal Al Shaini

A Thesis

Submitted to the
Civil and Environmental Engineering
College of Engineering
In partial fulfillment of the requirement
For the degree of
Master of Science in Civil Engineering
at
Rowan University
May 5, 2023

Thesis Chair: Adriana Trias, Ph.D. Assistant Professor, Department of Civil and Environmental Engineering

Committee Members:
Islam Mantawy, Ph.D., PE, Assistant Professor, Department of Civil and Environmental Engineering
Andres Roda, PE, Executive Manager, Design Standards, New Jersey Department Of Transportation

Dedications

I offer this thesis in gratitude and devotion to God, my constant guiding light. Your infinite love, wisdom, and grace have sustained me through the challenges and obstacles. This work is a token of my love and devotion to you.

I dedicate this thesis to my mother, Dr. Rima Muqattash, my role model and mentor. Your unwavering support, encouragement, and belief in me have been instrumental in helping me to achieve my goals. Your dedication to your own work and your family has been an inspiration to me, and I am honored to be your child.

To my father, Engineer Nidal Al Shaini, who inspired me to pursue a career in Engineering, thank you for your hard work, dedication, and expertise. Your constant guidance and support have been a source of inspiration to me.

I also thank my sisters, Reem and Victoria Al Shaini, for their love and support throughout my academic journey. Your unwavering belief in me has been a constant source of motivation, and I am grateful for your encouragement.

To my fiancé, Alaina Friend, and her family, Barbara Tichian, Joseph, Adrienne, and Julia Friend, thank you for your love, support, and understanding. Your encouragement, patience, and support have been essential in helping me to balance my academic pursuits and personal life.

Finally, I express my gratitude to all those who contributed to this work, including my team members, committee members, and research participants. Your support, guidance, and feedback have been invaluable, and I am honored to have worked with you all.

Acknowledgements

I would like to express my gratitude to all those who have contributed to the completion of this thesis. Your support and dedication have been invaluable in helping me achieve my goals, and I am forever grateful for your contributions.

Firstly, I would like to acknowledge Dr. Adriana Trias Blanco, our team leader, for her unwavering support and guidance throughout this research project. Her expertise in the field, leadership skills, and constructive feedback have been instrumental in shaping the outcome of this thesis.

I would also like to thank Juan Vera, Jessica Rosales, Jennifer Carson, and John Vrabel for their hard work, support, and dedication. Their guidance and expertise have been invaluable in shaping the final outcome of this thesis.

In addition, I extend my heartfelt appreciation to Andres Roda and Dr. Islam Mantawy, our committee members, for their invaluable feedback and support. Their guidance was instrumental in refining my ideas and improving the overall quality of this work.

I am grateful to have had the opportunity to work with such a talented and supportive team. Your contributions have been instrumental in the successful completion of this thesis, and I am honored to have had the chance to work alongside you.

Once again, I extend my heartfelt thanks to Dr. Adriana Trias Blanco, Juan Vera, Jessica Rosales, Jennifer Carson, John Vrabel, Andres Roda, and Dr. Islam Mantawy for their unwavering support, guidance, and encouragement throughout this journey. Your contributions have been invaluable, and I am grateful for the opportunity to have worked with you all.

Abstract

THE USE OF POINT CLOUD DATA TO SUPPORT CONCRETE BRIDGE DECK
CONDITION ASSESSMENT
Issa Al Shaini
Master of Science in Civil Engineering
Adriana Trias Blanco, Ph.D.

Bridge deck condition assessments are typically conducted through visual physical inspections, utilizing traditional contact sensors for Non-Destructive Evaluation techniques such as hammer Sounding and chain dragging which require the expertise of trained inspectors. However, the accuracy of these inspections is limited by the level of deterioration of the bridge deck, as the ability of the inspectors is proportional to the apparent level of damage. This study aims to improve the accuracy of bridge deck inspection processes by utilizing non-destructive evaluation techniques, including the analysis of point cloud data gathered via Light Detection and Ranging (LiDAR) as a geometry-capturing tool. The overall goal of this research is to evaluate and quantify the effectiveness and efficiency of LiDAR sensors in contributing to the suite of technologies available to perform bridge deck condition assessment. To achieve this, the research proposes to understand the deterioration pattern of New Jersey bridges, evaluate the results gathered from point cloud data collected on a full-scale bridge deck, quantify the information gained from deploying LiDAR on operating bridges in New Jersey, and investigate the costs related to current bridge condition assessment practices and the impact of incorporating the use of LiDAR sensors. Two data processing approaches were chosen to measure gross and fine dimensions of the evaluated bridge decks, resulting in an accuracy of 96% with respect to results gathered from inspection reports.

Table of Contents

Table of Contents (Continued)

Table of Contents (Continued)

Table of Contents (Continued)

List of Figures

List of Figures (Continued)

List of Figures (Continued)

List of Figures (Continued)

List of Tables

Chapter 1

Introduction

1.1 Motivation

There are over 617,000 bridges in the United States. Currently, 42 percent of them are over 50 years old, and 7.5 percent, or 46,154, are in poor condition , indicating they are in "poor" condition (ASCE, 2021); with the rapid deterioration pattern of bridge decks, implementing new reliable non-destructive evaluation (NDE) techniques is essential to maintain the structural health of reinforced concrete (RC) bridge decks and prevent deterioration before occurring. Research done on bridge condition assessment shows that the use of point cloud data captured via light detection and ranging (LiDAR) during construction (new or rehabilitation) can help to: (1) estimate the location of the rebar in the concrete deck by scanning during construction stage (Wang et al., 2017); (2) estimate rebar covers by comparing as built scans to construction scans (Kim et al., 2020); and (3) locate low points on the deck's surface where water can sit by analyzing point cloud data (Mohammadi et al., 2019). These aspects are critical factors in the performance of bridge decks, potentially causing early deterioration and shortening their service life.

Bridge inspection is currently being addressed through visual inspections and advanced testing techniques. Visual inspections are typically performed by trained inspectors who search for signs of deterioration in the form of cracks, steel corrosion, concrete spalling, section loss, and deformations that can impact the performance of the structure. Advanced testing techniques, such as non-destructive testing (NDT), complement visual inspections and provide more detailed information about the bridge's structural integrity. NDT methods include Visual Inspection, Ground Penetrating Radar,

Half-cell Potential and Electrical resistivity inspections. In recent years, new technologies such as LiDAR and drones have also been progressively used for bridge inspections, providing quantitative information on the bridge's condition and allowing for more efficient and accurate assessments. Overall, bridge inspections play a critical role in ensuring the safety and longevity of bridges, and continued advancements in inspection techniques, and technology are essential for maintaining the nation's infrastructure. This research presents the results of an analysis performed on point cloud data of bridge decks in New Jersey, USA, demonstrating the applicability of LiDAR sensors for assessing the condition of bridges. The first phase of this study consisted con gathering point cloud data on eight (8) bridges in the same region, which had varying deck conditions ranging from 3 to 9, on a 0 to 9 scale. The objective of the first phase was to identify critical aspects that accurately predict deterioration rates and extend the bridge deck's service life. Low-rated decks were selected to confirm the correlation between the bridge deck profile and the condition rating, while high-rated bridge decks were chosen to apply the knowledge gained for the deterioration pattern prediction. Table 1 obtained from FHWA Recording and Coding Guide for the structure inventory and appraisal of the Nation's Bridges depicts the rating scale for Bridges (FHWA, 1995) was followed.

Table 1

Condition Rating Code by FHWA Records and Coding Guide

Description	Code
NOT APPLICABLE (N): This rating indicates that the condition of the bridge cannot be evaluated based on the given criteria.	N
EXCELLENT CONDITION (9): A bridge with a rating of 9 is in excellent condition and does not have any issues or problems.	9

Description	Code
VERY GOOD CONDITION - no problems noted (8): A bridge with a rating of 8 is in very good condition and does not have any noticeable problems or issues.	8
GOOD CONDITION - some minor problems (7): A bridge with a rating of 7 is in good condition but may have some minor issues or problems.	7
SATISFACTORY CONDITION - structural elements show some minor deterioration (6): A bridge with a rating of 6 is in satisfactory condition but may show some minor signs of deterioration in its structural elements.	6
FAIR CONDITION - all primary structural elements are sound but may have minor section loss, cracking, spalling, or scour (5): A bridge with a rating of 5 is in fair condition and has all of its primary structural elements in sound condition, but may have some minor issues such as section loss, cracking, spalling, or scour.	5
POOR CONDITION - advanced section loss, deterioration, spalling or scour (4): A bridge with a rating of 4 is in poor condition and has experienced advanced section loss, deterioration, spalling, or scour.	4
SERIOUS CONDITION - loss of section, deterioration, spalling or scour have seriously affected primary structural components. Local failures are possible. Fatigue cracks in steel or shear cracks in concrete may be present (3): A bridge with a rating of 3 is in serious condition and has experienced significant loss of section, deterioration, spalling, or scour that has seriously affected its primary structural components. Local failures may be possible, and fatigue cracks in steel or shear cracks in concrete may be present.	3
CRITICAL CONDITION - advanced deterioration of primary structural elements. Fatigue cracks in steel or shear cracks in concrete may be present or scour may have removed substructure support. Unless the bridge is closely monitored, it may be necessary to close the bridge until corrective action is taken (2): A bridge with a rating of 2 is in critical condition and has experienced advanced deterioration of its primary structural elements. Fatigue cracks in steel or shear cracks in concrete may be present, or scour may have removed substructure support. If not closely monitored, it may be necessary to close the bridge until corrective action is taken.	2
"IMMINENT" FAILURE CONDITION - major deterioration or section loss present in critical structural components or obvious vertical or horizontal movement affecting structure stability. Bridge is closed to traffic, but corrective action may put back in light service (1): A bridge with a rating of 1 is in an "imminent" failure condition, with major deterioration or section loss present in critical structural components or obvious vertical or horizontal movement affecting its structure stability. The bridge is closed to traffic, but corrective action may allow it to be put back in light service.	1
FAILED CONDITION - out of service - beyond corrective action (0): A bridge with a rating of 0 has failed and is out of service with no possibility of correction.	0

On the second phase, six (6) additional bridges in New Jersey were scanned to increase the reliability of the information gained, and to develop a bridge deck deterioration trend based on Bridge Deck Characterization. The common factors between the bridges scanned to achieve the objectives of this study was: steel girders, concrete decks, single or

continuous two-span configuration, and similar Average Daily Traffic (ADT) and Average Daily Truck Traffic (ADTT).

The aforementioned bridge characteristics derive from a deep literature review and analysis performed on historical bridge condition data, which allowed to investigate further the deteriorating pattern of bridge decks in New Jersey. This data was extracted from the National Bridge Inventory (NBI) repository found on the Infobridge website managed by the Federal Highway Administration (FHWA); further information on the trends found during this analysis is explained further. According to FHWA's Recording and Coding Guide for the Structure Inventory and Appraisal of the Nation's Bridges (FHWA, 1995), concrete decks must be examined for cracking, scaling, spalling, leaching, chloride contamination, potholes, delamination, and full or partial depth failures before the structure is given a rating. Ratings of 0, 1, 2, 3, or 4 are associated with structurally poor; as 4 represents a Poor Condition, a rating of 3 depicts a serious condition, while 2 means that the bridge deck is in a critical condition, a rating of 1 identifies as a Failure Condition and 0 implies that the structure has failed while, a rating of 5-9 indicates that the bridge deck has some signs of deterioration but is generally still in good condition with only minor defects or damage that do not require immediate attention; as 5 refers to a Fair Condition rating, 6 shows a Satisfactory Condition, 7 and 8 mean that the Bridge is either in a Good or a Very Good condition; it would be rated a 7 as Good if the deteriorations are noticeable and 8 as Very Good if no Problems on the bridge deck were noticeable, Finally a rating of Excellent 9 is usually given to newly erected structures with no apparent issues or problems. However, it is essential to note that even decks rated 5-9 require regular

maintenance and monitoring to prevent further deterioration and ensure their continued safe operation.

This research seeks to implement point cloud data as a screening tool that contributes to the suite of non-destructive evaluation (NDE) techniques available for bridge deck inspection, effectively addressing early, efficient, qualitative, and quantitative bridge deck deterioration detection. Through the literature review performed on different NDE techniques and traditional inspection protocols, it was evident that the quality of the wearing surface, curbs, sidewalks, bridge rail, and all superstructure components are elements that need to be considered during the inspection; LiDAR has allowed us to gather quantitative data that complements with the information provided by the NDE. In the following chapters of this study, the correlation between the qualitative and quantitative data are presented and analyzed.

1.2 Objectives

The overarching goal of this research is to evaluate and quantify the effectiveness and efficiency of LiDAR sensors to contribute to the suite of technologies available to perform bridge deck condition assessment. In particular, this project will deploy LiDAR as a screening technique to address early bridge deck deterioration. To achieve this, this research proposes the following specific objectives:

(1) Understand the deterioration pattern of New Jersey bridges, focusing on the behavior of steel girder structures, by analyzing the time it takes from a bridge deck to drop one level on the condition rating scale.

(2) Evaluate the results gathered from the point cloud data collected on a full-scale bridge deck at different levels of deterioration by paring the information gained from implementing conventional NDE technologies.

(3) Quantify the information gained from deploying LiDAR on operating bridges in New Jersey to estimate the condition rating based on the level of damage on the decks' top surface.

(4) Investigate the costs related to current bridge condition assessment practices and the impact of incorporating the use of LiDAR sensors.

1.3 Methodology

To satisfy the objectives of this research, the following methodology explains the importance of implementing point cloud data captured via LiDAR in the condition assessment of bridge decks.

1.3.1 National Bridge Inventory Data Processing

A thorough literature review was conducted to understand the state-of-the-practice and identify gaps related to this research. Relevant journal papers, reports, and other literature related to bridge condition and preservation practices, as well as state-of-the-art data processing methods was reviewed. As part of this process, the National Bridge Inventory data will be thoroughly investigated. To process the NBI data and conduct studies on bridge deterioration based on change in deck condition rating by main construction materials, the following procedure was implemented. First, the National Bridge Inventory (NBI) data was obtained from a database maintained by the Federal Highway Administration (FHWA), which contained information on all bridges in the United States that certain bridges were chosen that met the research criteria of Bridges

having steel girders, concrete decks, single spans or continuous two-span configuration, Along with similar Average Daily Traffic (ADT) and Average Daily Truck Traffic (ADTT).. The NBI data could be obtained from the FHWA's website or through other sources such as BridgeData.net. Then, the NBI data was refined and preprocessed to remove errors, duplicates, or irrelevant information. Data refining and filtering techniques, such as data deduplication, data normalization, and data standardization, were employed during this step.

The data was then categorized based on the primary construction materials used in the bridge girders, such as concrete, steel, or timber. This categorization allowed to analyze how the choice of construction materials affected the rate of bridge deterioration. The deterioration rate was analyzed based on changes in ratings. Bridges that experienced a decrease in rating over time were identified, and their deterioration rate was investigated. This involved comparing the current condition rating of the bridge with its previous rating and calculating the rate of deterioration.

Finally, after analyzing the data, a comparison chart was created to show the time it takes for bridges to deteriorate one level within the condition rating scale (e.g., 9 to 8, 8 to 7, and so forth) based on their construction materials.

1.3.2 Evaluation of the Deterioration of a Full-Scale Bridge Deck

The evaluation of the deterioration of a full-scale bridge deck involves using LiDAR technology. The process begins with obtaining a LiDAR scanner, such as the Faro Focus S 150, and setting it up in a suitable location to capture the bridge deck surface. The surface is then scanned using the LiDAR scanner, and the scanning process is repeated for the entire bridge deck surface until all areas are captured.

The scans are then registered using Scene software provided by the Faro company. This involves aligning the scans to create a complete bridge deck surface point cloud. The registered point cloud is then imported into CloudCompare software for further processing and analysis. By analyzing the point cloud data using CloudCompare, low points where water can accumulate on the bridge deck surface can be identified. The analysis results can be used to plan maintenance and repair operations that can help extend the service life of the bridge deck.

In addition to the process above, the development of point cloud analysis methods involves gross-scale analysis, which includes curvature and slope analysis, and fine-scale analysis, which includes the evaluation of low points through extraction and analysis and curvature elimination, and plane fitting.

It is important to note that using LiDAR for bridge deck evaluation can be a complex process and may require specialized training and expertise to ensure accurate and reliable results. Figure 1 , demonstrates the steps taken to achieve our goal:
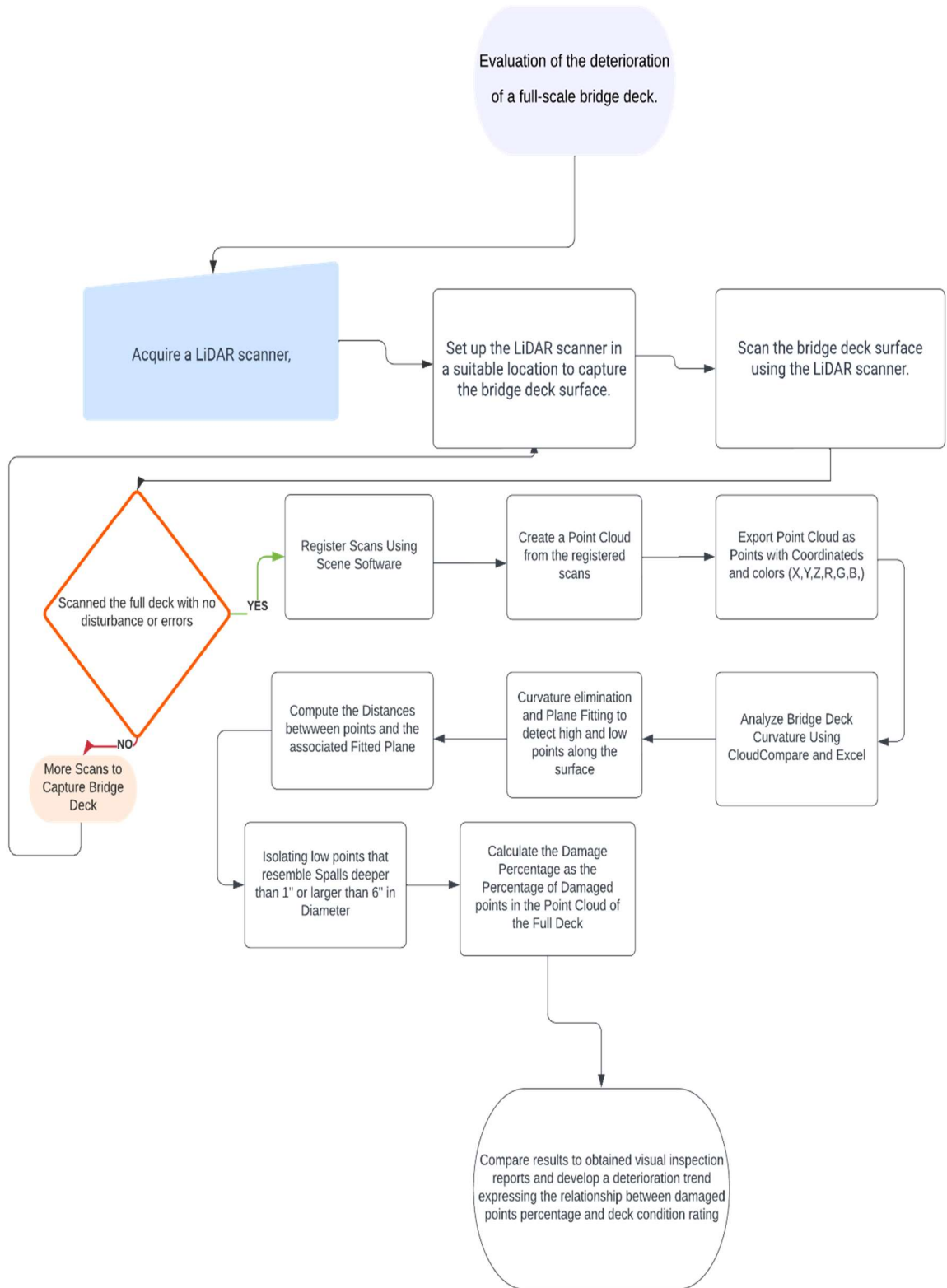
Figure 1. Methodology taken for the evaluation of the deterioration of a full-scale bridge deck.

1.3.3 Implementation of Knowledge Gained on Operating Bridges in NJ

To implement the knowledge gained on the information gathered from the full-scale bridge deck study, this section implements the two methodologies developed in *1.3.2* for the analysis of operating bridges in New Jersey, USA. The particular purpose is to develop a deterioration trend and evaluate its correlation to the patterns found on *1.3.2*.

Bridges in New Jersey will be scanned to collect data on bridge geometry, structural characteristics, and operational conditions. The collected data will be process and analyzed using common point cloud data management methods as pruning, filtering, and normalizing to remove outliers, errors, or inconsistencies. Curvature extraction and analysis will also be implemented using appropriate algorithms or techniques develop on 1.3.2, to extract curvature information from the collected data, and transform the shape of the top surface of the bridge decks into 2D planes.

Finally, a comparative analysis will be conducted to evaluate the effectiveness of both approaches in achieving the specific objective of this section. Results obtained from both methods will be compared to establish strengths and limitations of each, to propose cases for their application.

1.3.4 Incorporating LiDAR into the NDE Techniques Suite

Based on the information gathered on *1.3.3*, this section will focus on incorporating LiDAR technology into standard operating procedures (SOPs) for condition assessment. To achieve this, a cost estimation of current bridge deck condition assessment practices will be performed. On this section, knowledge gaps that can be bridged via point cloud data analysis (e.g., deck morphology) will be identified to propose its incorporation into

regulatory inspection procedures. This will include a revision of the benefits and shortcomings of implementing LiDAR sensors for bridge deck condition assessment, and its compatibility with existing infrastructure and data management systems. To evaluate the applicability of this incorporation, the proposed changes will be discussed with members of the bridge industry, including engineers, maintenance staff, and supervisors, to gather feedback and ensure everyone is on the same page.

Then, a plan for integrating LiDAR technology into the SOPs will be developed, including any necessary training or equipment upgrades. Consider the timeline for implementing the changes, considering any potential impacts on bridge operations and traffic.

Chapter 2

State-Of-The-Practice of Concrete Bridge Deck Condition Assessment

2.1 Bridge Deck Deterioration

From the ASCE 2021 infrastructure report. Figure 2, demonstrates the increase in the number of bridges rated as fair over the past years in the USA, which represents about 178 million trips per day each year. The total percentage of bridge deck areas identified as in poor condition was 7.5 percent in 2021 (ASCE, 2021). It is projected, that over the next 50 years, the deterioration trend will continue to increase unless significant work in done to our infrastructure. A systematic program for bridge preservation should be adopted, in which existing degradation is emphasized and preventative maintenance is prioritized.
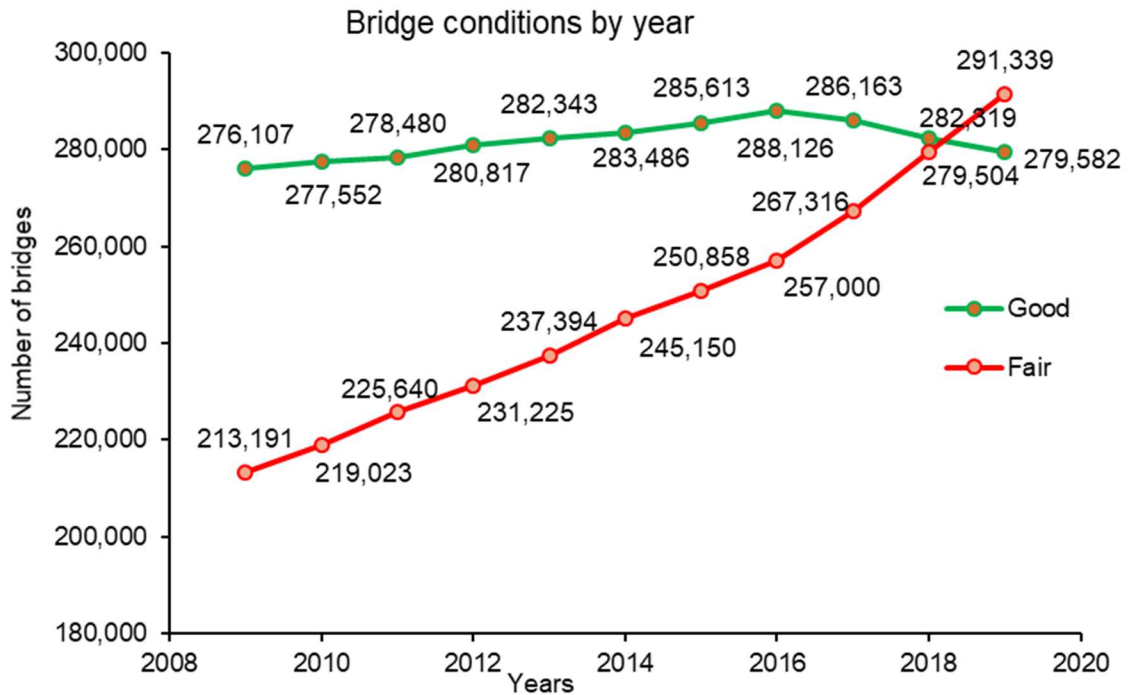
Figure 2. Bridges Condition Rating in the USA from ASCE 2021 infra-structure report.

2.1.1 Reinforced Concrete Deterioration

Reinforced concrete deterioration can be physically, chemically, or mechanically induced.(Alla & Asadi, 2020) Corrosion loads and mechanisms in concrete and reinforcement can be classified as external or internal physically induced deterioration (Penttala, Vesa, and Fahim Al-Neshawy. (2002)). External origin processes include freeze-thaw damage, chloride intrusion, carbonation, sulfate attacks, and acid attacks (Basheer et al., 1996) internal origin mechanisms include the effects of alkalis on specific aggregates or ettringite degradation. On the other hand, the chemical reactions that cause concrete structures to deteriorate include carbonation (Delatte, Norbert. (2009)), steel reinforcement corrosion, acid and sulfate impacts, delayed ettringite development, and alkali–aggregate reactions.. Carbonation of the concrete's surface layer can indeed affect the concrete itself over time. Carbonation occurs when carbon dioxide from the atmosphere reacts with the calcium hydroxide in the hydrated cement paste of the concrete, forming calcium carbonate. This reaction causes the pH of the pore water in the concrete to decrease, making it more acidic. When the pH of the pore water decreases, it can lead to a reduction in the alkalinity of the concrete. Alkalinity is important in concrete because it helps to protect the reinforcing steel from corrosion. When the pH of the pore water drops below a certain threshold (typically around pH 9), the passivating layer on the steel can break down, and corrosion can occur. Additionally, as the carbonation reaction progresses further into the concrete, it can cause the concrete to lose some of its strength and durability. This is because the reaction can cause the concrete to become more porous, which can allow water and other harmful substances to penetrate deeper into the concrete. (Panesar, 2019)

While carbonation can help to lower the pH of the pore water in the surface layer of the concrete, it is important to monitor the extent of carbonation to ensure that it does not progress too far into the concrete and cause more significant damage over time. (You et al., 2014). The absence of chlorides in the concrete is a requirement to avoid steel reinforcement corrosion. Additionally, Chloride intrusion in concrete can occur through several physical methods, including penetration through the surface, capillary absorption, permeation, diffusion, and carbonation. These mechanisms can act alone or in combination to cause chloride ions to penetrate concrete, which can affect the durability and performance of concrete structures. The severity of chloride intrusion and its impact on concrete depend on various factors such as the mix design, curing conditions, and exposure environment. (Zhang & Gjørv, 1994), but chlorides exacerbate steel reinforcement corrosion, so their effects are assessed alongside reinforcement corrosion. (Penttala, V. (2009)).

Reinforcement corrosion is the primary deteriorating mechanism that affects outdoor concrete structures, which account for roughly one-third of total concrete structures' volume (Penttala, 2009). Reinforcing steel corrosion is a common cause of reinforced concrete (RC) bridge deck deterioration, which occurs when the steel's passivity is weakened by concrete carbonation, chloride ion entry, or a combination of both. Steel expands as it corrodes, causing cracks within the concrete due to the internal tensile stresses. (Šavija et al., 2013). Cracking speeds up the damage mechanisms by allowing chloride ions, oxygen, and moisture to flow freely. As a result, subsurface fracture planes are formed. A rupture between the deck surface and the delaminated zone may develop as the deterioration progresses, resulting in concrete surface spalling and catastrophic

structural and functional failures, putting human lives at risk and causing severe economic loss. (Gucunski, N., and S. Nazarian. (2010))

2.1.2 Condition Assessment

According to the Federal Highway Administration's (FHWA) Recording and Coding Guide for the Structure Inventory and Appraisal of the Nation's Bridges, concrete decks must be examined for cracking, scaling, spalling, leaching, chloride contamination, potholes, delamination, and full or partial depth failures before the structure is given a rating. Timber decks and steel grid decks need to be examined as well. Inspection for broken welds, fractured grids, section loss, and growth of filled grids from corrosion is crucial for steel grids. It is essential to look for signs of rot, fastener failure, splitting, and crushing in wood decks.

Bridge deck condition assessment is an essential task in maintaining the safety and durability of bridges. While visual inspections remain the most common method of assessing the condition of bridge decks, there is increasing interest in using more advanced technologies such as non-destructive testing methods. These methods, including ground-penetrating radar and infrared thermography, are gaining popularity due to their ability to detect defects and deterioration below the surface. In addition, data-driven approaches, such as machine learning and artificial intelligence, are being explored for bridge deck condition assessment to improve accuracy and reduce the subjectivity of visual inspections. Long-term monitoring using sensors and automated systems is also being studied to provide continuous assessment of bridge deck conditions and detect changes over time. The growing emphasis on using a multi-faceted approach to bridge deck condition assessment, combining different methods and technologies, is promising in providing a

comprehensive understanding of the deck's condition. Such advancements in bridge deck condition assessment will lead to improved maintenance and preservation strategies, ensuring the safety and longevity of bridges for years to come.

2.2 Non- Destructive Evaluation

Due to concrete's heterogeneous nature, evaluating reinforced concrete bridge decks can take time and effort. Visual inspection is the most common method for bridge deck inspection, where hammer sounding and chain dragging are the most regularly utilized procedures to detect subsurface faults like delamination (Alsharqawi et al., 2018). However, it has several downsides, like the inability to discover concealed defects and the inspector's sensitivity. According to the findings, visual evaluation of bridge decks is a factor of the level of deterioration of the bridge deck, indicating that the inspector is capable of detecting damage after a certain level of development (Graybeal et al., 2002).

Various hand-held equipment such as hammers, steel rods, and chains are commonly employed to inspect concrete bridge decks. When the deck surface is struck, delamination in concrete usually produces a dull sound. While this technique is a low-cost technology, the operator's judgment and experience are required to interpret the produced sound. Hands-on approaches are required for such procedures, which can be labor-intensive and time-consuming. Inspectors must also have safe access to the bridge deck, which requires traffic management. The bridge community has been looking for better NDE technologies due to the inherent limits of visual examination and traditional sounding procedures. (Gucunski, et al. 2012). Some of the most common Non-Destructive evaluation (NDE) techniques used in the field can be seen in Figure 3.
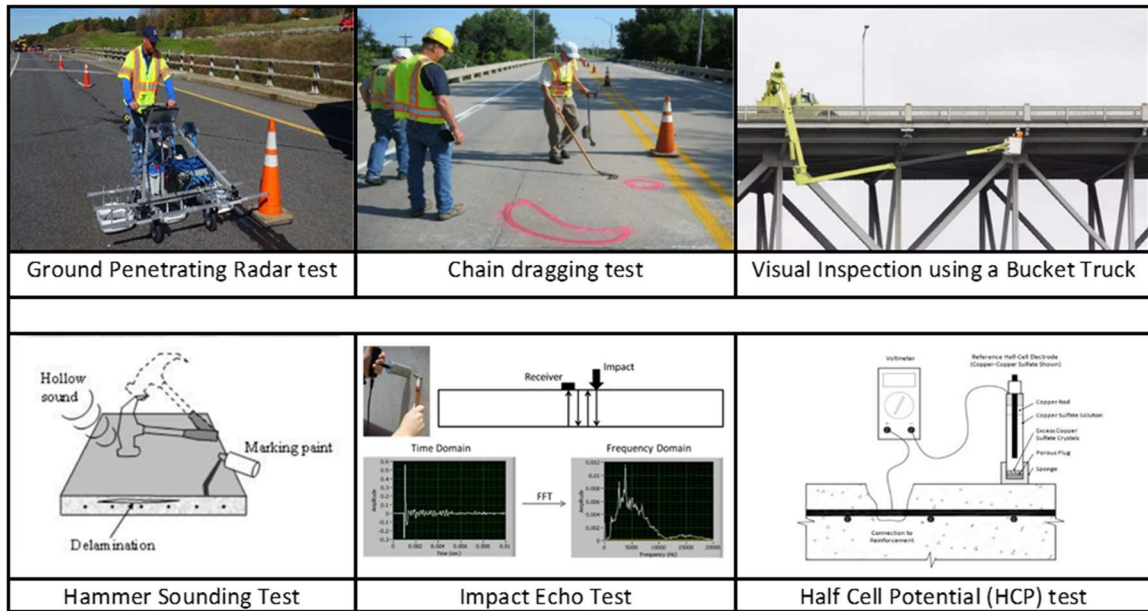
Figure 3. The most common NDE techniques used in the field.

2.2.1 Conventional Evaluation and Assessment Methods

2.2.1.1 Chain Dragging. Chain dragging is one of the primary conventional techniques for checking concrete decks for delamination. It is a straightforward procedure whereby the inspector merely drags heavy chains across the concrete deck, producing a unique sound over any probable delamination-prone spots. All Currently used NDE techniques standards can be found in the Bridge Inspector's Reference Manual provided by the Federal Highway Administration (FHWA, 2013). Then, these locations are mapped and labeled for later analysis. Usually, when using this technique, several chains may be added to cover huge regions swiftly. However, because there might be a lot of background noise, this approach depends on the inspector's ability to identify the various noises (Kashif Ur Rehman et al., 2016). Due to the need to shut the lane being tested, the test also disrupts moving traffic.

2.2.1.2 Visual Inspection. One of the most typical methods of bridge inspections is a visual examination. This approach entails skilled inspectors inspecting a structure with their unaided eyes for flaws such as potholes, cracks, spalling, corrosion, joint condition, and other faults on a bridge surface. In the past, this has involved personally visiting the building and performing a visual inspection. Inspectors would utilize bucket trucks to examine the problems beneath a bridge when necessary. However, the deployment of Remote Visual Inspection (RVI) has only just begun. Drones are used in RVI to explore challenging regions of the structure securely (Alsharqawi et al., 2018).

Only qualified inspectors with thorough training programs recognized by the Federal Highway Administration (FHWA) can conduct a traditional visual inspection. Controlling traffic is one of this method's drawbacks, along with optical clarity, color vision, complexity, accessibility, and expense. Particularly if a bucket truck wants to operate on the bridge, traffic must be managed on both sides of the structure. Visual acuity and color vision are terms used to describe how well the inspector(s) doing the inspection can perceive clarity and sharpness at a distance of 20 feet and color. Another restriction is the difficulty, expense, and cost-effectiveness of a structure's examination since there may be locations on the bridge that are difficult to access and other options (Scott et al., 2003). Such as drones or heavy machinery; the cost of purchasing big machinery or drones would be high. This approach is often quite reliable for locating apparent damage, but more is needed to provide an adequate evaluation of what happens inside the building.

2.2.1.3 Hammer Sounding. A hammer-sounding test offers a qualitative assessment of the under-consideration concrete. The concrete is pounded with a hammer during this non-destructive operation, and the noises it creates at various points on the

concrete are analyzed. Concrete is more durable when hammer vibrations are louder and more powerful. The weaker the concrete, the hollower it sounds, and the lower its pitch, the more like a drum (Henderson et al., 1999). This technique is effective for locating voids and deformations in the top layer of concrete but is ineffective for determining the state of the concrete farther into the member. Another drawback of this approach is the inability to detect any flaws hidden under overlays. Like chain dragging and visual inspection, the inspector's experience is crucial for assessing the deck condition (Abu Dabous et al., 2017).

2.2.2 Modern Approaches – Non-Destructive Evaluation (NDE)

The absence of accurate geospatial information, the length of time needed to conduct the evaluation, and the subjective character of the data are significant drawbacks of the aforementioned traditional assessment techniques. Capturing geospatial data would allow to map and quantify the damaged regions more precisely and objectively. Modern NDE techniques help mitigate some drawbacks of traditional inspection techniques. Current NDE digital data offers geometric data that maps the information received, which permits to quantify the dimensions of the damage discovered. Next, the most often employed NDEs are discussed.

2.2.2.1 Ground Penetrating Radar (GPR). A prevalent form of Non-destructive evaluation method for bridges is Ground Penetrating Radar. For this method, electromagnetic wave pulses are transmitted via an antenna which is then collected by a radar receiver to make an image of the subsurface features in a bridge deck or pavement. As the pulse encounters a discontinuity, they are reflected, which could indicate the presence of delamination. Therefore, GPR has been found helpful for evaluating bridge decks on determining the depth of concrete and spot potential deterioration (e.g.,

delamination) (Hugenschmidt & Mastrangelo, 2006). A shortcoming of GPR technology is the limitation of waves penetrating through metal, blocking the possibility of detecting voids, delamination, or cracks under the rebars. On the other hand, this means that GPR is useful in determining the location of steel rebars within the deck (Abdelkhalek & Zayed, 2020).

2.2.2.2 Impact Echo (IE). An NDE method called Impact Echo uses the acoustical resonance of a material's intrinsic faults to identify subsurface delamination. A brief impact on the deck during this test causes internal defects and stress waves to travel through the material back and forth between the impacted and opposite surfaces. A time domain and frequency domain will be obtained to examine the data and find any internal faults, including delamination, fractures, voids, and honeycombing (Hendricks et al., 2020)

The Impact Echo method has limitations that may affect its accuracy and reliability in certain situations, according to (Kee et al., 2012). The method may not be effective in detecting relatively small voids or cracks in the concrete, as they may not produce strong echoes. In addition, reinforcing steel and other metallic objects may interfere with the signals and produce false readings. The thickness of the concrete layer may also affect the accuracy of the results, as thicker layers may absorb more energy and reduce the signal strength. Furthermore, the method may not be suitable for use in high-traffic areas or situations with high noise levels, as this can interfere with the data collection. (Abdelkhalek, 2022) Despite these limitations, the Impact Echo method remains valuable for bridge deck evaluation and provides helpful information about the condition of the concrete and the presence of defects.

2.2.2.3 Half Cell Potential (HCP). A technique called half-cell potential can be used to assess the likelihood of corrosion or the occurrence of corrosion on the steel used as reinforcement in concrete. This technique measures the potential difference between a reference electrode and the reinforcing steel that is being evaluated. ASTM C876 then provides the likelihood of steel corrosion activity based on the measured potential (Amiri et al., 2021).

However, the HCP method has several limitations. The method only provides a qualitative indication of the corrosion activity and does not provide information about the extent or rate of corrosion. The HCP measurements are also sensitive to the surface condition and moisture content of the concrete, and the presence of coatings or cathodic protection systems can affect the accuracy of the measurements. Additionally, interpreting the HCP measurements requires experience and knowledge of the concrete structure. The method is impractical for detecting corrosion in steel reinforcement deeply embedded within the concrete. Despite these limitations, the HCP method is still widely used in practice due to its ease of use and cost-effectiveness (Gucunski et al., 2010).

2.2.2.4 Electrical Resistivity (ER). The strength of the resistance to the flow of an electric current is described by the material attribute known as electric resistivity. Because the concrete's electrical resistance regulates the potential corrosion rate, this is crucial to the bridge inspection. This test complements the HCP test because both assess the possible corrosion rate. The electrical resistivity method is a non-destructive testing method that measures the electrical resistance of concrete to determine its quality and condition. This method involves using electrodes placed on the surface of the concrete to send an electrical current through it. The electrical resistance of the concrete is then measured, which can

provide information about the presence and extent of cracks, voids, or other defects within the concrete.

However, there are limitations to the electrical resistivity method. The accuracy of the measurements can be affected by factors such as the concrete structure's size and shape, the concrete's moisture content, and the presence of reinforcing steel or other conductive materials. Additionally, the electrical resistivity method cannot provide information about the depth or location of defects within the concrete. Therefore, it is often used in conjunction with other testing methods to provide a complete picture of the condition of the bridge deck. (Le et al., 2017). The effects of the studied concrete's water-to-cement ratio represent a significant restriction of ER. Lower electrical resistivity is produced by higher porosity percentages, which are produced by higher w/c ratios. Supplemental cementitious materials' inclusion also has an impact on these values. Since the presence of water inside the concrete would diminish its porosity, the presence of water throughout the data-collecting period must also be considered when interpreting the results (Su et al., 2002).

Non-destructive evaluation (NDE) technologies are used to detect potential damage or defects in concrete structures without causing any harm to the material itself. Each NDE technology has a unique physical concept that enables it to identify different types of flaws. Half-cell potential measures the electrochemical potential of reinforcing steel within concrete to detect the early stages of corrosion. Ground-penetrating radar (GPR) uses high-frequency electromagnetic waves to detect interfaces or discontinuities within the material, allowing engineers to locate features such as rebar, post-tensioning cables, and voids. Electrical resistivity (ER) measures the electrical resistivity of concrete to identify areas

where the concrete may be weaker or more susceptible to damage. Impact echo generates stress waves within the concrete using a mechanical impact, which can be detected by sensors placed on the surface of the concrete to determine the thickness of the concrete and locate potential damage or defects. By using these NDE techniques, engineers and technicians can select the appropriate method for a given application and interpret the results accurately to ensure the safety and longevity of concrete structures.

Over the last decade, there has been a burst of new NDE assessment tools. Still, their documentation must be more complete (across refereed and no refereed literature). It requires actual performance statistics for specific technologies and products (Long-Term Bridge Performance. FHWA)." Of geographical information, the length of time needed to conduct the evaluation. The subjective character of the data is a significant drawback of the aforementioned traditional assessment techniques. Capturing geometrical data would make it possible to map and quantify the affected regions more precisely and objectively.

Modern NDE techniques help mitigate some drawbacks of traditional inspection techniques. Current NDE digital data offers geometric information that maps the data received, including the depth of the damage discovered. The most common modern NDEs used are Ground Penetrating Radar (GPR), Impact Echo (IE), Half Cell Potential (HCP), and Electrical Resistivity (ER).(FHWA-HRT-21-004, Vol. 85 No. 2)

The data from the NDE above provide 2D information that is extrapolated to create a predictive 3D data mapping. There is a pressing need for a means to reflect ground truth 3D data and serve as a platform where multiple NDE technologies can be combined. This

research utilizes point cloud data from LiDAR as the linking platform, ultimately serving as a predictive bridge deck condition assessment tool.

2.2.3 The Urge for Robust Non-Contact SHM Techniques

Infrastructure worldwide, including roads, buildings, and bridges, have deteriorated due to limited durability and increasing natural disasters. Inspection techniques are necessary to assess damage and safety of our infrastructure but traditional approaches, as visual inspections, can increase the risk of the inspectors. Non-contact or remote sensors are increasingly being used for Structural Health Monitoring (SHM) as they do not require physical contact with the structures. Non-contact sensors can be either passive or active. Passive sensors use optical setups to capture images or videos, while active sensors emit a signal or energy and measure the reflected or emitted signal. Active sensors can emit a range of spectral bands or frequencies depending on the specific application. Both types of sensors are widely used in various industries and applications. Non-contact sensors, such as cameras, smartphones, unmanned aerial vehicles, satellites, and ultrasonic devices, are used for structural inspections. However, the quality of data collected from optical sensors can be impacted by environmental factors, and ultrasonic devices are limited to analyzing the surface of structures. Non-contact sensors have limited applications in specific types of monitoring, making them difficult to use in a generalized setting (Huang et al., 2018). For this, there's a need for a robust system that can integrate technologies that supplement each other, combining the advantages of all to deliver fast, reliable, quantitative, and objective infrastructure assessment.
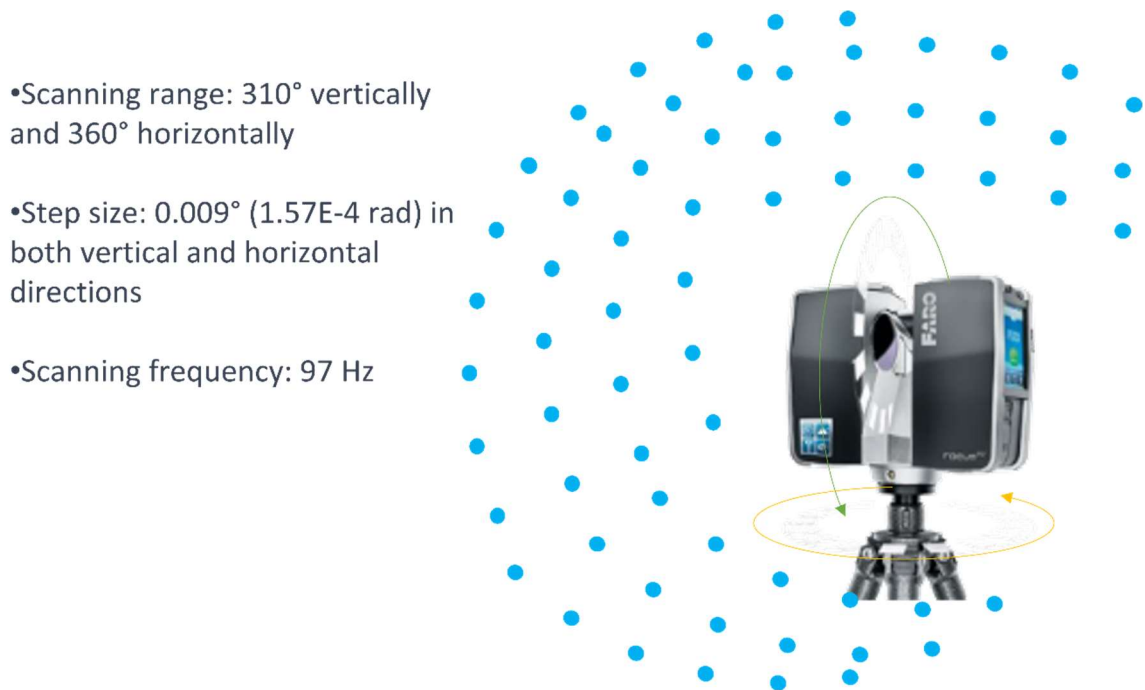
2.3 LiDAR Sensors

LiDAR is an acronym for light detection and ranging. It is also known as LADAR or Laser Altimetry Detection and Ranging. It is a remote sensing technology that uses intense, focused beams of light to detect reflections and measures distance by estimating the time it takes for the beam of light to be emitted, bounce from the scanned surface, and return to the scanner. LiDAR is similar to RADAR (radio detection and ranging), but using discrete laser light pulses instead of continuous radio waves. The coordinates in three dimensions of the targeted objects (x, y, z or longitude, latitude, and elevation) are calculated using: (1) the time it took for the laser pulse to travel between being emitted and being retrieved, (2) the angle at which it was emitted, and (3) the scanner's exact location above or on the Earth's surface. LiDAR was first developed as a fixed-position ground-based instrument for studying atmospheric composition, structure, clouds, and aerosols. It is a valuable tool for climate observations around the world (Mijić, 2018). LiDAR sensors are also used to scan specific targets, such as bridges, buildings, and beaches, and are mounted on fixed-position tripods. Tripod-based LiDAR systems produce centimeter-level point data and are frequently used for localized terrain mapping applications that require frequent surveys. (Dong, Pinliang, and Qi Chen. (2017))

The operational processes of standard LiDAR scanners involve the emission of laser beams over a range of 300° (vertical) by 360° (horizontal) on steps with angular distances as small as 0.009° (1.57E-4 rad), providing a maximum resolution of 111 points per degree angle. The effective range of the scanner will depend on the model, but it usually varies between 10 m to 300 m. The originated pulses bounce back from the object's surface

to the scanner. Then, points are registered on a global coordinate system based on the pulses' time of flight and the vertical scanner's distance and horizontal rotational angles.

Different kinds of software can process and produce 3D images using X, Y, and Z coordinates. Figure 4 depicts how a typical LiDAR scanner operates. LiDAR's biggest drawback is that it cannot scan the interior of structures; thus, numerous scans may be required depending on the application and the level of detail needed.

•Scanning range: 310° vertically and 360° horizontally

•Step size: 0.009° (1.57E-4 rad) in both vertical and horizontal directions

•Scanning frequency: 97 Hz

Figure 4. Principals of Operations of Standard Terrestrial LiDAR.

2.3.1 Lidar Sensor Types

There are multiple applications for when LiDAR sensors can be deployed to acquire geometrical data of the scanned objects. Each application requires certain level of local accuracy, therefore, different platforms for LiDAR sensors have been created to meet the

needs. LiDAR sensors can be categorized into three main types based on their mode of operation and platform: terrestrial, mobile, and aerial.

2.3.1.1 Terrestrial LiDAR Sensors, or terrestrial laser scanning (TLS), are mounted in a fixed position and can capture dense point clouds from various locations near the ground. TLS scans are typically merged to create larger point clouds, and the size of the point cloud depends on the range of the scanner. TLS sensors use two laser measurement techniques: phase-based, fast but limited to short distances, and time-of-flight-based, which can measure more considerable distances but are slower and less accurate. Different models of TLS sensors offer various speeds, resolutions, and accuracies, with some capable of capturing 2000-120,000 points per second and providing precision within a few millimeters. TLS sensors help build information modelling, structural inspection, and reconnaissance surveys. While using TLS may require more handling and time per scan than mobile laser scanning (MLS) during data collection, TLS point clouds are generally more detailed and with smaller precision (Kaartinen et al., 2022).

2.3.1.2 Mobile Laser Scanning (MLS) is a LiDAR sensor mounted on mobile equipment such as drones, airplanes, cars, or helicopters. It can capture scans while the equipment is in motion, typically at speeds up to 100 km/h. MLS devices are equipped with GPS receivers and inertial measurement units (IMUs) to accurately record the location and orientation of the equipment during data capture (Wang et al., 2019)

2.3.1.3 Airborne Laser Scanning (ALS) is a specific type of MLS that is particularly useful for capturing point cloud data of large areas of land, hard-to-reach surfaces such as skyscrapers or signature bridges, and terrain with limited access such as

post-disaster situations. ALS is typically mounted on airplanes, helicopters, or drones and captures point clouds at different heights and distances without manual operation. The GPS receiver allows for accurate recording of the location of reflections on the scanned surfaces, while the IMU records the orientation of the system to account for its tilt, roll, yaw, and pitch. The airborne system's speed, angle, and rotation are crucial factors in calculating each point's elevation in the point cloud (Schlögl et al., 2022)

2.3.2 Faro Laser Scanners

For this research, the scanner chosen to collect data was the Faro Focus S-150; this device is a stationary LiDAR system that produces centimeter-level point data and is frequently used for localized terrain mapping applications requiring frequent surveys. (Dong & Chen, 2017). This study utilizes data collected through a Faro Focus-S 150 laser scanner. These sensors are also used in industries such as architecture, engineering, construction, public safety and forensics, and product design for indoor and outdoor measurements to capture real-world data that is analyzed, collaborated on, and made decisions in a digital space to improve and manage projects or product quality. (Hohenthal, et al. 2011).

The Focus-S 150 Laser Scanner series, used to collect the data for this research, allows the user to adjust the scanner's features based on the task's requirements. Table 2, summarizes the specifications of the terrestrial laser scanner used.

Table 2

Faro Focus-S 150 Specification From Faro User Manual

Unambiguity	614m for up to 0.5 mil pts/sec 307m at one mil pts/sec
Operating	5 °C to 40 °C: (41°F to 104°F)
Extended	-20 °C to 55 °C: (-4°F to 131°F)
Range Accuracy	+/- 1 mm
3D Position	2mm @ 10m; 3.5mm @25mm
On-site	Available
On-site	Available
Accessory Bay	Available
Integrated Color	Available
Retake Photo	Available
Digital Hashing	Available
Scan Groups	Available
Sensors	Dual-axis compensator, Height sensor, Compass, Integrated

2.3.3 LiDAR-Based Structural Health Monitoring (SHM)

The SHM research community has extensively studied LiDAR devices and methods for generating 3D point clouds and analyzing structures over the past ten years. Numerous studies have proposed techniques for optimizing the collection and processing of data to create more time-efficient and cost-effective SHM systems. For example, (Bolourian & Hammad, 2020) implemented an unmanned aerial vehicle-based LiDAR with an optimized flight path decision-making paradigm to inspect surface defects in bridges. Additionally, advanced algorithms have been developed for detecting structural elements and damages with millimeter precision and minimal error (Pereira et al., 2021) and (Trias et al., 2021). Although several literature reviews have been conducted on using LiDAR devices for SHM, most have broadly assessed non-contact sensing techniques for damage detection rather than focusing specifically on LiDAR devices (Kim et al., 2019). Moreover, current LiDAR-based literature reviews tend to concentrate on limited areas

within SHM, such as the deformation monitoring of buildings (Mukupa et al., 2016). bridge inspection (Rashidi et al., 2020). and moisture detection in structures (Suchocki & Katzer, 2018). LiDAR technology has various applications in SHM, including analyzing 3D objects, structural geometries, deformations, and crack information using highly accurate and precise 3D datasets. These applications can be broadly categorized into two types: phase-based, which is rapid but limited to short distances, and time-of-flight-based, which is slower but can measure more considerable distances (Mukupa et al., 2016). There are a variety of laser scanners available, with speeds ranging from 2000 to 120,000 points per second, maximum resolutions typically between 1 and 100 mm at 50 m, and accuracies typically between 3 and 50 mm at 100 m (Ranyal et al., 2022). These scanners can be used for as-built building information modeling, structural inspection, and reconnaissance surveys by capturing 3D data and meta-data of the target several hundred meters away to a precision of a few millimeters. Using LiDAR in SHM can significantly improve efficiency and reduce costs associated with traditional inspection methods while ensuring the safety and longevity of critical infrastructure such as buildings and bridges.

2.3.3.1 LiDAR for Structural Health Monitoring of Bridges. LiDAR has been increasingly gaining recognition for bridge structural health monitoring (SHM), focusing on characterizing the geometric features of components like girders and decks. One common application is to measure the vertical clearance under bridges to ensure safe passage for large vehicles (Kaartinen et al., 2022). LiDAR has also been utilized to examine the relationship between environmental factors, such as loading, temperature, precipitation, and bridge deformation. Some studies have also employed LiDAR to detect structural damages, such as spalling and cracks. For instance, (Teza et al., 2009)study proposed an

automated method for identifying mass loss in concrete bridges using TLS, which involved three steps: subdividing the point clouds into sub-areas, applying Gaussian filtering and parabolic fitting to each point, and classifying each sub-area as damaged or undamaged based on the curvature distribution.

Researchers have investigated various uses of LiDAR technology for bridge evaluation and monitoring. One study by (Liu et al., 2010) used a phase-based laser system to compare distance and gradient-based methods for quantifying material loss in a bridge. Combining these methods improved the capability of LiDAR for identifying and quantifying defects. Another study by (Liu et al., 2012). developed an automatic technique for measuring bridge clearance using TLS, which achieved millimeter-level accuracy. Watson et al in 2012 evaluated the impact of various parameters on bridge clearance measurements using periodic TLS scans. In (Liu & Chen, 2013), the applications and reliability of LiDAR for bridge health monitoring were assessed through sensitivity analyses on a full-scale bridge, including tests of range measurement ability, the accuracy of the scanner, and automatic inspection algorithms.

In a study (Riveiro et al., 2013). A method was introduced for measuring the minimum vertical clearance of bridges and obtaining the profile of prestressed concrete beams using photogrammetry and TLS surveys. To estimate the vertical clearance and beam cambers, a 3D curve-fitting algorithm was developed, which achieved high statistical correlation coefficients when implemented on a full-scale bridge. Geometrical information of bridges, including elevation, span length, girder spacing, bottom flange width, and web height, was recorded by a LiDAR (Dai et al., 2014), and the girder deflections were calculated by comparing the girder elevation coordinates of the scans with and without

truck weight. The proposed approach proved to e accurate and more accessible than contact methods, even in estimating the bridge's natural frequencies. In addition, a fully automated TLS point cloud segmentation procedure was developed by (Riveiro et al., 2016) for the structural health monitoring of masonry arch bridges. The proposed algorithm used a voxelization process to filter out redundant data and used topological constraints to establish individual structural elements' spatial relation and order. When tested on five datasets, the algorithm showed coherent results with minor issues due to poor point cloud quality. (Sánchez-Rodríguez et al., 2017) Suggested an automated method of processing laser scanning data for structural health monitoring (SHM) of masonry arch bridge piers. They segmented a full-scale bridge into its structural components and identified structural faults by analyzing the geometric parameters of pier faces and their topological relationship with other bridge elements.

SHM technology for masonry bridges using TLS data and Ground-Penetrating Radar (GPR) was presented by Pérez et al., in 2018. They compared TLS measurements with historical drawings to identify anomalies in hyperbolic reflections and determine the bridge filling configuration. Ziolkowski et al., in 2018 introduced a TLS-based framework for detecting structural deformation in composite footbridges. They generated two mesh models using the Fast Marching algorithm and compared them to check for changes after applying a load to the bridge. Kim et al., in 2018 investigated a crack identification and quantification approach for concrete structures using unmanned aerial vehicles. They generated a point cloud-based background model of the structure and applied convolutional neural networks to high-resolution images for crack detection. They used transfer learning and 384 crack images for classification and localization on a full-scale bridge. Cha et al.,

in 2019 proposed a deflection and deformation measurement application for bridges using a shape information model constructed from improved octree data structure and TLS data. The deflection was estimated based on the octree space division and validated using LVDT. The research developed a new bridge inspection technique using UAV imagery point clouds, constructing a triangular mesh and density map to reduce errors in data. The iterative closest-point algorithm was applied with TLS data to measure thickness, point distribution, and point-to-point distances for a full-scale bridge.

Lee et al., in 2019 introduced a reflector-based framework for measuring long-term bridge displacement using LiDAR. The framework included a reflector positioning strategy, measuring the reflector coordinates, and calculating the displacement. The proposed method was validated using a prestressed concrete bridge. Liu et al. in 2019 used TLS to construct a Digital Surface Model and identify the potential damage area of a bridge. Ground-based microwave interferometry was used to confirm the damage, and interferometry synthetic aperture radar was applied to analyze the causes of the damage to a full-scale bridge. Bolourian & Hammad, in 2020, introduced a 3D path planning technique for LiDAR-equipped UAVs to inspect bridges. The approach involved three steps: (1) assigning essential values based on the moment and shear force values from structural analysis, (2) selecting Viewpoints of Interest for perpendicular and overlapping views, and (3) calculating the optimal collision-free path using a Genetic Algorithm and A* algorithm. After testing on a full-scale bridge, the method reduced flight time, processing time, and workload while enhancing visibility, reliability, and accuracy. Erdélyi et al.in 2020 developed a deformation monitoring method using TLS and ground-based radar interferometry data, which was also tested on a full-scale bridge. By comparing the

two methods, the authors found similar results. Cha et al.in 2020, proposed a displacement estimation method for bridge structures using four laser scanning-based techniques. The method involved rearranging points in a 3D space and creating nodes to calculate the displacement. The proposed method reduced the time required for displacement estimation but increased data processing time compared to other approaches.

According to Rashidi et al.in 2020, TLS has been mainly used for quality inspection of structural members to identify surface defects and the presence of water. For measuring point-wise aspects, Kwiatkowski et al.in 2020 used a combination of TLS and photogrammetric techniques on a historic suspension bridge and found that the accuracy of the measurements was influenced by the distance and complexity of the bridge, with TLS performing better than photogrammetry. Kermarrec et al.in 2020 Tested the B-spline surface method for approximating and filtering point clouds using TLS on a bridge under load and concluded that mathematical approximation was necessary for accurate computation.

2.4 Goals for Data Collection

Recent research has found a possible link between the top surface geometry of the deck and its degradation pattern and stage. Dr. Trias' investigation (Trias et al., 2021) comparing the geometric information recorded by LiDAR of the top surface of a bridge deck with its correspondent NDE data revealed clear indications of linkage. Figure 5, shows evidence of the relationship between the shape of the scanned deck and its degradation pattern, by presenting the elevation heat map generated from the point cloud data (on the left), and the results of the rebar cover derived from GRP data (on the right).
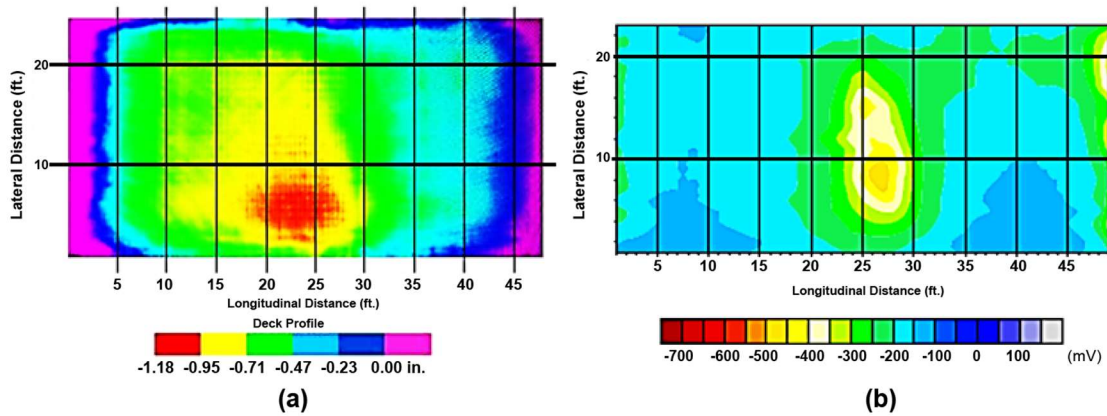
Figure 5. Half Cell Potential Vs. LiDAR. (a) LiDAR data of deck surface; (b) Half Cell Potential data of deck after deterioration. Source: Trias-Blanco, A. (2022).

Motivated by the evidence shown above and understanding: (1) the behavior of concrete bridge deck deterioration; (2) the state-of-the-art of NDE technologies; and (3) the need for rapid and qualitative data collection; this research seeks to introduce consistent evidence of the contribution that LiDAR sensors can provide to the existent suite of NDE technologies available for deck condition assessment. It is expected that LiDAR sensors can be used as screening tools to provide informative judgement in a timely manner.

2.5 Advantages and Limitation of Current Practices

Non-Destructive Evaluation (NDE) techniques are widely used for assessing the properties and characteristics of materials, components, and structures without causing any damage. When it comes to bridge deck inspection, these techniques offer several advantages.

One of the most significant benefits of NDE techniques for bridge deck inspection is safety. NDE methods do not require any invasive procedures, ensuring the safety of the

inspectors and the structural integrity of the bridge. Moreover, NDE techniques can detect small cracks, voids, or other defects in the bridge deck that might not be visible to the naked eye. This allows for early detection and repair of defects, ensuring the safety and longevity of the bridge.

NDE techniques are also cost-effective for bridge deck inspection. They can be performed quickly and efficiently, reducing the time and costs associated with bridge maintenance and repair. Additionally, NDE techniques are non-destructive, meaning that they do not cause any damage to the bridge deck or its components. This allows for multiple inspections without affecting the structural integrity of the bridge.

Furthermore, NDE techniques for bridge deck inspection are versatile. There are multiple techniques available, including visual inspection, ground-penetrating radar, infrared thermography, Impact Echo testing, and Electrical Resistivity inspection. This allows for a tailored approach to each inspection, maximizing accuracy and efficiency.

However, there are also some limitations to NDE techniques for bridge deck inspection. Some NDE techniques require the surface of the bridge deck to be cleaned and prepared before the inspection, which can be time-consuming and costly. Additionally, the accuracy and reliability of NDE techniques can depend heavily on the skills and experience of the operator. Some NDE techniques may not detect defects at a micro level, limiting their effectiveness in detecting certain types of defects. Moreover, certain NDE techniques may not be suitable for use in certain environments, such as extreme temperatures or high humidity.

Overall, NDE techniques offer significant advantages for bridge deck inspection, including safety, early defect detection, cost-effectiveness, and versatility. However, their effectiveness can be limited by factors such as surface preparation, operator dependence, limited sensitivity, and environmental limitations.

2.6 Advantages and Limitations of LiDAR Sensors

The most significant advantages of LiDAR devices over traditional non-contact sensors is that they do not require physical instrumentation or accessibility to structures. This feature saves time and labor costs, improves workplace safety, and makes LiDAR devices excellent field measurement tools.

Traditional non-contact sensors often require physical contact with the target surface or proximity to the surface to perform accurate measurements. This requirement can pose several challenges, such as the need for physical access to the target, which can be time-consuming and require additional resources. In contrast, LiDAR devices can be used from a distance, and they do not need physical contact with the target. This feature allows for quick and accurate measurements without the need for time-consuming and costly preparatory work.

Moreover, the use of LiDAR devices also improves workplace safety. Traditional non-contact sensors often require inspectors to access high or difficult-to-reach locations, posing potential safety hazards. In contrast, LiDAR devices can be operated from a safe distance, eliminating the need for inspectors to access these hazardous locations. Additionally, the non-contact nature of LiDAR measurements eliminates the risk of physical injury, making them an ideal tool for hazardous work environments.

Finally, LiDAR devices are excellent field measurement tools. The portable nature of these devices allows for quick and easy deployment to field sites, providing accurate measurements and high-resolution images of structures and environments. LiDAR devices are particularly useful for inspecting and monitoring large structures, such as bridges and buildings, where traditional measurement tools may not be practical or feasible (Kaartinen et al., 2022).

In summary, LiDAR devices have significant advantages over traditional non-contact sensors. They do not require physical instrumentation or accessibility to structures, improving workplace safety, saving time and labor costs, and making them excellent field measurement tools. These advantages make LiDAR devices ideal for a range of applications, from surveying and mapping to structural inspection and monitoring. However, while LiDAR devices offer several advantages for field measurements and inspections, there are also limitations to their use that SHM (Structural Health Monitoring) researchers have been working to overcome in recent years.

One of the primary limitations of LiDAR devices is their dependence on weather conditions. Poor weather conditions, such as rain, fog, or dust, can interfere with the accuracy of LiDAR measurements, limiting their effectiveness. Additionally, LiDAR devices can experience performance degradation with distance, resulting in reduced accuracy and increased costs (Dorafshan & Maguire, 2018).

Another limitation of LiDAR devices is the need to remove non-structural components using specific filters. This can be time-consuming and require additional resources to perform accurate measurements. Moreover, the capture of massive datasets by

LiDAR devices can require long computational processing times, limiting their usefulness in time-sensitive applications. Additionally, strategic positioning is necessary to avoid overlapping or targetless scans, which can be challenging in complex environments. Finally, the need for multiple scans at different points can require object extraction or interpolation techniques, further adding to the complexity of data processing (Chen et al., 2019).

Despite these limitations, SHM researchers have been working to overcome them and maximize the potential of LiDAR devices. For example, researchers are developing new filters to remove non-structural components more efficiently, and new data processing techniques to reduce computational processing times. Additionally, researchers are exploring the use of LiDAR devices in combination with other technologies to improve accuracy and reduce limitations.

In conclusion, while LiDAR devices have limitations, researchers are continuously working to overcome these limitations and improve the performance and accuracy of LiDAR devices in structural health monitoring and inspection applications.

Chapter 3

National Bridge Inventory Data Analysis

This chapter aims to satisfy Objective 1 by analyzing the National Bridge Inventory (NBI) database, which contains information on the condition, design, and construction of all bridges on public roads in the United States. In order to understand the deterioration pattern of New Jersey bridges, with a focus on steel girder structures, an analysis was conducted using the NBI data. The aim was to determine when a bridge deck would drop one level on the condition rating scale. Analyzing this data makes it possible to identify steel girder bridges' behavior and predict future deterioration rates. This information can be used to develop strategies to extend these bridges' service life and prioritize repair and maintenance efforts. The analysis results provide insights into New Jersey bridges' condition and the factors contributing to their deterioration.

3.1 NBI Deck Condition Rating

On a scale of 0 to 9, the National Bridge Inventory (NBI) evaluates the deck, superstructure, foundation, and culvert of all bridges in the USA. Condition ratings were explained in Table 1 (Chapter 1).

3.2 Deck Condition Rating for NJ

The information obtained from LTBP on Infobridge suggests that more than half of the bridge decks in New Jersey have a deck condition rating of Satisfactory (6) or less. This indicates that a significant portion of the bridge infrastructure in the state may be in need of repair or maintenance. The data from Figure 6 highlights the importance of regular

inspections and upkeep to ensure the safety and longevity of these critical transportation structures. It also underscores the need for investment in infrastructure to address the current state of disrepair and prevent further deterioration.

Figure 6. Bridge deck condition ratings for New Jersey from the LTBP website.

3.3 Bridges Main Construction Material

According to Figure 7 from the data obtained from LTBP, the majority of bridges in New Jersey are constructed using steel, representing 61.43% of all bridges. The next most commonly used material is prestressed concrete, which represents 26.85% of the

bridges. The remaining materials, such as concrete, timber, aluminum, and masonry, are used to a lesser extent, with each representing a smaller percentage of the total number of bridges in the state. It is evident from the data that steel and prestressed concrete are the two most commonly used materials for bridge construction in New Jersey.

Bridges Main Construction Materials and the Amount of Bridges Each Represents in New Jersey

	Steel	Prestressed Concrete	Concrete	Wood or Timber	Aluminum	other	Masonary
Bridges %	61.43%	26.85%	7.19%	4.02%	0.29%	0.12%	0.10%
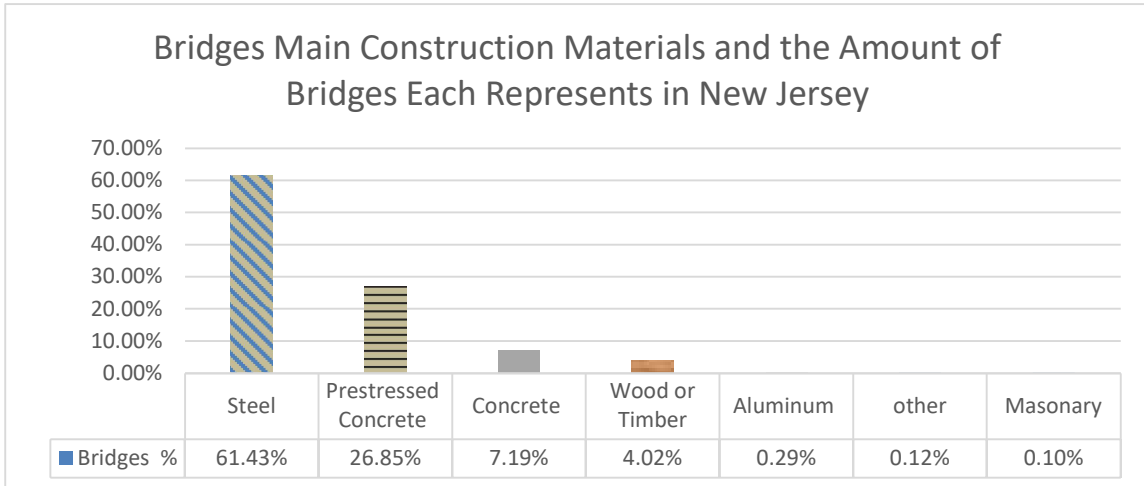
Figure 7. Bridges Main Construction Materials in New Jersey.

3.4 Long-Term Bridge Performance (LTBP) Data Analysis

Data analysis was performed to study the deterioration pattern for the 6801 bridge decks, started by studying the time in years it takes for each bridge to change in condition; through the study, it was found that a lot of the bridges had jumps in condition ratings either an upgrade or a downgrade. Some deck conditions upgraded from a rating of 0 to an eight as a one-step upgrade, and some deteriorated from a rating of 8 to a failed rating of 0, as well as a one-step downgrade.

As the study is interested in deterioration patterns, the first step of data cleaning and modification started with the upgrades in conditions, as it usually means the bridge deck was rehabilitated, reconstructed, or repaired, along with the deteriorations that ended up in a failed deck condition rating (0); as these values are primarily due to some unforeseeable disastrous conditions such as natural hazards and not due to usual deteriorating factors. Therefore, data containing these values were excluded and considered outliers for our research purposes.

Second, Data modification was done on the deterioration patterns, which showed degradation of more than one value in condition rating for it to be divided into seven one-grade drops in deck condition rating value. For example, from the data obtained, It can be seen that it takes an average of 4.558 Years for the deck condition rating of the studied bridges to degrade from a rating of 8 to a rating of 5; this interval was modified to represent the three steps' degradation from (8 to 7), (7 to 6) and (6 to 5) each having a value of 1.519 years (18.23 months), the same process was repeated for each value representing more than one value degrade in deck condition rating. Further studies were made based on the bridge's construction material; the data was also modified for each material, as done in the previous part, to find the deterioration pattern for bridge decks constructed on different materials; these studies can be summarized in Figure 8.

Different materials deterioration patterns

	Steel	Prestressed Concrete	Concrete	Wood or Timber	Aluminum	Other
9 TO 8	1.78	2.52	1.67	2.33	1.28	0.00
8 TO 7	1.64	2.71	2.38	1.56	6.25	3.49
7 TO 6	2.11	4.51	3.48	1.87	5.90	1.25
6 TO 5	2.12	4.35	3.34	1.73	4.62	3.00
5 TO 4	1.79	2.17	2.77	1.43	1.50	2.33
4 TO 3	1.69	1.94	5.48	1.48	1.00	1.00
3 TO 2	1.93	0.00	1.00	2.55	0.00	0.00
2 TO 1	0.60	0.00	0.00	1.82	0.00	0.00
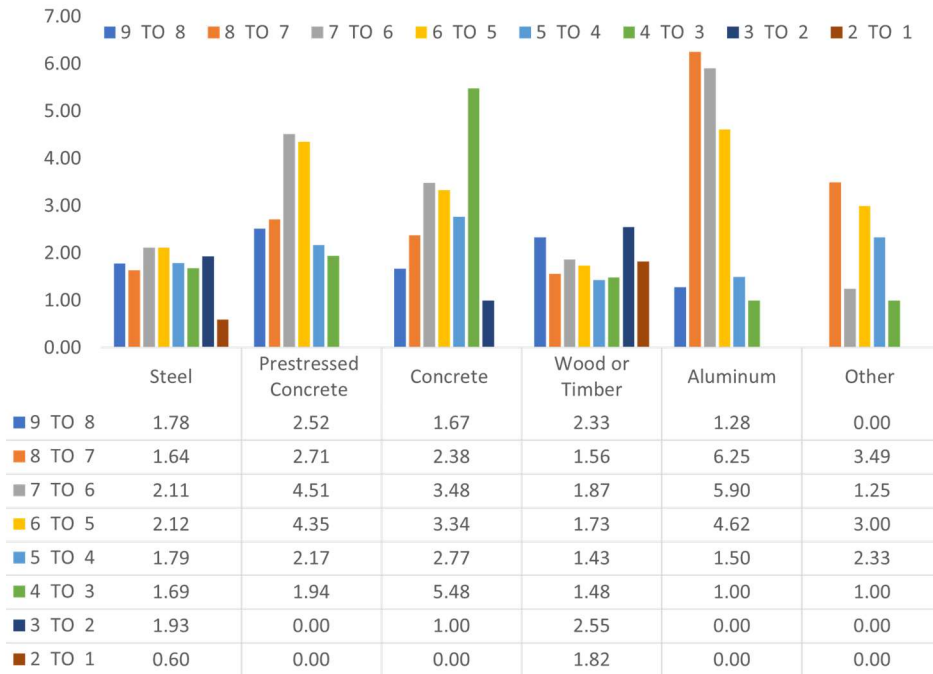
Figure 8. Detriment of Condition Rating Pattern for Different Bridge Main Construction Materials.

By the analyzed data of all materials, Steel showed a deterioration pattern closer to the average patterns for all different materials; On the other hand, Steel was the most representative material of the bridges in New Jersey, as it represents 61.43 %, while prestressed concrete scored second, representing 25.96 %. These two main bridge construction materials were the focus of the research as they represented 87.39 % of the bridges in NJ.

By analyzing the data from the 6801 bridges for the period (1983-2020), it shows that it takes 2.125 years (around 26 months) on average for any bridge to deteriorate one grade from its previous deck condition rating, while the inspection is being performed once

every two years, at first glance this inspection should be sufficient. However, by shifting the focus to be on the most representative bridges by main construction material, which would be steel in this case, it can be seen in Figure 9 that, on average, it only takes 1.45 years for the bridge deck condition rating to drop by one grade from its previous rating.
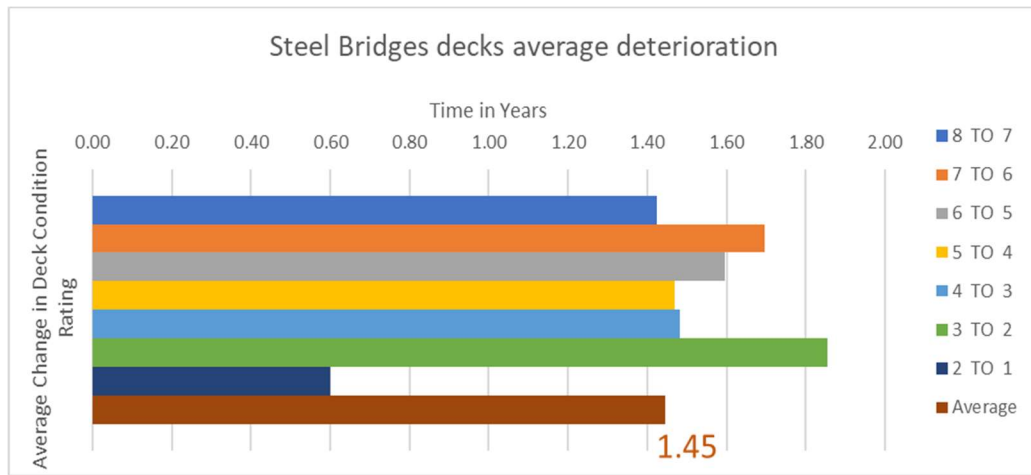
Figure 9. Change in deck condition rating for steel bridges.

Hence, implementing new reliable NDE technologies that can detect early signs of deterioration is essential to maintain the structural health of RC bridge decks preventing deterioration before occurring. After collecting, refining, and modifying the data, the next step was field research. The research team focused on eight bridges in New Jersey based on a request from NJDOT. The following section will talk about the methodology of the implemented NDE Technique and deploying TLS as a screening tool to prioritize detail deck inspection.

Chapter 4

Evaluation of Full-Scale Bridge Deck

Evaluating bridge deck deterioration is essential to bridge maintenance and repair operations. In recent years, LiDAR has emerged as a powerful tool for bridge deck evaluation due to its high precision and efficiency. This chapter satisfies the goals of Objective 2, by presenting a methodology for using LiDAR to evaluate the deterioration of a full-scale bridge deck. For this, a 50-feet long bridge specimen tested at Rutgers University's Bridge Evaluation And Structural Testing (BEAST) lab was chosen as testbed to perform a comparison between the NDE and point cloud data collected.

This BEATS test specimen consisted of four steel-rolled beams of W27x84, covering a total span of 47ft-11 ¼in. The four lines of diaphragms were composed of C15x33.9 sections. On top of the girders, a haunch that varied from 1 in deep at Abutment 1 (fixed end) to 3 in deep at Abutment 2 (expansion end), received the concrete deck, which had a total length of 50ft-1 ¼in and an out-to-out width of 27ft. Two curbs of 1ft-5 ¼ in wide by 6 in deep ran along the top outside edges of the deck leaving a curb-to-curb distance of 24ft-1 ½ in.

The BEAST specimen was subjected to continued deterioration imposed inside the lab's chamber, which included live load cycling, freeze-thaw, and brine water spray. Additionally, the deck, girders, and parapets were fully instrumented to record internal stresses, displacements, and changes in temperature. Figure 10, presents a point cloud of the BEAST lab with the bridge specimen on an elevation heat map. The NDE data collection was performed throughout the length of the test at different deterioration stages.

LiDAR data was collected: (a) during the construction of the bridge, recording the as-built dimensions, (b) during an intermediate deterioration stage, and (c) at the end of the first phase of the BEAST specimen project.
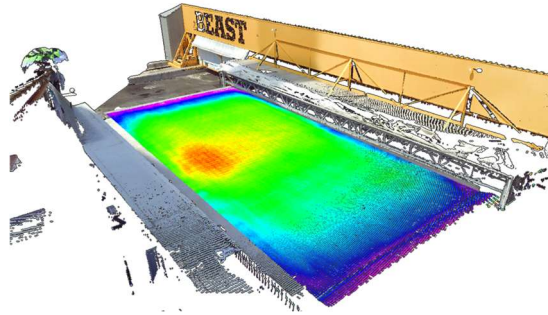
Figure 10. The BEAST Bridge Scanned Point Cloud.

The methodology for point cloud data collection, consisted of placing the scanner at four different locations surrounding the bridge specimen to capture the bridge deck surface. Then, the scans are registered through the scanner's software, Faro SCENE, by using targets (white spheres of 23 cm in diameter) placed at key locations during data collection. The registered point cloud data was processed and analyzed using software tools such as CloudCompare and Excel, through two different approaches that allowed to characterize the geometry of the deck: (1) Curvature Extraction and Slopes Analysis, and (2) Least Square Method Plane Fitting. The results analysis can be used to identify low points on the bridge deck surface where water can accumulate, which allows to plan maintenance and repair operations.

The tested bridge specimen is unique in its use of advanced materials, and Structural Health Monitoring technologies, making it significantly more robust and resilient than traditional bridges. This means that the bridge requires less maintenance over time, reducing overall costs and minimizing disruption to traffic flow.

In addition to its durability, the BEAST specimen is also designed with efficiency in mind. Its modular construction allows for quick and easy assembly, which could significantly reduce construction time and costs compared to traditional bridge-building methods. The bridge is also equipped with sensors that can detect changes in temperature, humidity, and other environmental factors, allowing engineers to monitor its performance and identify potential issues before they become significant problems.

This research utilized the information gathered from the BEAST specimen to validate the results gather from point cloud data captured via LiDAR. This comparison allowed to understand the correlation between internal element transformation and external symptoms of the bridge deck due to the continued deterioration. The development of clear correlation trends was possible given the amount of NDE data available at different deterioration stages for one single specimen. By comparing the LiDAR results with the inspection reports for the BEAST specimen, we demonstrated the data's accuracy and the potential for this approach as screening tool to potentially reduce the need for immediate costly repairs and minimize traffic disruption.

4.1 The BEAST Visual Inspection Reports

The inspection reports obtained for the BEAST showed that at the time of scanning, The Bridge had a rating of 5 for the Bridge Deck Condition Rating. This result

correlated to the damaged area, which had 35 square feet of spalls equal to or deeper than 1" or 6" in diameter. The images from the visual inspection report captured in July 2021 can be seen in Figure 11.

<p align="center">(a)   (b)</p>

Figure 11. Images from visual inspection reports of the BEAST (a) Small to large spalls (35 SF total) looking east (b) 25 SF large spalls looking south.

Moreover, a summary of the inspection report for the deck condition rating can be seen in Table 3. This table indicates, based on visual inspection, the amount of surface area damage. Where, the damage is indicated for each condition rating (e.g., spall >1").

Table 3

Bridge Deck (58) Visual Inspection Report From The BEAST Bridge Inspection Reports Indicating Damages

RATING	COMPONENT	REMARKS
5	Wearing Surface	(1/2" Integral wearing surface) One large area of moderate scaling near mid-span east half of the deck (180 SF). Some minor scaling at random locations (30 SF). Some pop-outs and insignificant cracking at random locations.
5	Top of Deck	Some deep spalls (>1"), mostly with exposed rebar near mid-span of the deck (35 SF total)
8	Underside of Deck	Bay 1: SIP forms with isolated rust along connection to the top flange of girder. Bays 2 & 3: Reinforced concrete with no significant defects

The BEAST has a 7.27 m x 15.27 m Deck forming a total area of 111 m^2 or 1195 square feet, and since the reports are showing damage of 35 square feet which represents a damage percentage of 2.93% which is very close to the result of 2.83 % obtained by analyzing the point cloud and based on these results a trend was developed to tie Bridge Deck Condition rating to the percentage of damaged points in the point cloud of the decks, more profound explanation of the developed trend will be demonstrated in Chapter 5.

4.2 BEAST NDE vs Point Cloud Data

A detailed analysis of the comparison of the NDE data collected from the BEAST versus the point cloud data captured via LiDAR was performed to correlate the internal damage detected from the non-destructive evaluation technologies, and the external changes in geometry on the top surface of the bridge deck. Table 4, present a summary of

the results gathered from the test performed including, half-cell potential, ground penetrating radar, electrical resistivity, ultrasonic wave, impact echo, and point cloud captured via LiDAR.

Table 4

NDE and Point Cloud Data Collected From the BEAST Specimen
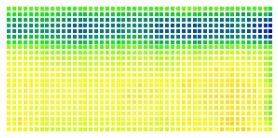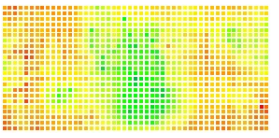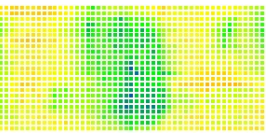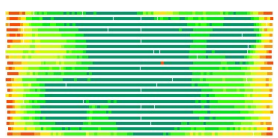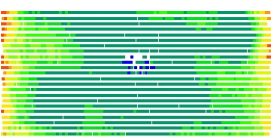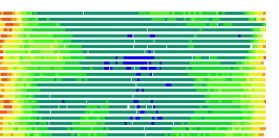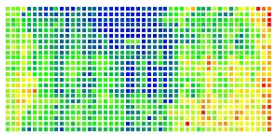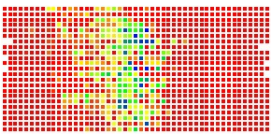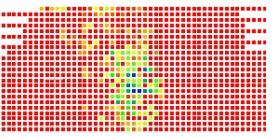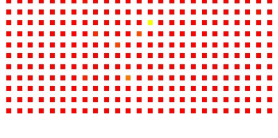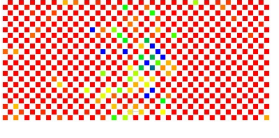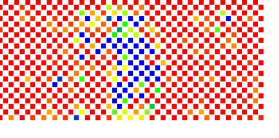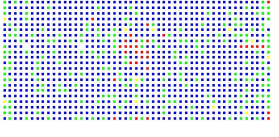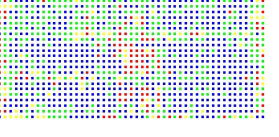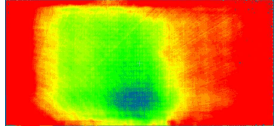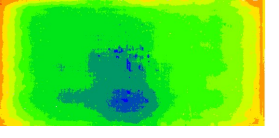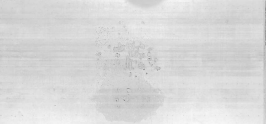
NDE	2019 – 07 – 30 (construction)	2021 – 02 – 24	2021 – 07 – 21	Scale & Units
HCP				135.0 -620.0 (mV)
GPR (top cover)				7.6 3.8 0.0 (cm)
ER				5.0 1.1 (KΩ.cm)
USW				4500 3000 (ksi)
IE				4 1 (index)
LiDAR (elevation)		Not available		0 3.5 -4.5 (cm)
Deck's Image		Not available		NA

Table 4, indicates that the point cloud data was the only NDE capable of detecting

the geometry of the bridge deck from the first set of scans. GPR data correlates to the point

cloud data, as it indicates a shallow top cover for the reinforcing steel, but this data is not a direct indication of the depression at midspan as it could indicate an issue with the rebars instead, leaving point cloud data as the only clear evidence of the local anomaly.

The NDE data collected on February 24th 2021 and July 21st 2021, clearly evidenced deterioration in the bridge deck, which originated around midspan as predicted given the depression of the bridge deck detected by LiDAR scanning.

4.3 Curvature and Slope Analysis Approach on BEAST Specimen

This project evaluated the presence of various aspects using the point cloud data collected for each bridge deck. These aspects include: (a) Rutting percentage: expressed as a percentage of the deck's total area and indicate the extent of rutting; (b) Percentage of overall potholes: expressed as a percentage of the deck's total area and indicate the extent of potholes; (c) Section loss at joint locations: expressed as a percentage of the deck's area and indicate the amount of section loss at the joints; (d) Longitudinal curvature: each deck will be analyzed to determine whether there is a correlation between low points in the deck and the condition stage; (e) Transverse curvature: the transverse slope will be compared to the evaluate the presence of the recommended 2% slope on the bridge decks and ensure proper water drainage. The following figures (Figure 12, Figure 13, and Figure 14) show the location where the longitudinal and transverse cross sections were taken from the BEAST bridge deck. This approach was taken to better visualize the curvature of the deck, which was first explored and analyzed through the elevation heat map presented in Figure 12.
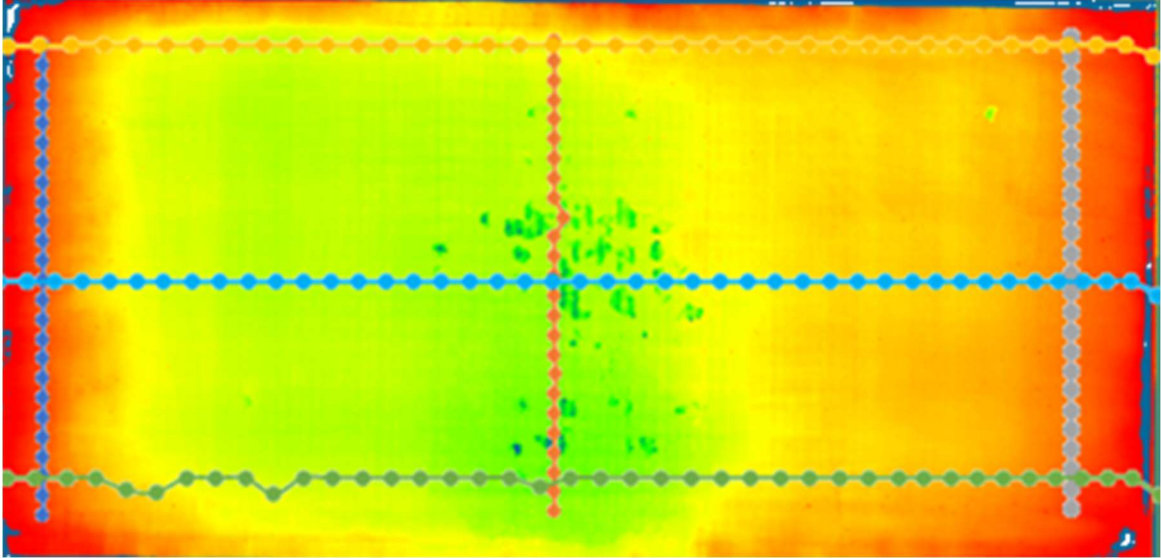
Figure 12. Location of transverse and longitudinal cross-sections.
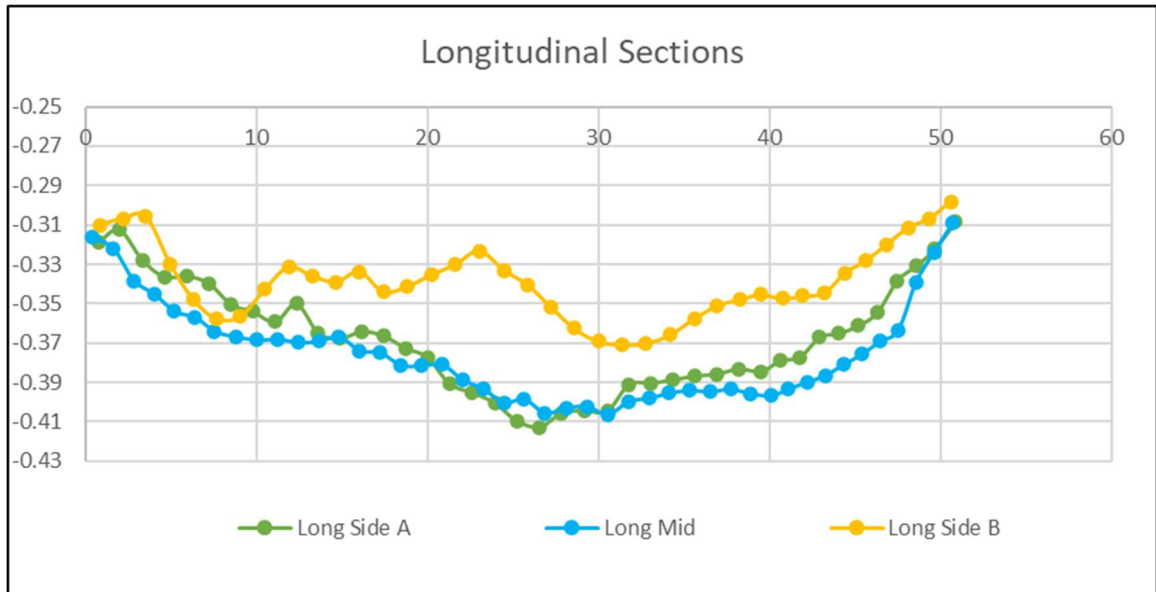
Figure 13. BEAST Deck - Longitudinal sections.
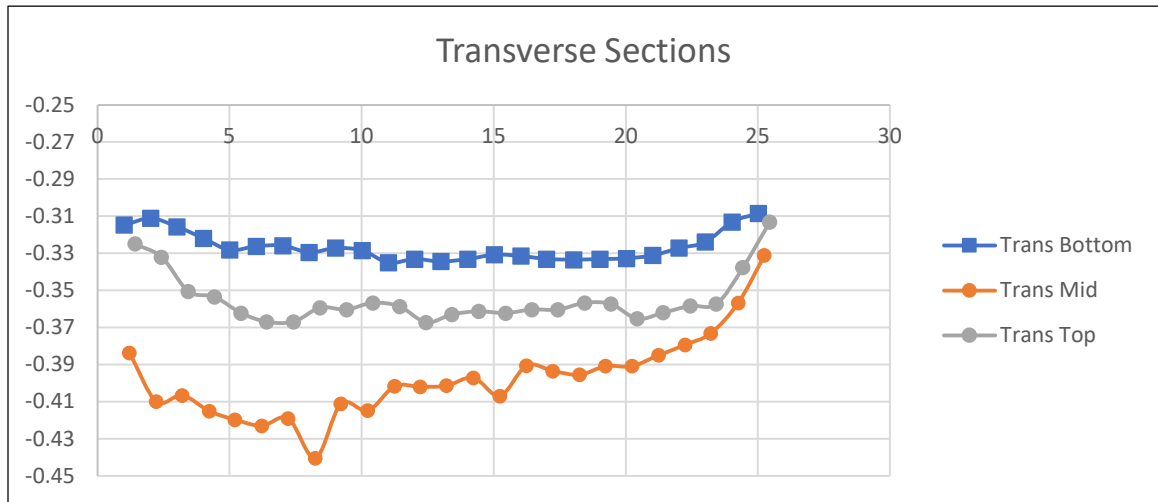
Figure 14. BEAST Deck Transverse sections.

4.4 Least Square Method Plane Fitting on BEAST Specimen

After performing the analysis of curvature and slope of the BEST deck, where multiple cross-sections were evaluated, a second data analysis approach was taken to better characterize the damage found. For this, horizontal projections and planes fitting was completed showing areas of interest where distances from the fitted planes were -36 mm (-1.4") below the fitted planes, indicating a accentuated depression. Figure 15, presents an elevation heat map of the deteriorated bridge deck (data collection date: 10 Oct., 2022), where is clear that potholes where already developing on the surface of the deck. Once this potential damaged area was isolated, the points below -6 mm (-0.24")were highlighted and classified as actual damage. This criterion is based on the assumption that the surface roughness of a concrete bridge deck is 0.003 to 0.005 (0.16"), then a surface irregularity of 0.006 m would represent approximately two times the roughness. Figure 16, presents a

closer look to the area of study, where the figure on the top (a), encloses the area that was selected to perform the percent damage evaluation, and the image on the bottom (c), is the points that correspond to the points classified as actual damage.

(a)

(b)
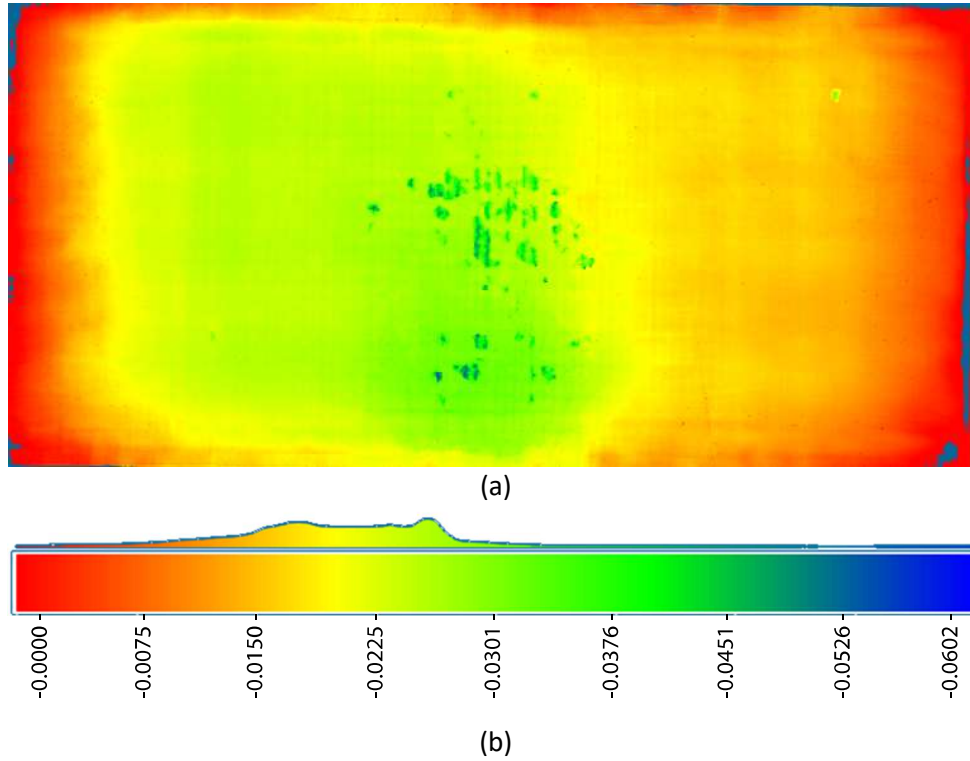
Figure 15. Heat Map of The BEAST Bridge Deck: (a) Plan view of deck's heat map by elevation; (b) Elevation scale from 0.00 to -0.06 in.
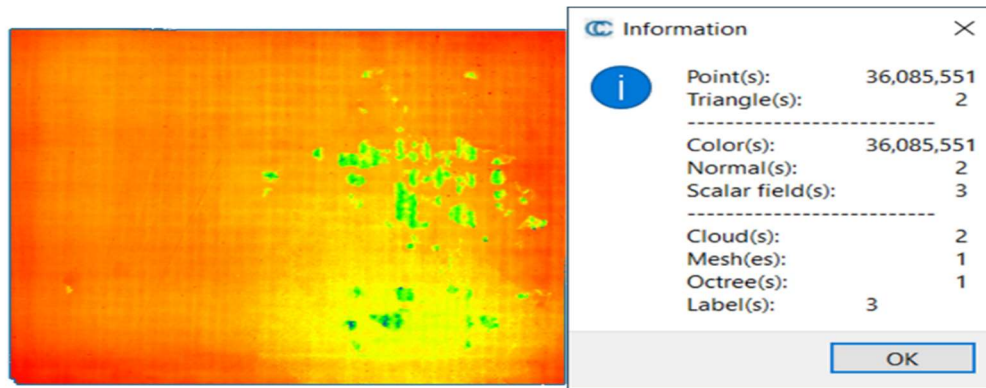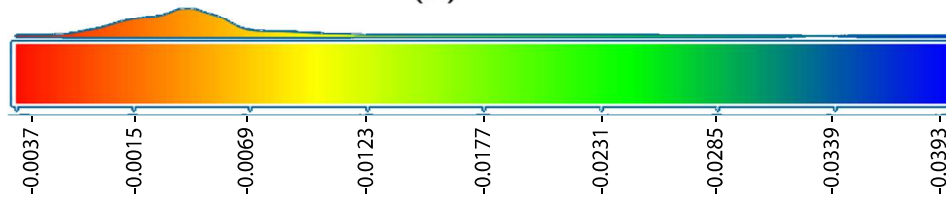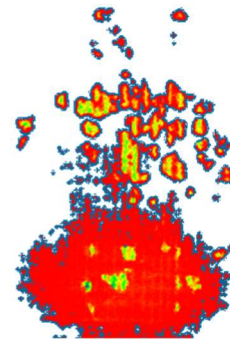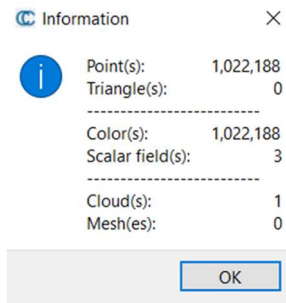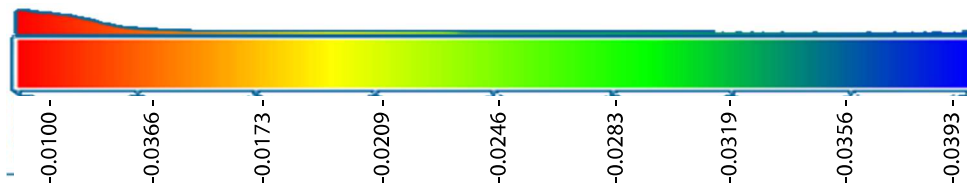
Figure 16. Analysis of The BEAST Bridge Deck

(a) area of interest as it was a dipped surface and a fitted plane to that area along with the total number of points in the beast bridge deck (b) Elevation scale showing Elevations from 3.8 to - 39.5 mm (c) Isolated damaged points along with the number of points in the isolated cloud that represent damage, (d) Elevation scale showing elevations from -10 to -39.3 mm

The BEAST analysis was conducted on a specific area of the bridge deck that was identified as an area of interest due to its progressive damage and slight deflection indicated in previous scans. The analysis was focused on matching the damage location from the Visual inspection reports, which indicated 35 SF of damage on the top of the deck of spalls > 1" deep or > 6" in diameter.

The results of the point cloud analysis showed a total of 1,022,188 points identified as damaged points out of the 36,085,551 points in the full bridge deck point cloud. This indicates that the damage represents 2.83% of the total area of the bridge deck, which is equivalent to 1195 SF. The damaged area was found to be equal to 33.85 SF, which is a 96% accuracy level compared to the 35 SF documented in the visual inspection reports. These results suggest that the BEAST analysis is a reliable method for identifying and quantifying damage on bridge decks.

The table presented with the results is an important tool for visualizing and summarizing the data obtained from the BEAST analysis. The table shows the number of points identified as damaged, the percentage of damage, and the damaged area of the bridge deck. This allows for a more detailed and localized analysis of the damage, which can aid in prioritizing repair and maintenance efforts.

In conclusion, the BEAST analysis proved to be an effective method for identifying and quantifying damage on bridge decks. The results obtained were highly accurate and matched the damage locations documented in the visual inspection reports.

Table 5, summarizes the results found from performing Least Square Plane Fitting Method, showing The BEAST's information and the damage percentage analysis result.

Table 5

Damaged Points Analysis Results for The BEAST's Specimen

Bridge #	County	ADT	ADTT	Deck Condition	Damage Percentage
0821155	Middlesex	15000	0	5	2.83%

The results of comparing the damage detected by the LiDAR at a similar time to the inspection report show a compelling pattern of deterioration. These findings are displayed in a clear and concise manner in Figure 17. This comparison highlights the efficacy of the LiDAR technology in detecting and monitoring damage over time, and demonstrates its potential as a valuable tool in infrastructure maintenance and management.
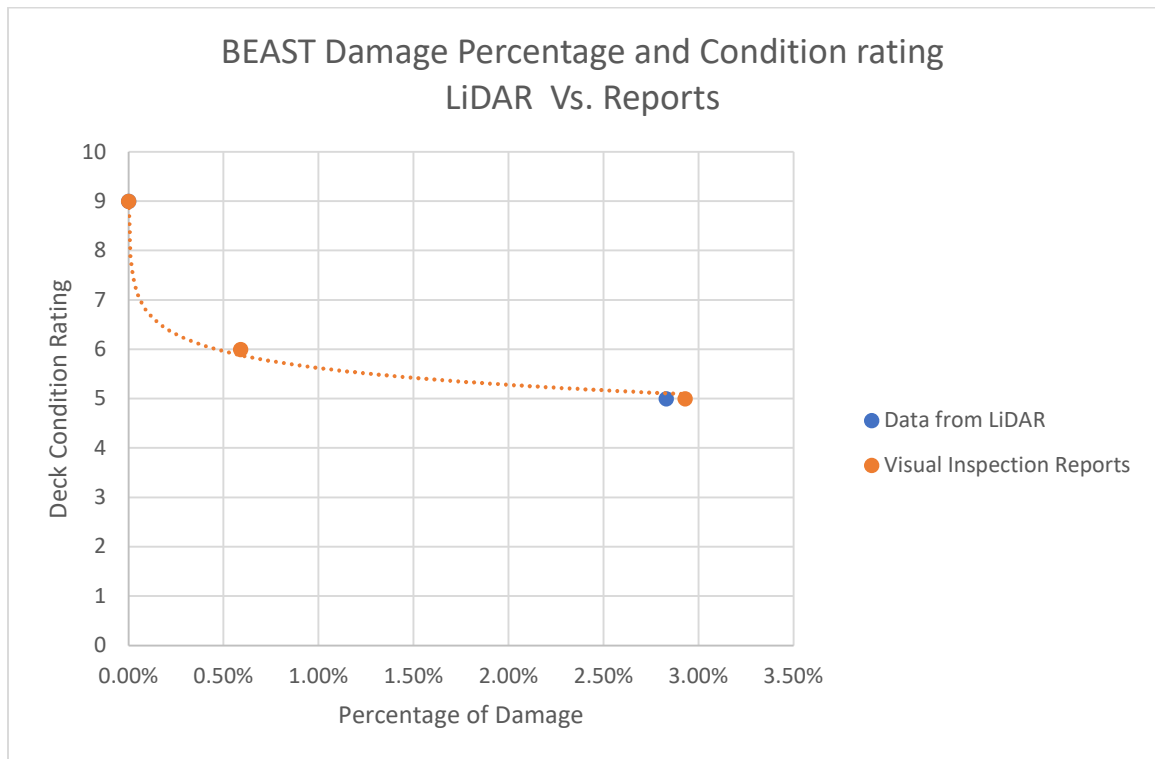
Figure 17. BEAST Damage Percentage and Condition rating LiDAR Vs. Reports

Chapter 5

Evaluation of Operating Bridges in New Jersey

Based on the information gained from studying the NDE and LiDAR data captured from the full-scale bridge deck, this chapter presents the evaluation of 14 operating bridges in New Jersey and the analysis of The BEAST bridge specimen. LiDAR was deployed during operating conditions, allowing the point cloud data to capture the undisturbed condition of the decks.

5.1 Field Research – Selected Structures

For our research on the deterioration pattern of New Jersey bridges, a total of 8 were initially selected by New Jersey's Department of Transportation (NJDOT) from 7 counties in the state. Additionally, after the preliminary research, another eight bridges were scanned to expand the analysis, which was carefully chosen by the research team. Locations of the chosen bridges can be seen in *Figure 18*, and an aerial view with a brief description of each structure can be seen in Figure 19.
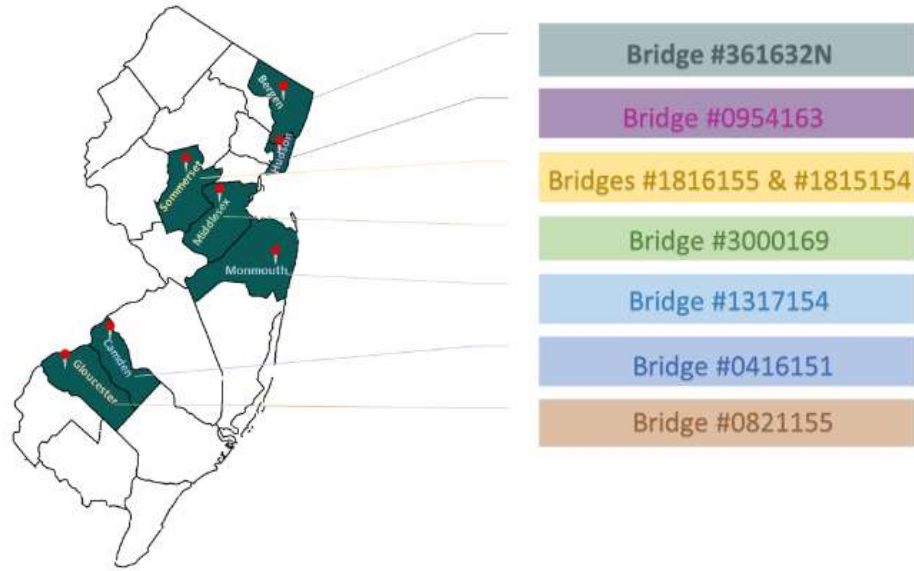
Figure 18. Locations of the selected bridges.
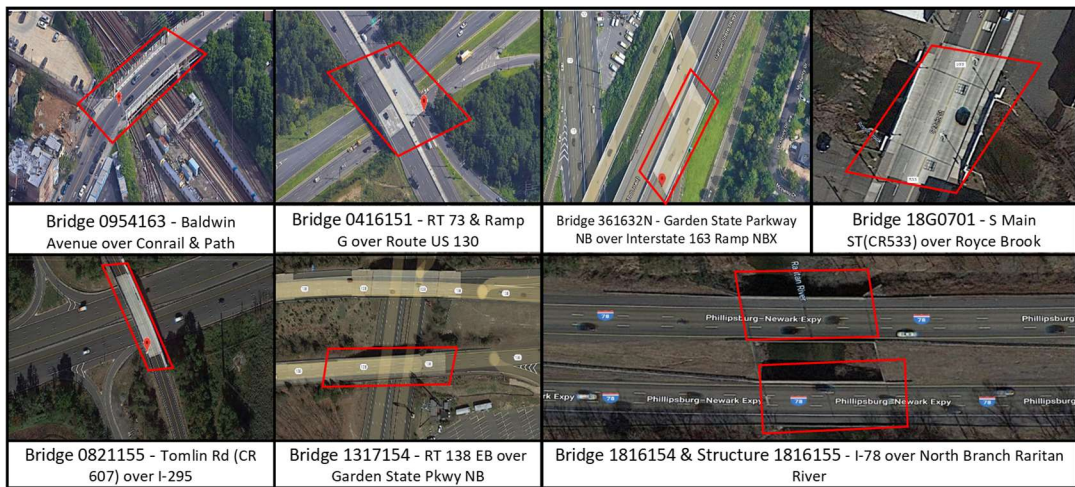
Figure 19. Description of the selected structures.

5.2 Bridge Decks Scanning

The researchers utilized a Faro Focus terrestrial laser scanner to gather information on the bridge decks. They visited each bridge and determined the scanner's position and scans based on its characteristics, such as span length, curb-to-curb dimension, obstructions, and traffic flow during scanning. The scanner was placed on the side of the road (shoulder or sidewalk) to prevent traffic disturbances, as depicted in *Figure 20*.

Figure 20. Typical location of scanner: (a) Scanner located on deck's shoulder; (b) Scanner located on the sidewalk.

Two (2) to three (3) scans at minimum were taken from different locations on the shoulder to ensure the whole deck's geometry was captured with at least 30 % overlap between scans for the most accurate results.

The evaluation of the scanner settings was not considered in the analysis. Due to the size of the object scanned and the overlapping of multiple scans, fixed settings for the scanner's resolution were used. For this project, a resolution of 1/3 was used, resulting in

an angular distance between points of 0.027 degrees. This resolution produced a data point distance of 0.05 ft at a range of 10 ft from the scanner. To obtain a colored point cloud, some scans were taken while collecting real-time photos.

5.3 Scans Processing

The process used to transform individual scans into a combined point cloud and disseminate the data for each bridge deck in this project is a multi-step procedure using three software: Faro Scene, CloudCompare, and Microsoft Excel. A typical processed point cloud data resulting from the registration using Faro Scene is shown in Figure 17, which also shows the location of every single scan that was performed to capture the entire top surface of the bridge deck. The captured scans were imported to the Scene software provided by Faro Company. The goals and application determined the point cloud processing method chosen. This process compares the scans based on their plan view and cloud-to-cloud distance, and Scene provides feedback on the accuracy of the registration.

To increase the precision of the registration, it is recommended to pre-process each scan by removing potential noise and unnecessary points that can affect the final registration. The goal of point cloud processing methods in bridge engineering is to recognize structural features in the point cloud and then apply the algorithm that best meets the project demands (e.g., geometry capturing, condition assessment, structural evaluation) (Trias-Blanco, A., (2020).). An example of one set of registered point cloud containing a bridge deck analyzed in this research is shown in *Figure 21*.
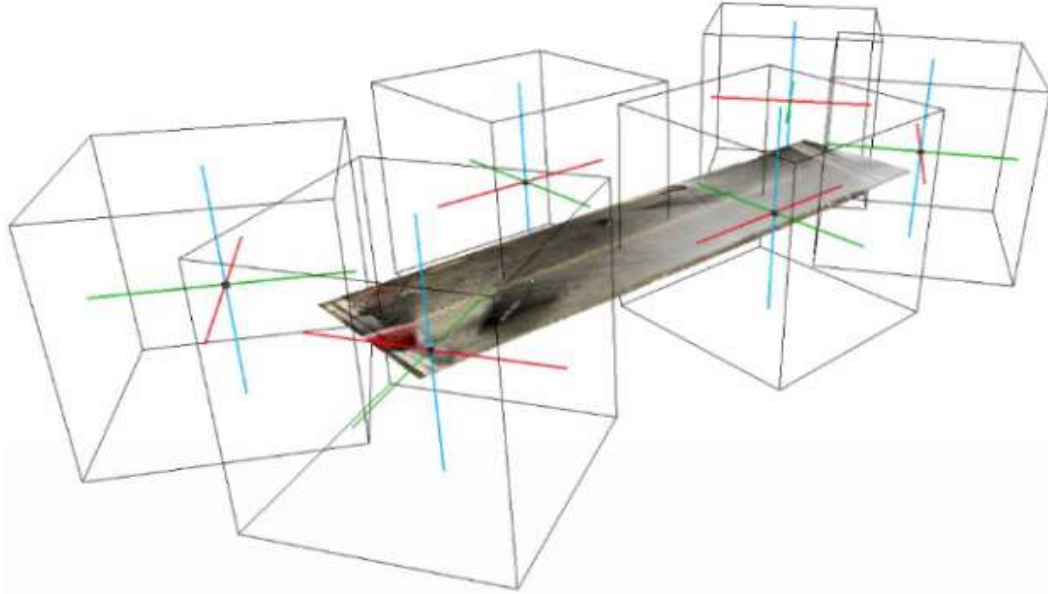
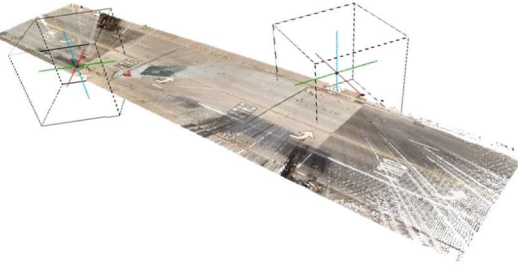*Figure 21*. Processed point cloud of a bridge deck.
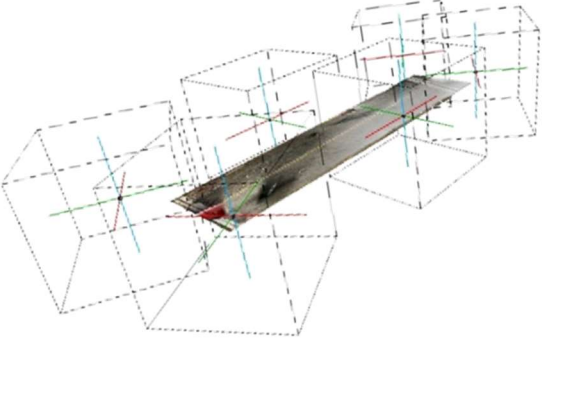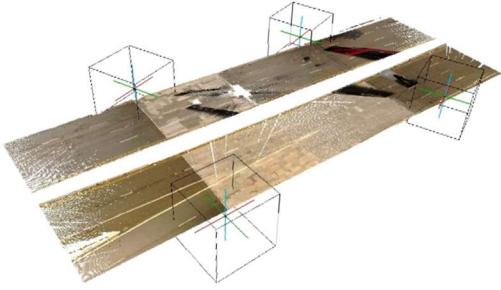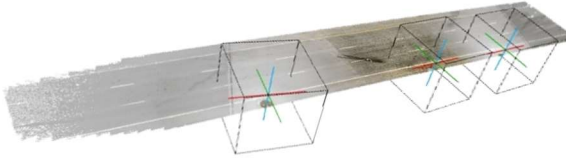
TLS can get accurate location information from GNSS receivers and target point clouds simultaneously; this information can then be used to integrate the various point clouds directly. (Rönnholm, P., and H. Haggrén. (2012)). In this procedure, extracting feature points is crucial, and the extraction outcome directly impacts point cloud registration accuracy. Artificial items are frequently more mathematically regular than natural surroundings and objects, and their geometric feature information is also relatively accurate. (Cheng, Liang, et al. (2018).
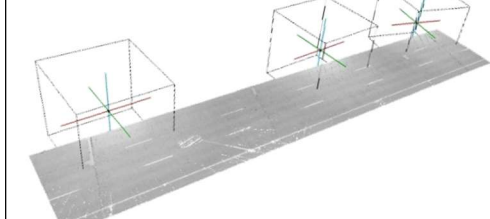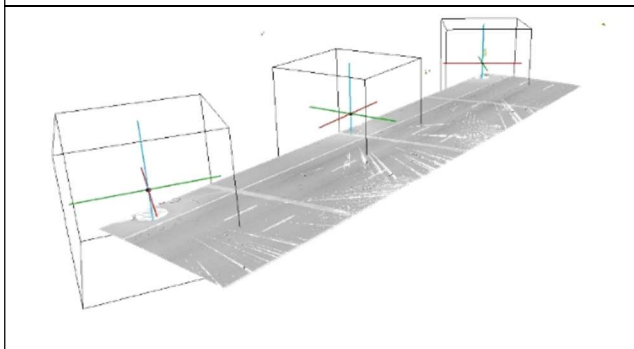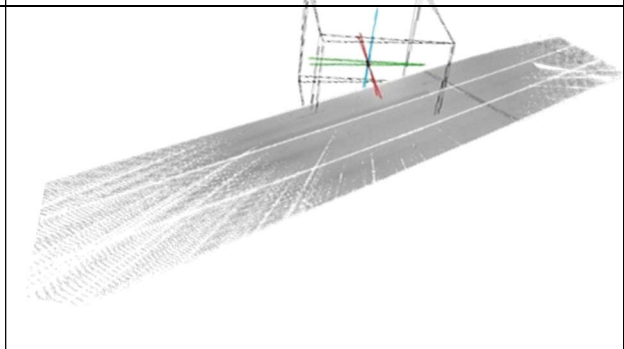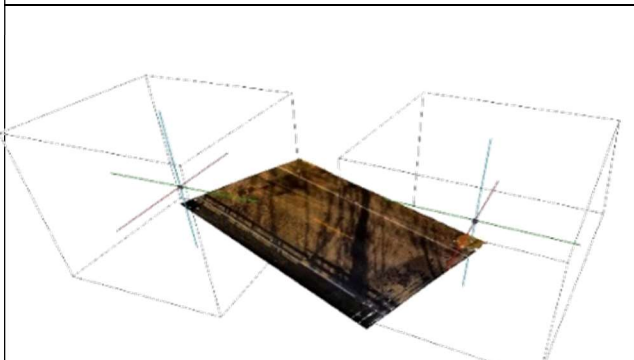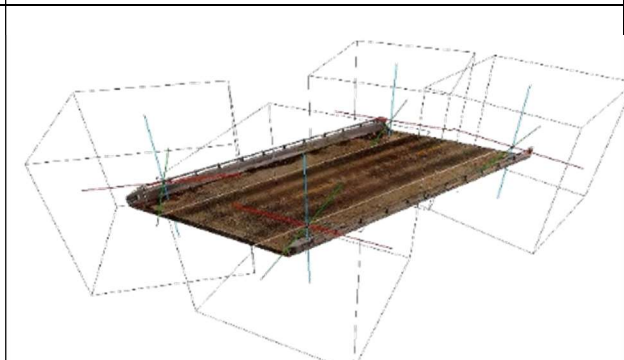
5.4 Registered Bridge Decks Scans

The following table (Table 6) presents a description of the bridges chosen for this research. The description of all structures: number, year built, year of reconstruction (if any) span length, cur-to-curb length, total area, and condition rating with its correspondent year.
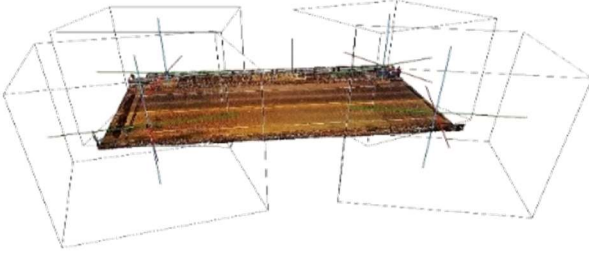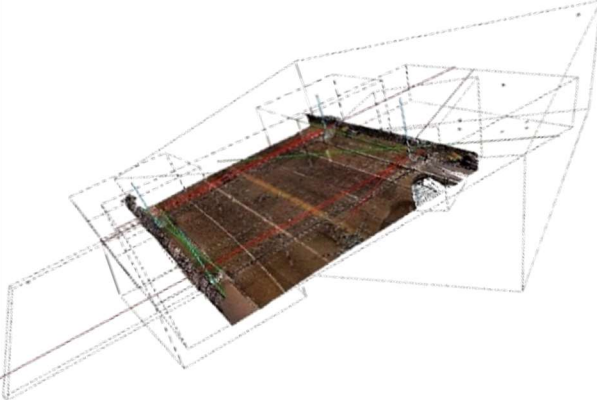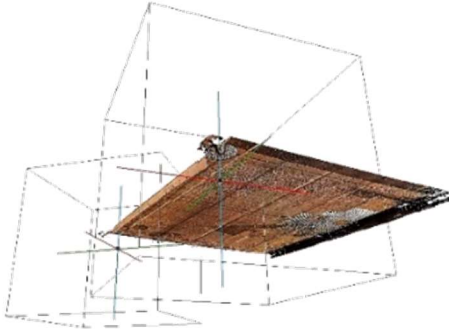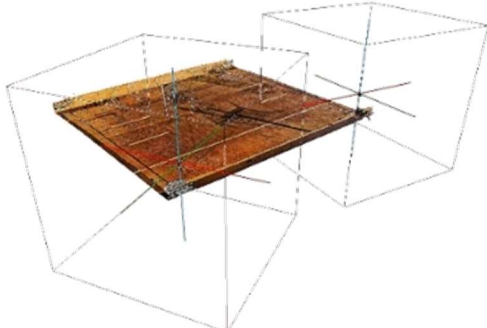
Table 6

Array of Bridges Chosen for This Research

Structure 0954163, built in 1928, Deck reconstructed 1990, Total length of 166 ft, curb-to-curb width of 32.2 ft, total deck area is 5609.9 sq. ft. deck condition rating for the year 2022the is 4 (Poor)	Structure 0416151, built in 1930 The total length of 148 ft, with a curb-to-curb width of 100.4 ft, total area of the deck is 19903.5 sq. ft deck condition rating for the year 2022 is 4 (Poor).
Structure 361632N, built in 2016. The total length is 210 ft, a curb-to-curb width of 58.1 ft, Total area of the deck area is 12951 sq. ft with a skew angle of 22°. The deck condition rating for 2022 is 8 (Very good).	Structure 18G0701, built in 2019. The total length of 75.1 ft, with a curb-to-curb width of 46.3. The total deck area is 4905. 2 sq. ft. with a skew angle of 9°. The deck condition rating for the year 2022 is 9 (Excellent).

Structure 0821155, built in 1953. The total length is 159.1 ft, with a curb-to-curb width of 29.9 ft Total area of the deck area is 6525. 6 sq. ft with a skew angle of 15°. The deck condition rating for the year 2022 is 9 (Excellent).	Structure 1317154, built in 1974. The total length of 194.9 ft, with a curb-to-curb width of 42.3 ft. The total area of the deck is 9910.3 sq. ft with a skew angle of 13°. The deck condition rating for the ear 2022 is 7 (Good).
Structure 1816154, built in 1965. The total length is 112.9 ft, with a curb-to-curb width of 50.9The total deck area is 6331.8 sq. ft. with a skew angle of 11°. The deck condition rating for the year 2022 is 6 (Satisfactory)	Structures 1816155, built in 1965. The total length is 112.9 ft, and the curb-to-curb width is ft. The total area of the deck is 6331.8 sq. ft. with a skew angle of 11°. The deck condition rating for the year 2022 is 3 (serious).
Structure 0805F03, built in 1997. The total length is 55.1 ft, and the curb-to-curb width is 34.1 ft. The total area of the deck is 2079.8 sq. ft. The deck condition rating for the year 2022 is 7 (Good).	Structure 0807P01, built in 2010. The total length is 77.1 ft, and the curb-to-curb width is 37.4 ft. The total deck area is 3136.6 sq. f twith a skew angle of 29°. The deck condition rating for the year 2022 is 7(Good).

Structure 0809Q03, built in 1997. The total length is 71.9 ft, and the curb-to-curb width is 40 ft. The total area of the deck is 3182.3 sq. ft. The deck condition rating for the year 2022 is 6 (Satisfactory)	Structure 0833150, built in 2005. The total length is 64 ft, with a curb-to-curb width of 66.9The total area of the deck is 5415. The deck condition rating them for the year 2022 is 7 (Good)
Structure 0411163, built in 1956. The total length is 56.1 ft, and the curb-to-curb width is 50.9 ft. The total area of the deck is 3313.1 sq. ft. The deck condition rating for the year 2022 is 5 (Satisfactory)	Structure 0411163, built in 1956. The total length is 56.1 ft, and the curb-to-curb width is 50.9 ft. The total area of the deck is 3313.1 sq. ft. The deck condition rating for the year 2022 is 8 (Very Good)

5.5 First Approach: Curvature Extraction and Slopes Analysis

Cross sections along the transverse and longitudinal directions were generated by creating slices of the point cloud of the deck. *Figure 22*, represents an RGB image of a sample of the bridge decks used in our research structure number 18G0701.

Figure 22. RGB Of Structure 18G0701.

One-Foot-Wide longitudinal cross sections were taken along the Bridge Deck on either side and the middle span. As can be seen in Figure 23 (a). The process was repeated for transverse sections, where 1'-wide strips were taken at both supports and at the middle span, a reference location of the strips can be seen in Figure 23 (b), and Figure 23 (c).
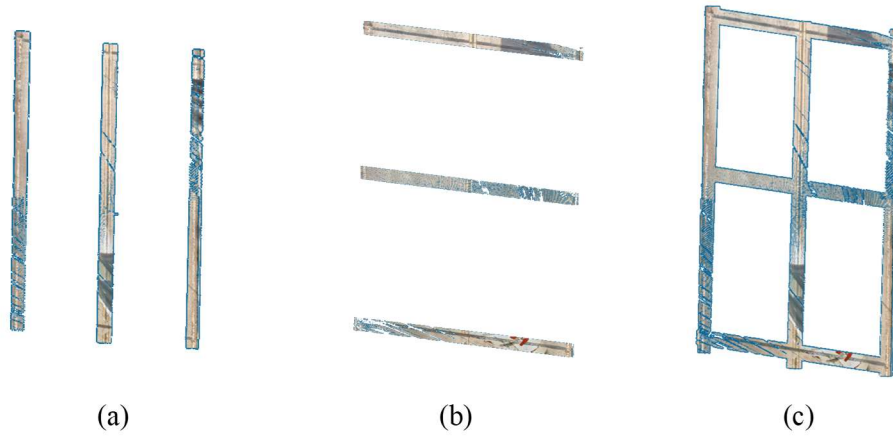
(a)   (b)   (c)

Figure 23. Sections of bridge 18G0701: (a) Location of longitudinal cross-sections; (b) Location of transverse cross-sections; (c) Location of both longitudinal and transverse sections.

The next step was to select points one foot apart along the cross sections to study the variation of coordinates (X, Y, Z) between points. This process was done manually through the point-picking tool in Cloud Compare as can be seen in Figure 24.
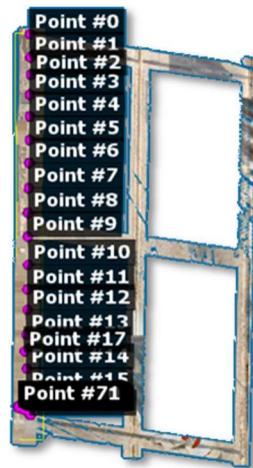

Figure 24. A visualization of selected points along the cross-section.

These points were chosen on all sections, and then points were exported to a text file and analyzed using Excell The following results were obtained, and these results can be found in the report submitted to NJDOT (CAIT-UTC-REG52)

5.6 First Approach Results

5.6.1 Bridge 18G0701

Figure 25. RGB of Structure 18G0701/

Structure 18G0701 has a recently reconstructed Deck. Based on the visuals provided in Figure 26, Figure 28 and Figure 29, it has been constructed with appropriate slopes to facilitate drainage in both the longitudinal and transverse directions. However, it should be noted that there are a few depressions or low points on the deck, as can be observed in Figure 28 that shows Longitudinal sections and Figure 29 for Transverse sections, which could pose potential problems in the future.

Figure *27* displays a blueprint of the deck, indicating the locations of the longitudinal and transverse sections. Additionally, Figure 25 provides a colored view of the top surface of the deck. And

Figure 26. Structure 18G0701 Elevation heatmap.
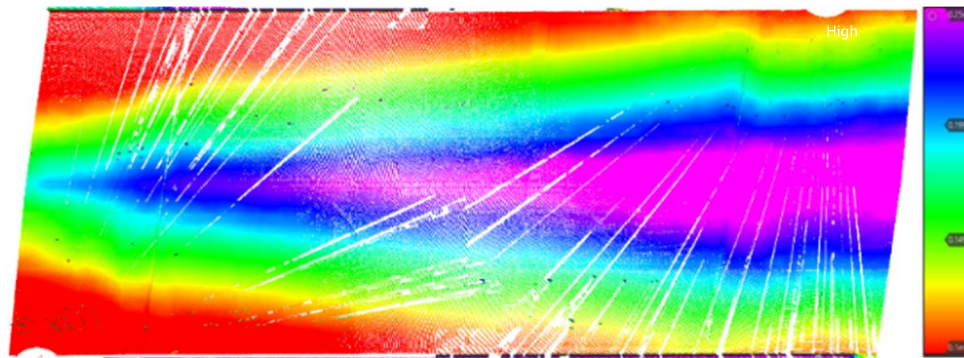
depicts a Heat map of the Bridge Deck.

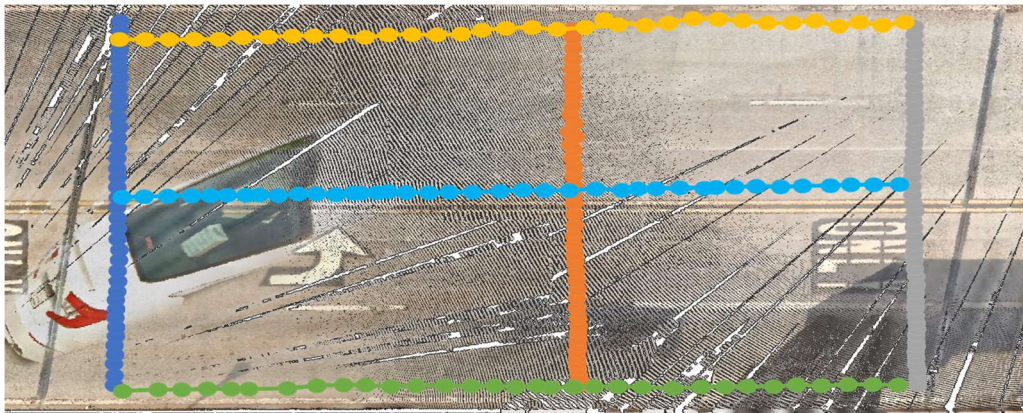*Figure 26*. Structure 18G0701 Elevation heatmap.

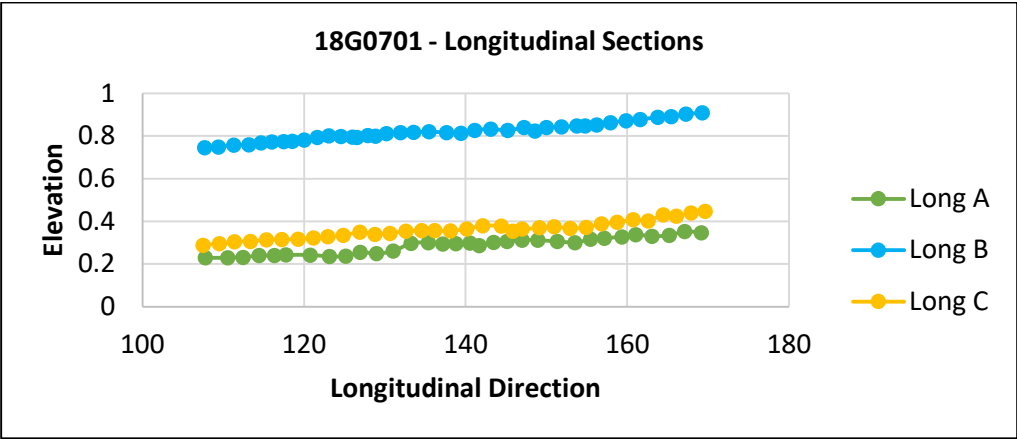*Figure 27*. Approximate Cross Sections Locations on the Deck Surface

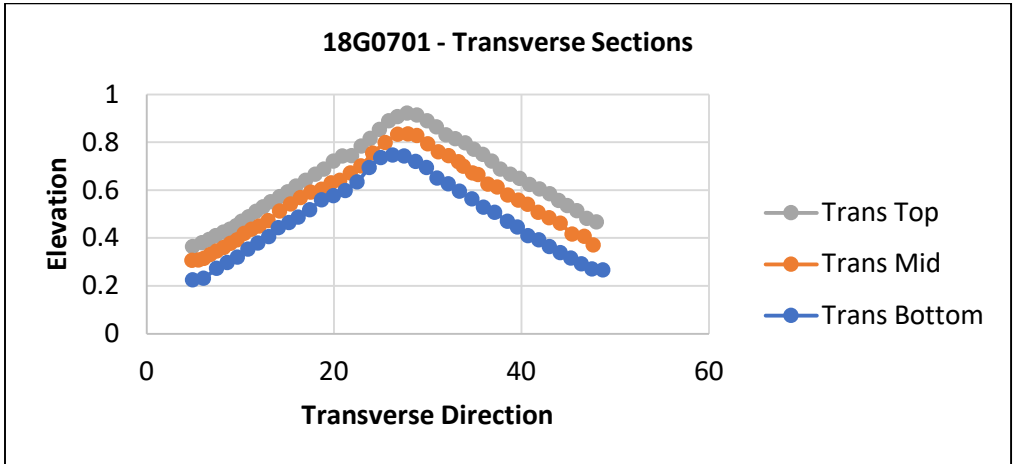*Figure 28.* 18G0701 - Longitudinal Sections

Figure 29. 18G0701 - Transverse Sections

5.6.2 Bridge 0954163

Figure 30. RGB of Structure 0954163

The longitudinal cross-sections produced for this structure illustrate multiple areas with depressions, as displayed in Figure 32. These low points are prone to accumulating water for extended periods, speeding up the reinforcing steel's deterioration. Furthermore, the longitudinal slope was approximately 0.5%, which hinders water drainage, based on Figure 32. The transverse cross-section slope ranges from 0 to 0.8%, falling below the recommended 2% as seen in Figure 33. Figure 31 presents a plan view that pinpoints the placement of the longitudinal and transverse sections within the deck.
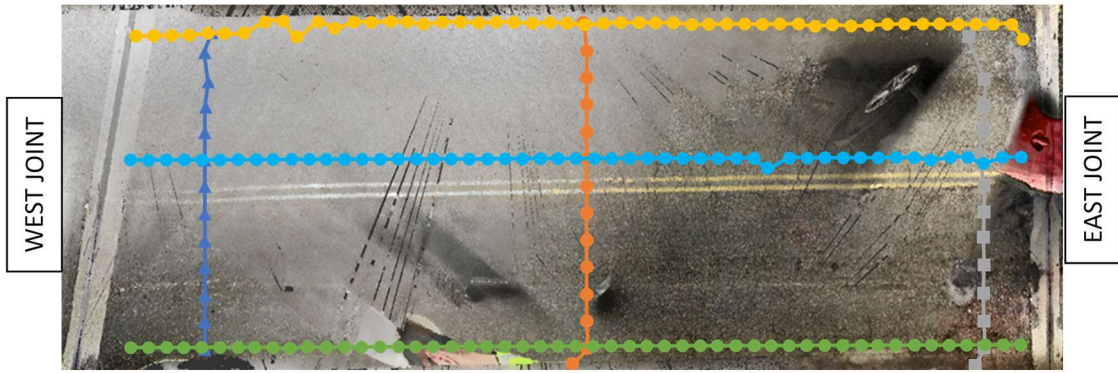
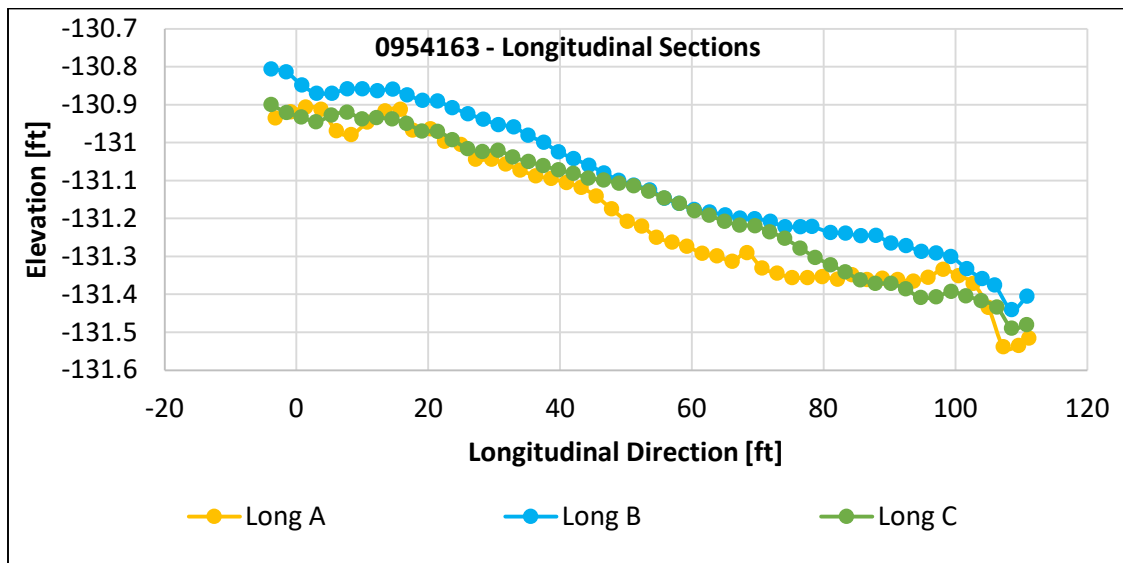*Figure 31*. Approximate Cross Sections Locations on the Deck Surface

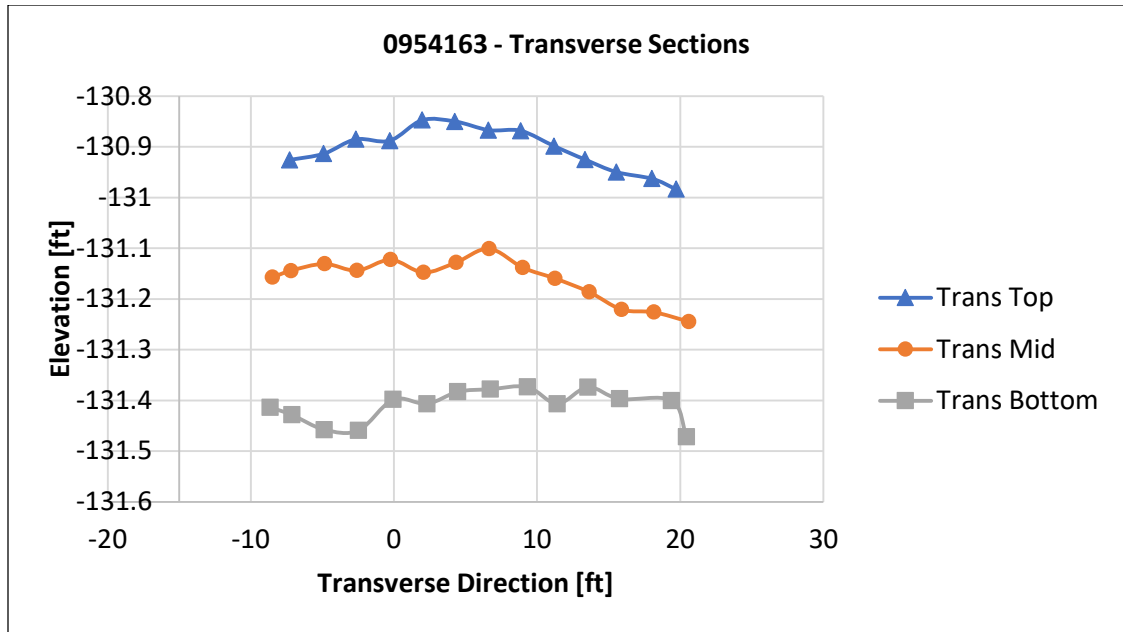*Figure 32*. 0954163 - Longitudinal Sections

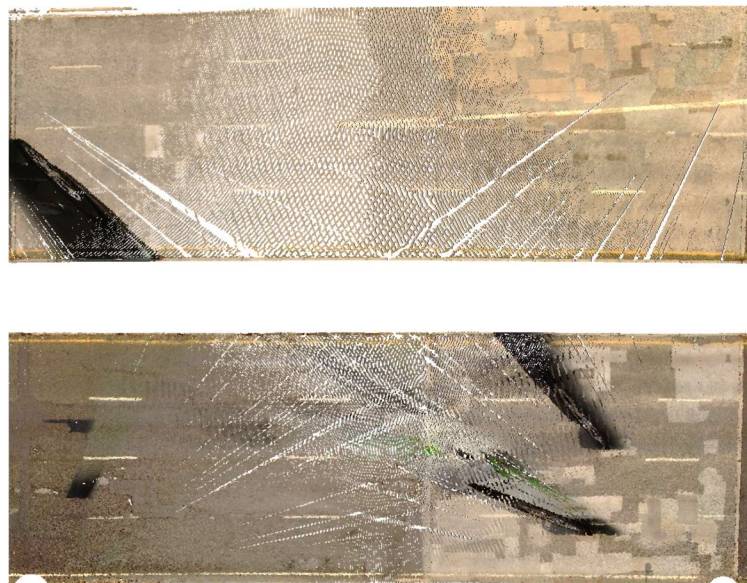*Figure 33*. 0954163 - Transverse Sections
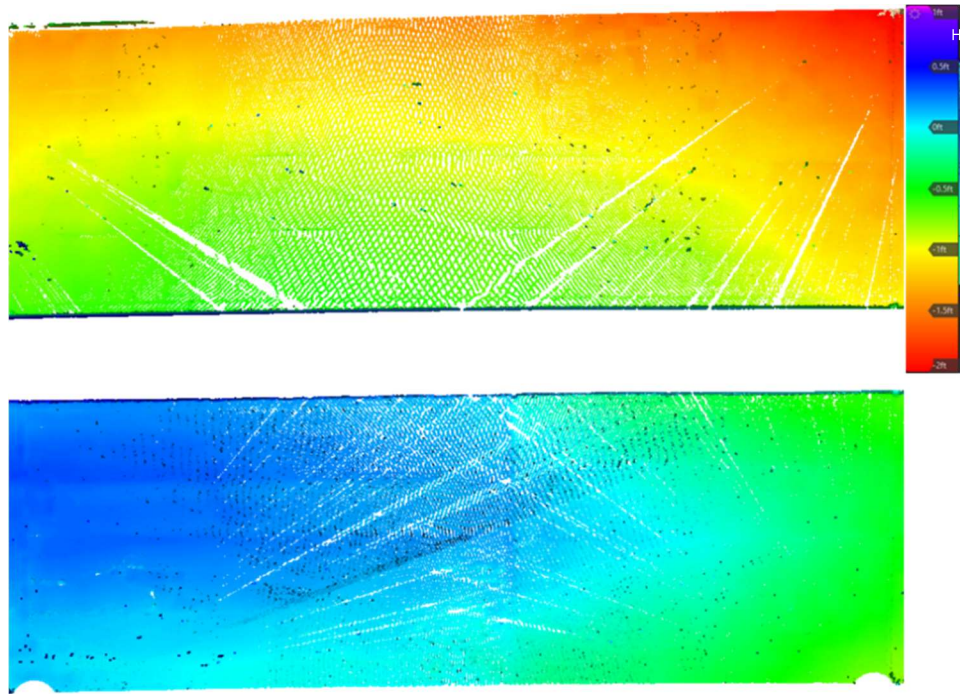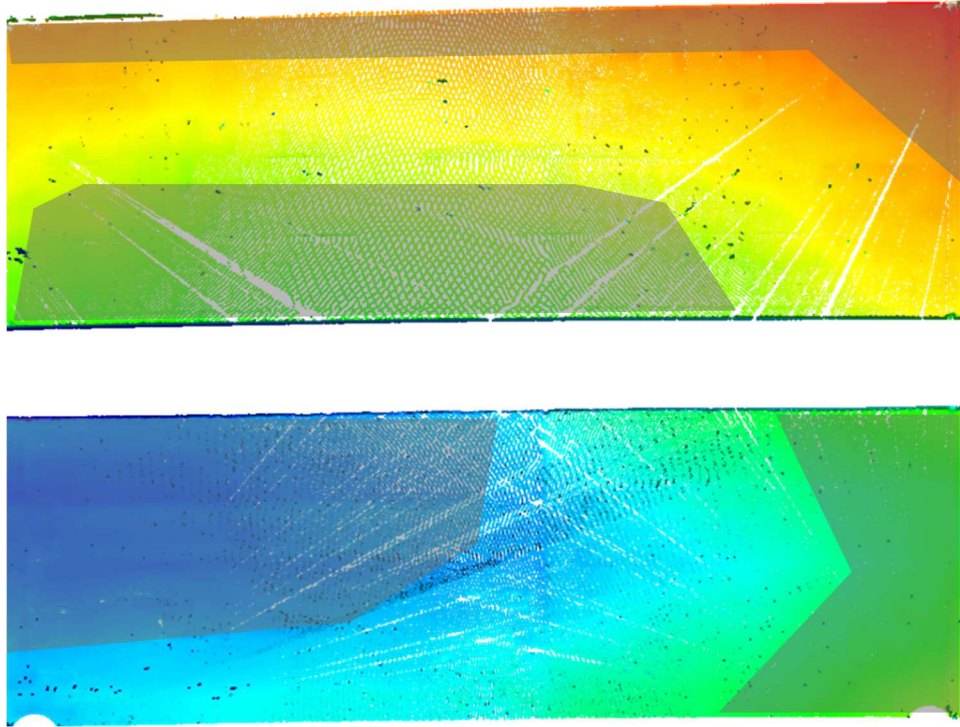
5.6.3 Bridge 0416151

Figure 34. RGB of Structure 0416151.

Bridge 0416151 was observed to have significant flat regions, as depicted in Figure 35 and Figure 36. Figure 35 portrays the differences in height on the top surface of the deck, while Figure 36 points out the areas that are level and devoid of changes in elevation or slope. Figure 34 shows an RGB view of the deck's top surface. These flat regions have an impact on the way water flows off the bridge. The flat areas are prone to accumulating water, which can seep into the deck and heighten the risk of corrosion on the reinforcing steel.


Figure 35. Heat Map of structure 0416151

Figure 36. Flat regions of structure 0416151

Figure 37 illustrates the rough location of the above-mentioned cross sections within Bridge 0416151. where Long A, Long B, Long C, and Long D are the sections that run along the length of the bridge, and Trans Top, Trans Mid, and Trans Bottom are the sections that run across the bridge's width. Based on the information provided in Figure 38 and Figure 39, it can be inferred that the longitudinal and transverse cross sections range from 0 to 0.6%, which impedes proper water drainage.
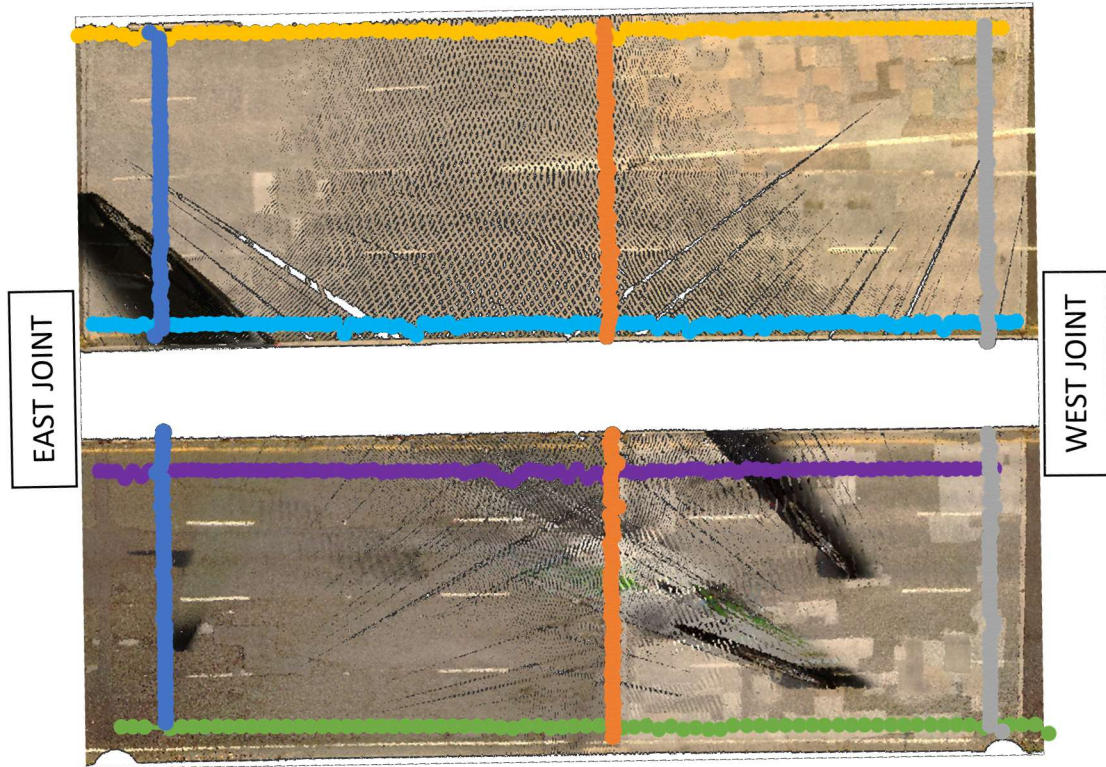
Figure 37. Approximate Cross Sections Locations on the Deck Surface

The high points depicted in Figure 38 and Figure 39 may indicate the possible existence of surface irregularities, such as minor potholes on the deck. The gap is evident in Figure 39 due to the barrier on the deck.
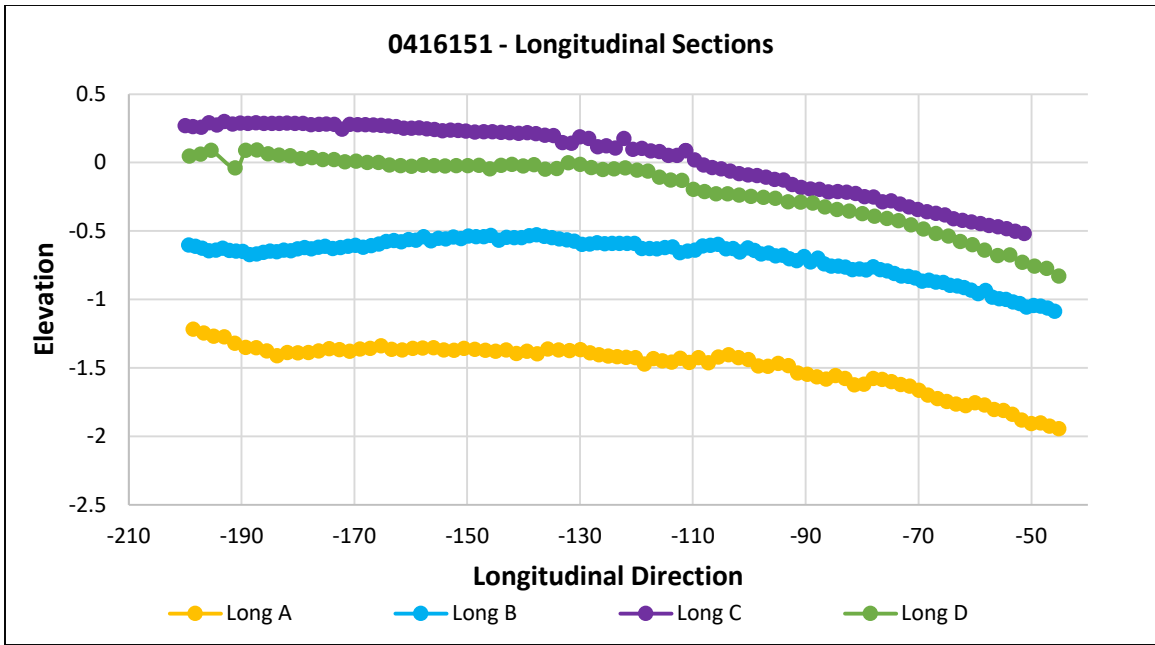
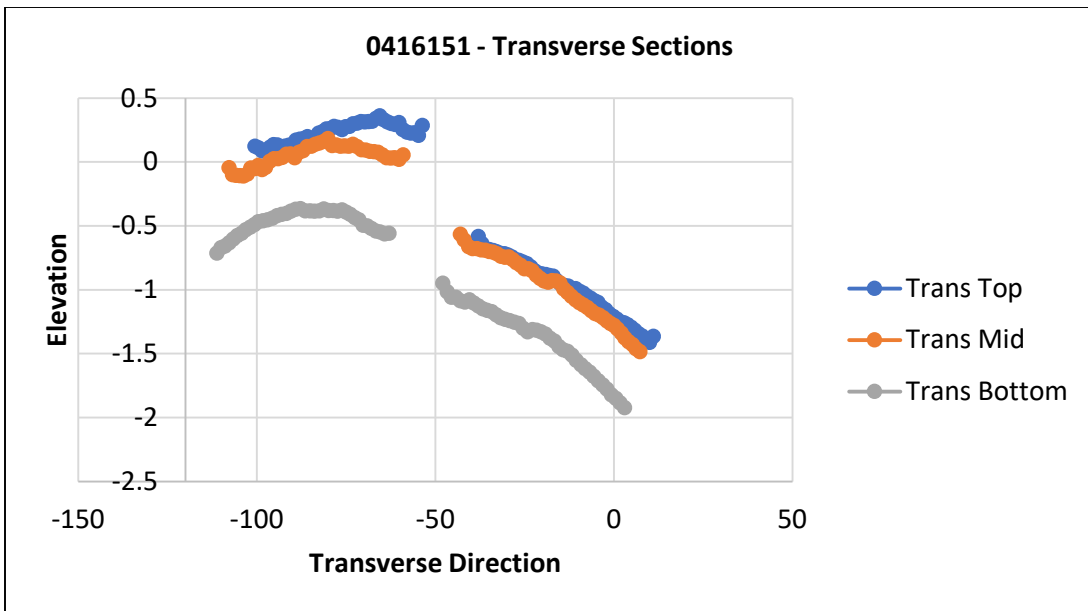*Figure 38*. Structure 0416151 - Longitudinal Sections

Figure 39. Structure 0416151 - Transverse Sections

5.6.4 Bridge 361632N

Figure 40. RGB of Structure 361632N

Figure 41 shows an elevation map, and Figure 43 estimates a 1 to 1.5% longitudinal slope. These indicate that the surface conditions allow water to run off the deck efficiently. Additionally, Figure 44 estimates a transverse slope of approximately 2%. There is no clear evidence of areas on Structure 361632N prone to early deterioration. However, it is worth noting that the first half of the deck (upstream) has a lower slope than the second half. This could affect performance by causing water to sit longer on flatter areas and accelerating deterioration. Figure 40 provides an RGB view of the top surface of the deck.
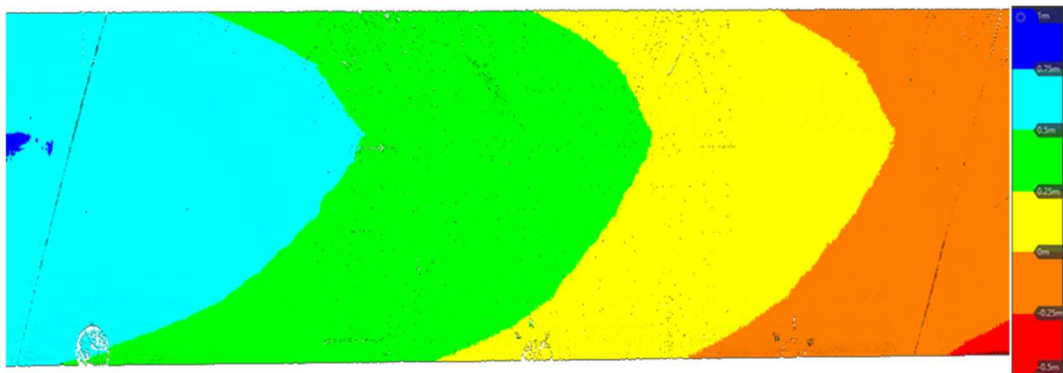

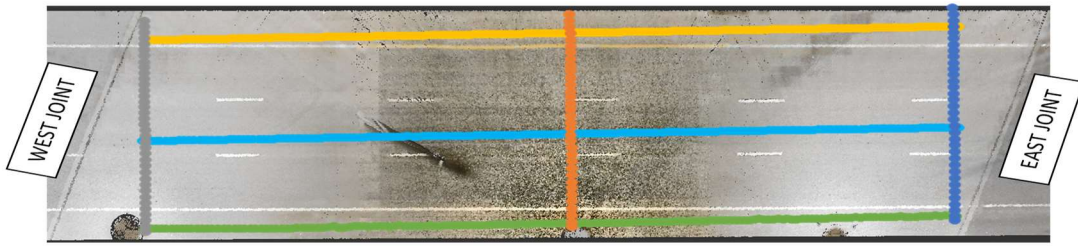*Figure 41*. Structure 361632N Heat Map

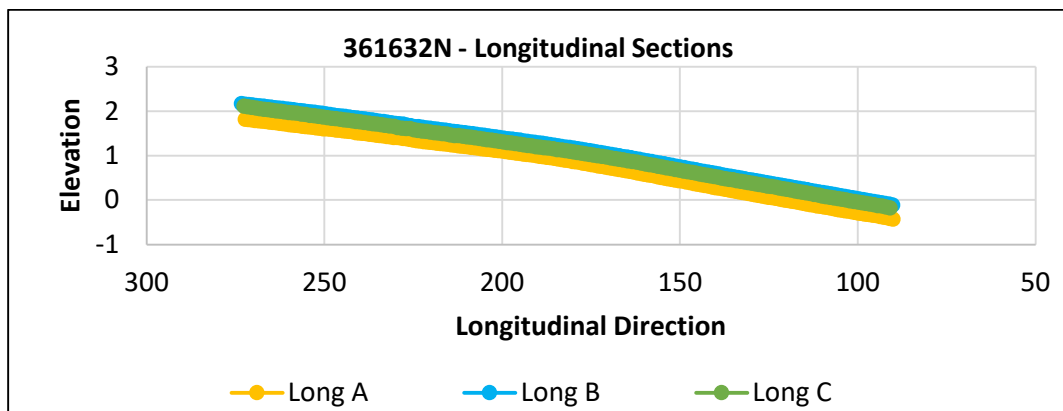*Figure 42*. Approximate Cross Sections Locations on the Deck Surface

Figure 43. Structure 361632N – Longitudinal Sections
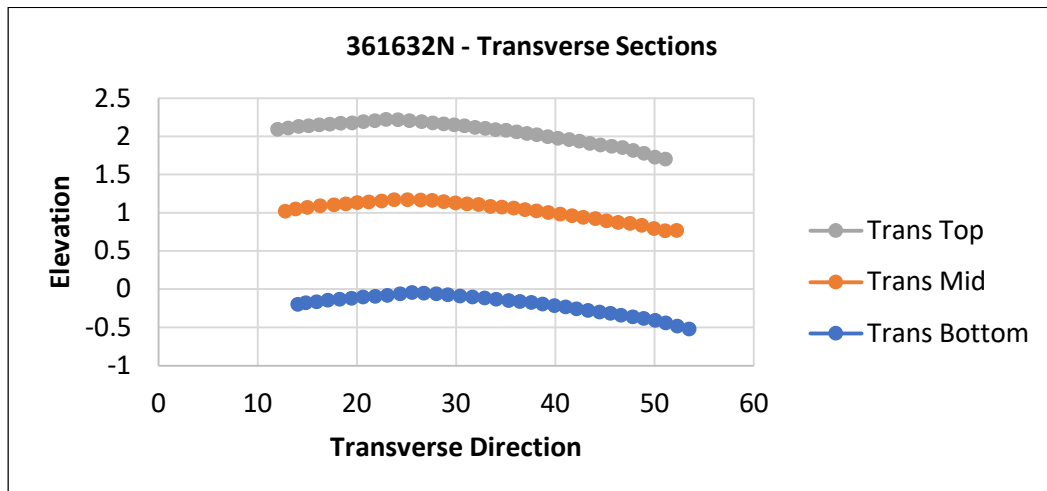
Figure 44. Structure 361632N - Transverse Sections

5.6.5 Bridge 0821155
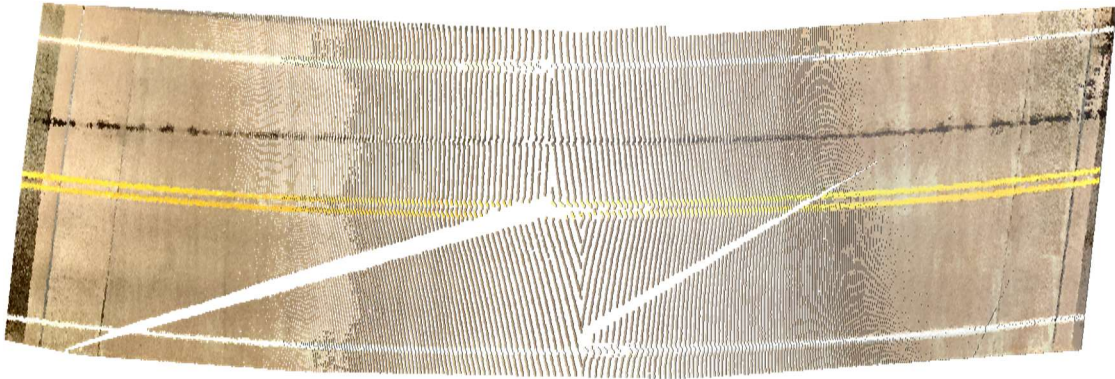
Figure 45. RGB of Structure 0821155

Structure 0821155 is recently built. Figure 46 and Figure 48 show a flatter area on the left side that may cause problems in the long run. The transverse cross-section slope of the deck is around 1.4%, which is slightly lower than the recommended 2%, as estimated from the data in Figure 49. Figure 45 shows an RGB view of the top surface of the deck.
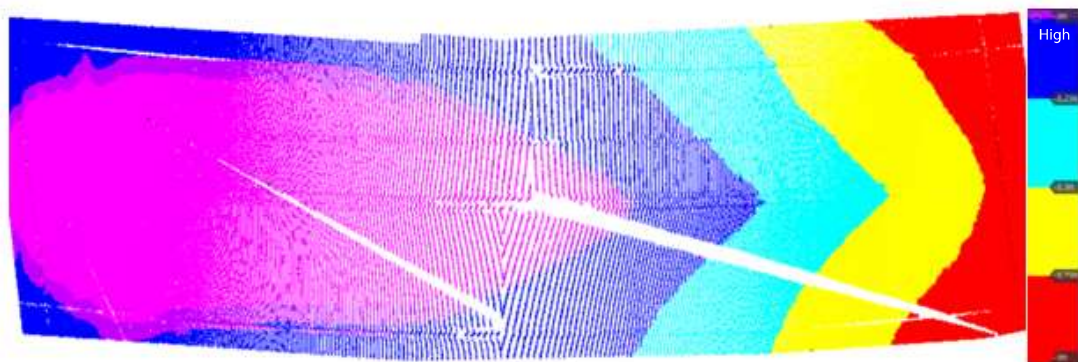
Figure 46. Structure 0821155 Heat map

Figure 47 provides an estimated location for each cross-section within structure 0821155.

Figure 47. Approximate Cross Sections Locations on the Deck Surface
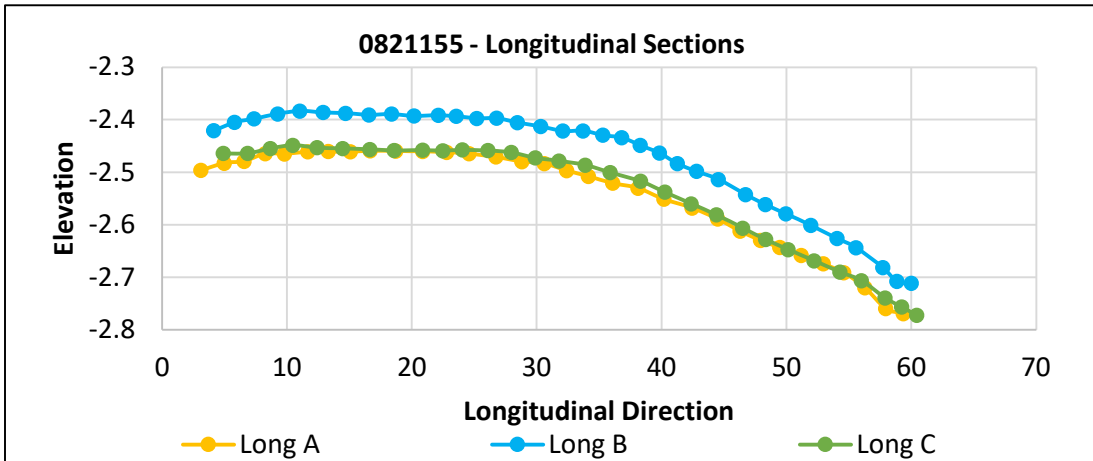
Figure 48. Structure 0821155 - Longitudinal Sections
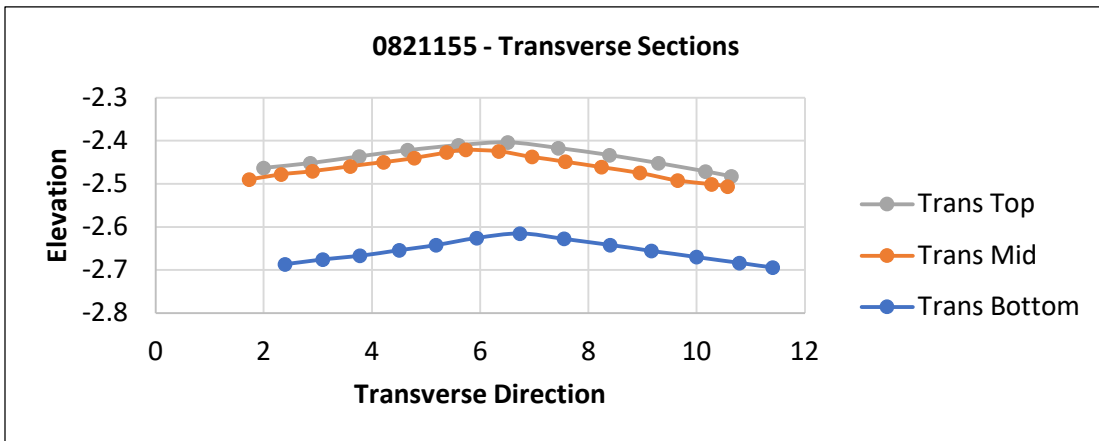
Figure 49. Structure 0821155 - Transverse Sections

5.6.6 Bridge 1317154
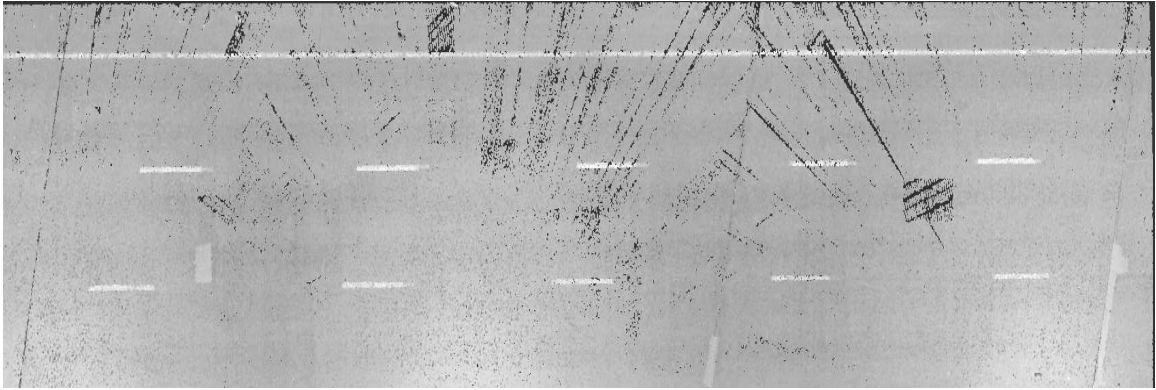
Figure 50. Plan View of Structure 1317154

The slope of Structure 1317154 is uniformly inclined at about 3% longitudinally, according to Figure 51 and Figure 53. As estimated in Figure 54, the transverse slope is slightly below the recommended 2%, at approximately 1.6%. There is no particular area of concern where the structure might deteriorate prematurely. However, the transverse slope observed in this deck is worth noting; Figure 52 provides an approximate location of each cross-section in Structure 0821155. Long A, B, C, and D refer to cross sections in the longitudinal direction. Trans Top, Trans Mid, and Trans Bottom denote cross sections in the transverse direction.

Figure 51. Structure 1317154 Heat Map

Figure 52. Approximate Cross Sections Locations on the Deck Surface

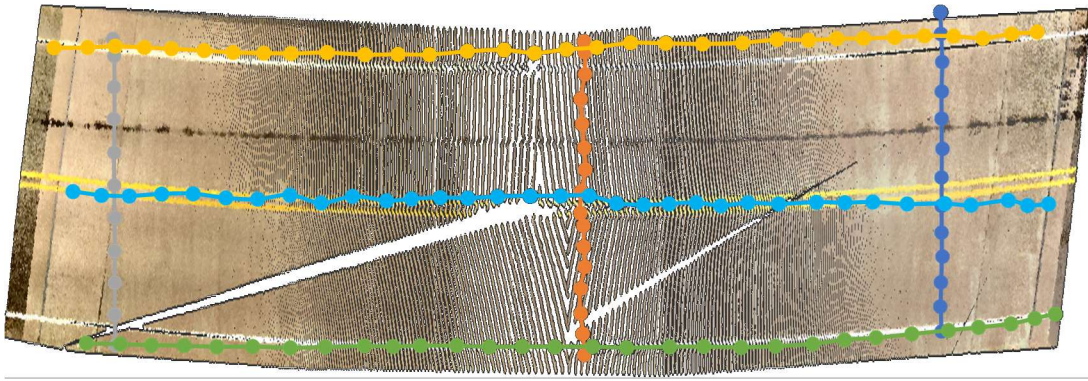*Figure 53.* Structure 1317154 - Longitudinal Sections
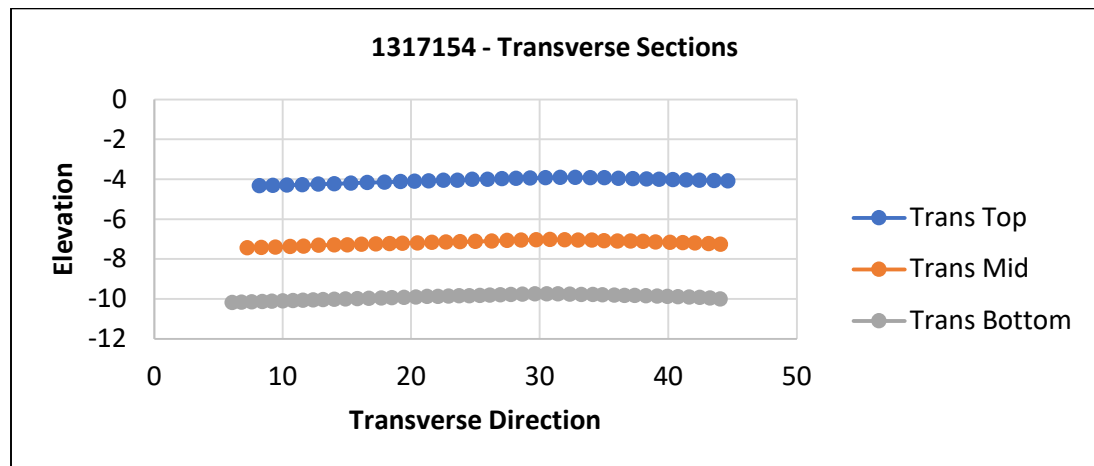
Figure 54. Structure 1317154 - Transverse Sections

85

5.6.7 Bridges 1816154 & 1816155
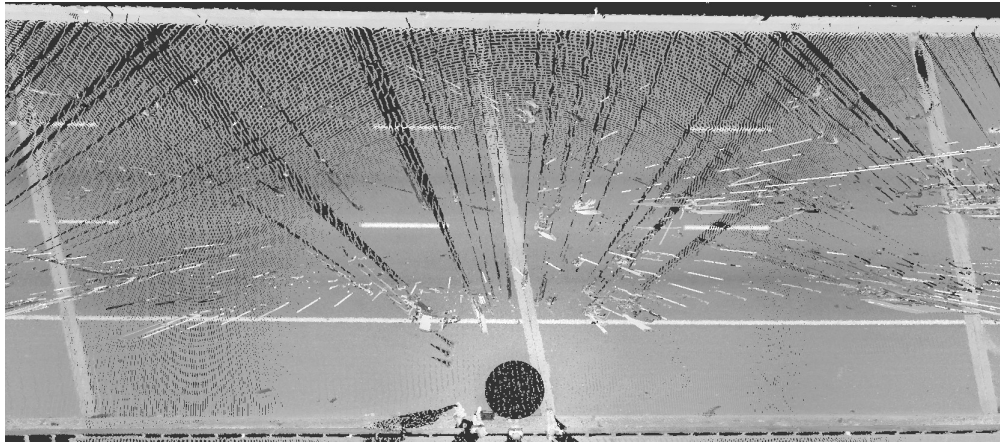
Figure 55. Plan view of Structure 1816154

In this section, we will compare Structures 1816154 and 1816155, included in the project, as a case study presented by NJDOT. The twin bridges initially had different levels of deck condition, with 1816155 having a rating of 3 and 1816154 having a rating of 6. Figure 55 and represent a top view of bridges 1816154 and 1816155, respectively.

Figure 56. Plan view of Structure 1816155

This was concerning as the structures have the same level of traffic and dimensions of their structural components. Figure 57 and Figure 58 show the elevation maps of the top surface of the structures, both of which have a longitudinal slope of approximately 2.3%, as can be seen in Figure 60 and Figure 63. Structure 1816154 has a transverse slope of 1-1.3%, demonstrated in Figure 61, while structure 1816155 has a uniform transverse slope of 1.3%, visible in Figure 64.
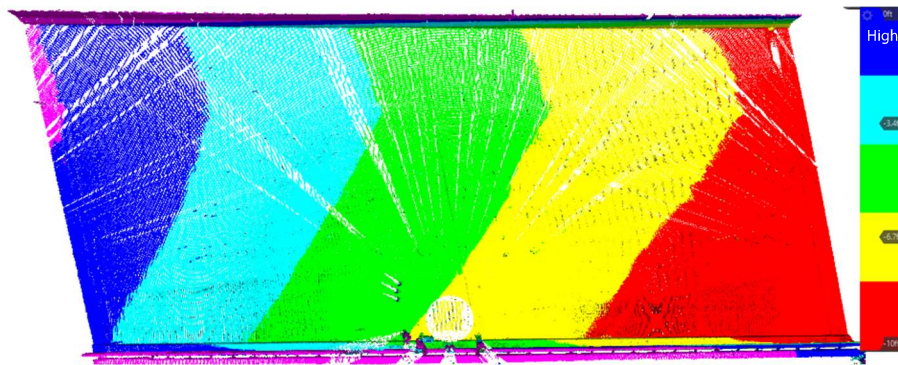
Figure 57. Structure 1816154 Heat Map
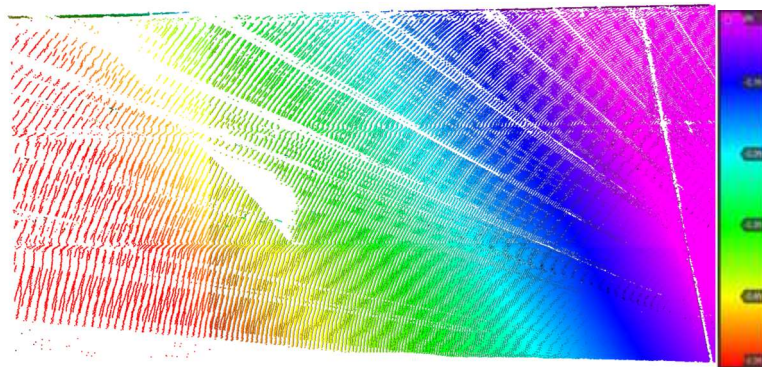
Figure 58. Structure 1816155 Heat Map

During the data collection for Structure 1816155, construction work was being performed on the bridge, which obstructed part of the deck and limited access for the research team. As a result, only half of the deck was available for data collection.
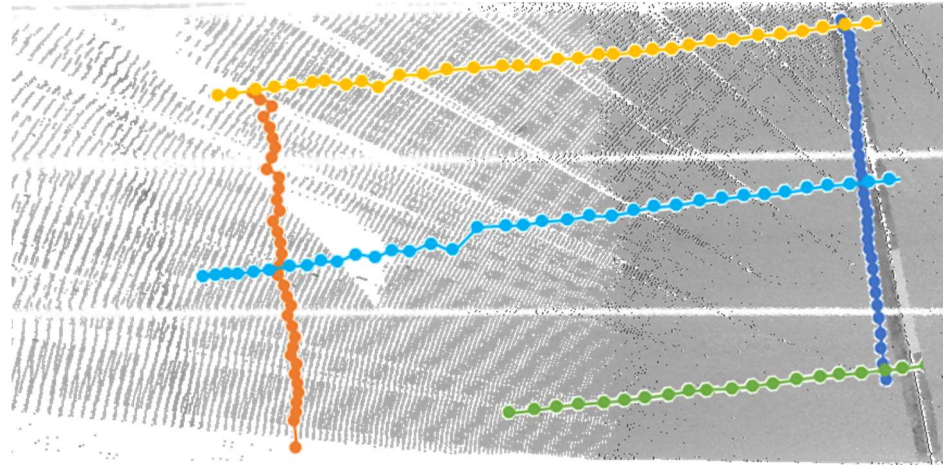
Figure 59. Approximate Cross Sections Locations on the Deck Surface
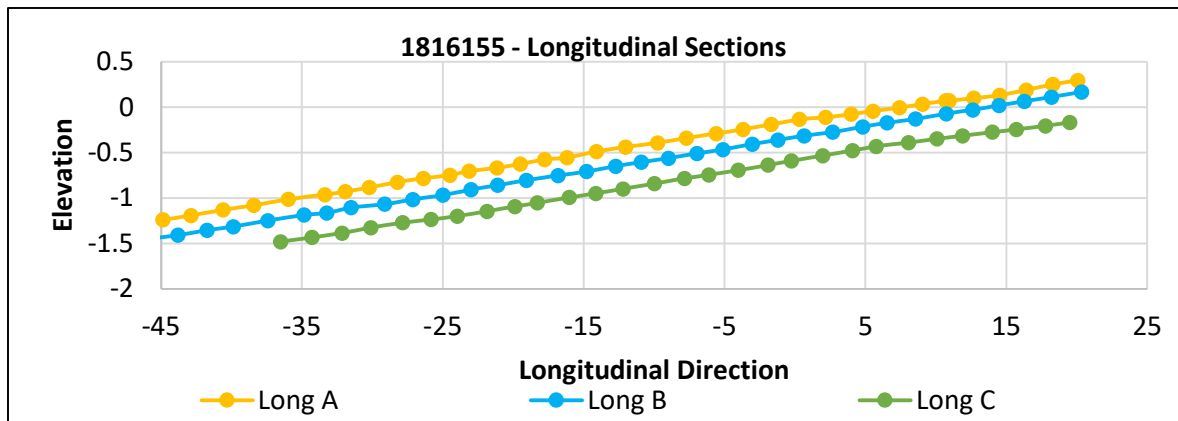
Figure 60. Structure 1816155 - Longitudinal Sections
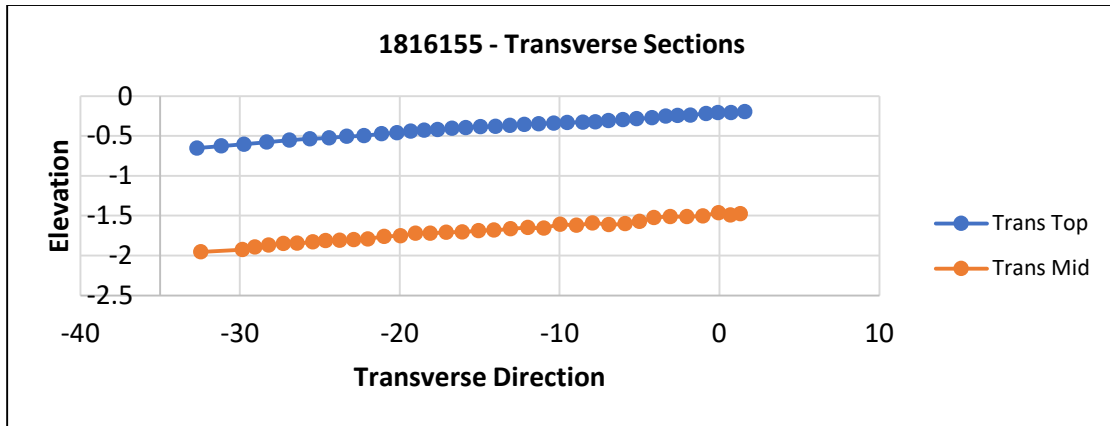
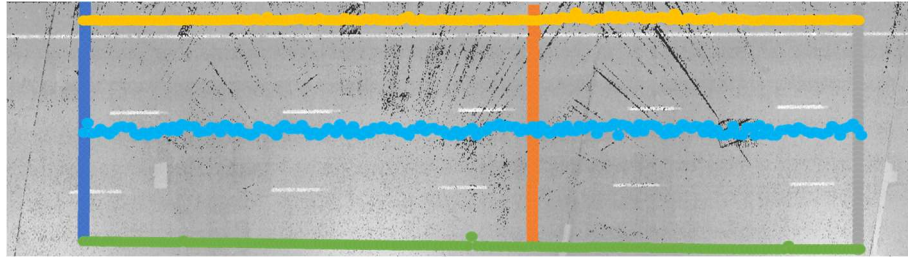*Figure 61*. Structure 1816155 - Transverse Sections
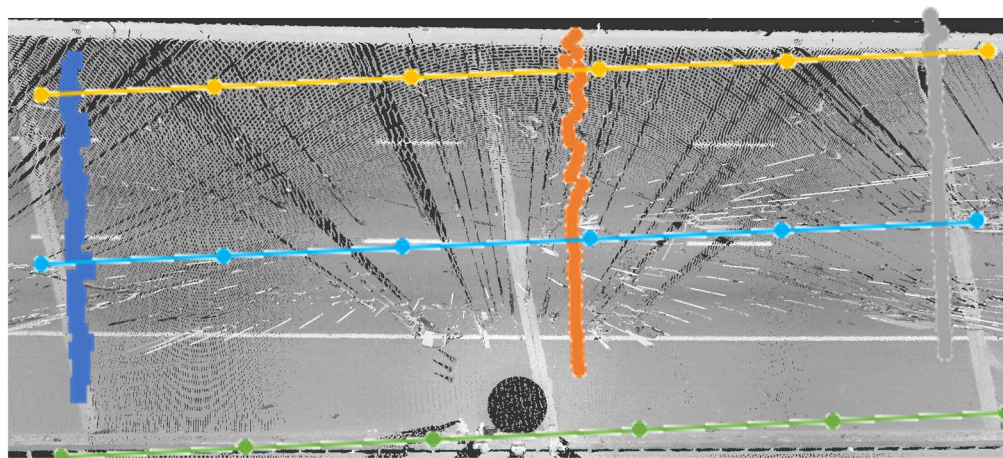
Figure 62. Approximate Cross Sections Locations on the Deck Surface –
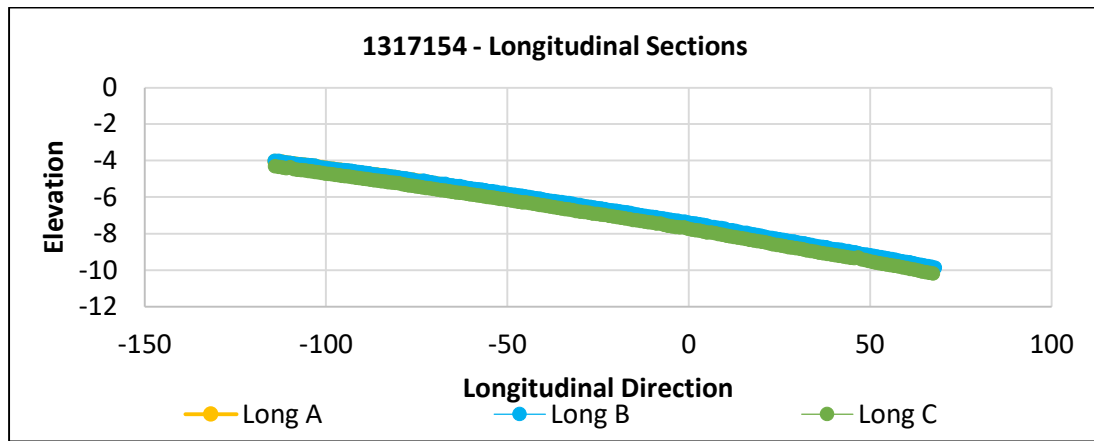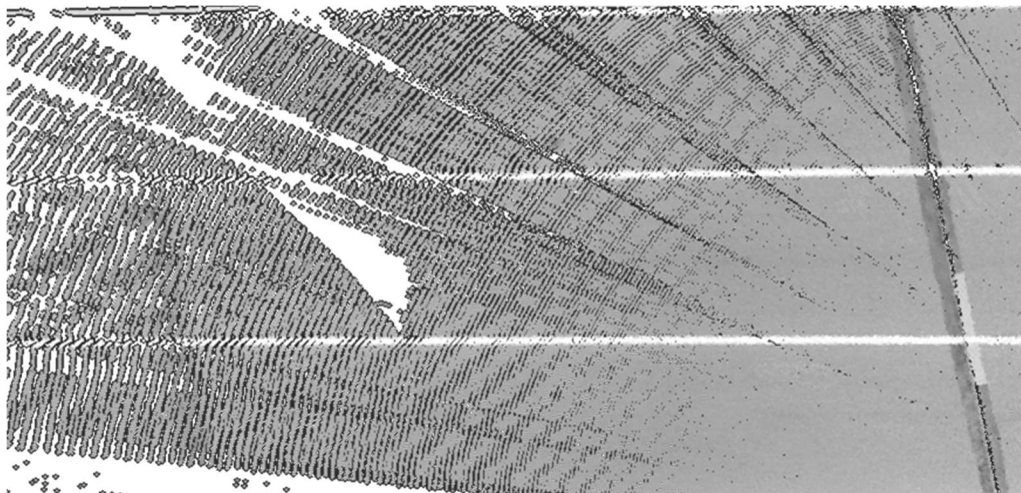
Structure 1816154
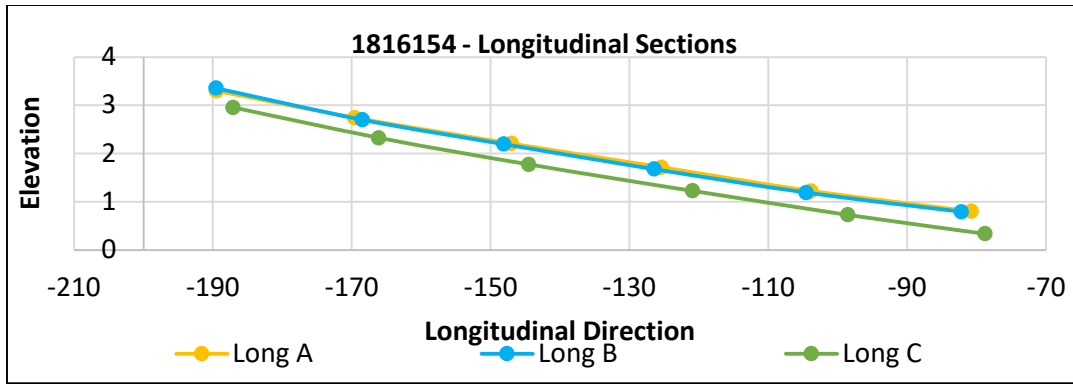
Figure 63. Structure 1816154 - Longitudinal Sections
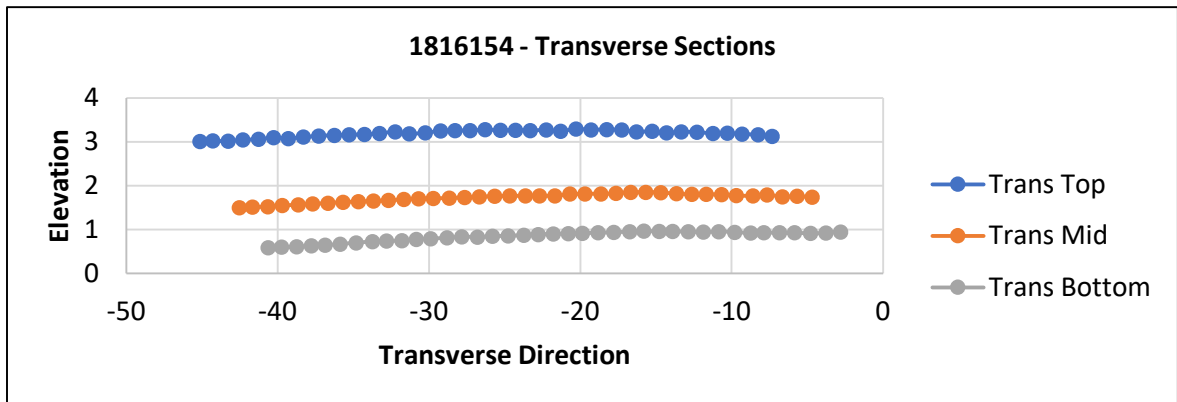
Figure 64. Structure 1816154 - Transverse Sections

Mild rutting was observed in all transverse directions, indicating areas where water may sit for extended periods and increasing the possibility of early deterioration. The point cloud data analysis did not provide clear evidence of the cause of the difference in condition between the two structures. The main signs of deck damage observed were rutting and low points of vertical curvature, which had a clear correlation with the deterioration stage of the deck. After the data analysis, NJDOT conducted a detailed deck survey, resulting in a

deck condition rating of 3 for both structures. This aligned with the information in the point cloud data analysis, as there was no clear evidence of significant differences between the two decks.

5.7 Second Approach: Least Square Method Plane Fitting

The goal of this approach for analyzing bridge deck point cloud data is to establish a trend that links the condition rating of a bridge to the percentage of damaged areas. To achieve this, a methodology was developed that involved projecting the deck onto a horizontal plane, eliminating longitudinal slopes, and creating cross-sections wherever crowns or a change in slope was present. Each cross-section was then flattened to create a plane, enabling the identification of high and low points along the surface. By joining these sections, deeper spalls greater than 0.75 inches (19.05 - 25.4 mm) were isolated as damaged points. The ratio of these points to the total surface area represented the percentage of damaged areas. It is worth noting that the data was validated through scanning and comparing results of The BEASE bridge specimen, which increases the reliability and accuracy of the results. *Figure 65* shows a heat map of the Bridge Deck of structure #1816154, showing the Longitudinal slope, Transverse slopes, and Deck Dimensions
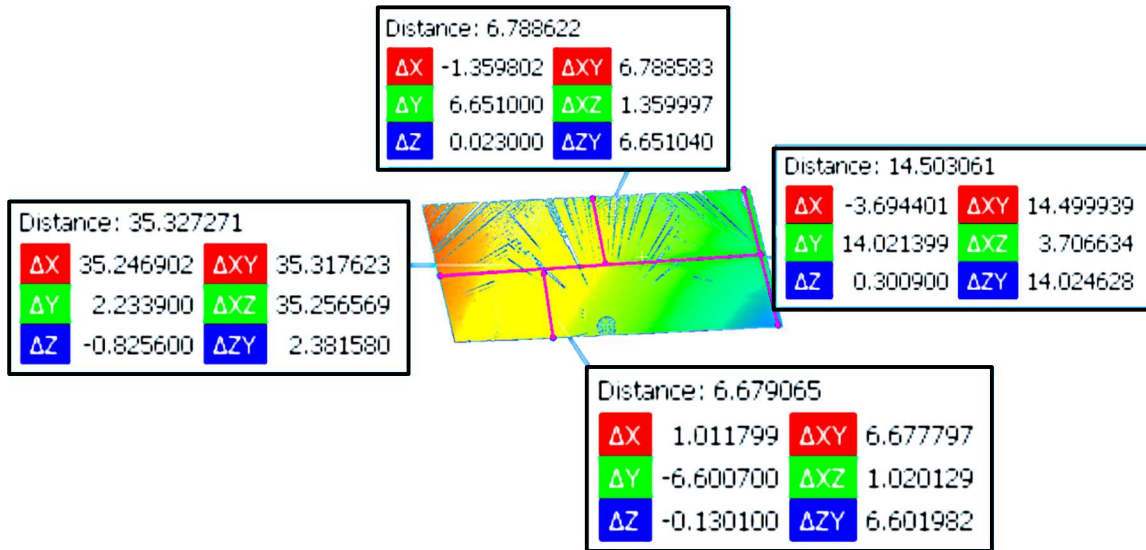
Figure 65. Points Coordinates and slopes Variation along the Deck

The following process, as seen in Figure 66, was the horizontal projection of the Bridge deck, and the goal was to eliminate the Longitudinal slope. It was done by obtaining the matrix that would transform the point cloud so that the normal vectors are pointing toward Positive Z. Figure 66 shows the updated scalar field after the projection. After the transformation has been made, a recheck of slopes can be seen in Figure 67 to identify further curvature and determine areas of interest on the deck.
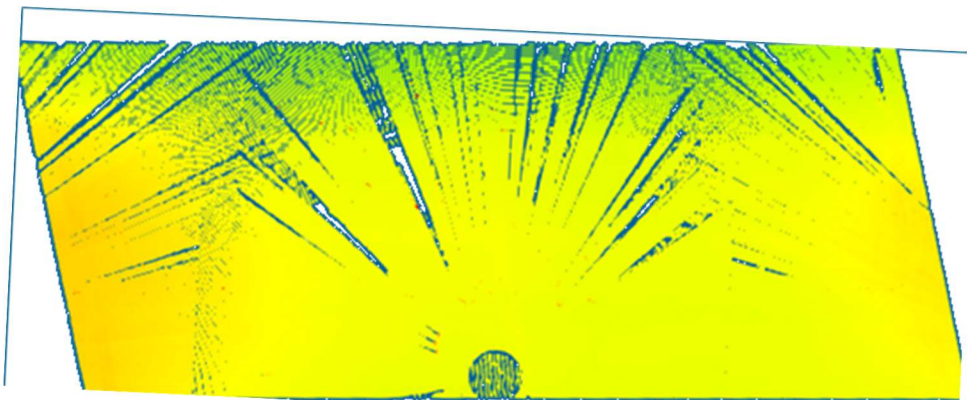
Figure 66. Horizontally Projected Bridge Deck

92

Distance: 7.356003
ΔX	0.858433	ΔXY	7.355210
ΔY	-7.304945	ΔXZ	0.865195
ΔZ	0.107962	ΔZY	7.305742

Distance: 17.723001
ΔX	-17.658724	ΔXY	17.722998
ΔY	-1.508013	ΔXZ	17.658728
ΔZ	-0.011918	ΔZY	1.508060

Distance: 35.647706
ΔX	35.556412	ΔXY	35.647705
ΔY	2.549602	ΔXZ	35.556412
ΔZ	-0.007111	ΔZY	2.549612

Distance: 17.128086
ΔX	17.006287	ΔXY	17.128084
ΔY	2.038999	ΔXZ	17.006287
ΔZ	0.006547	ΔZY	2.039009

Distance: 14.274690
ΔX	-2.738419	ΔXY	14.274396
ΔY	14.009263	ΔXZ	2.739948
ΔZ	-0.091541	ΔZY	14.009562

Distance: 6.699353
ΔX	0.865154	ΔXY	6.699346
ΔY	-6.643248	ΔXZ	0.865209
ΔZ	-0.009720	ΔZY	6.643255

(a)

0.8052 0.6813 0.5574 0.4334 0.3095 0.1856 0.0617 0.0621 -0.1860

(b)

Figure 67. (a) Points Coordinates and slopes Variation After Horizontal Projection, (b) Elevation Scale proving the elimination of Longitudinal slope with Plane Projection.

By adjusting the color scale for finer change in elevation visualization, Figure 68 shows a heat map that reflects the different elevations of points in the point cloud after the Longitudinal slope was eliminated.

Figure 68. Heat Map of the Horizontally Projected Decks

It can be seen that the longitudinal slope has been eliminated. However, we still have much curvature in the deck and some dipping in the mid-span, probably due to deflection and deformation of the substructure, superstructure, and the wearing surface material. So, surface damage still could not be detected at this point. However, the location can be predicted based on the elevation difference. The areas where the surface is depressed will be an area of interest as it is prone to more water collection and eventually further deterioration.

The next step was to section the deck based on the elevation changes and repetition of the projection procedure to locate further curvature and get the most accurate curvature-free Deck surface so plane fitting could be relevant and accurate results could be obtained. Figure 69 shows the deck cross sections generated and separated the right and left spans along with a separate horizontal projection for further curvature detection.
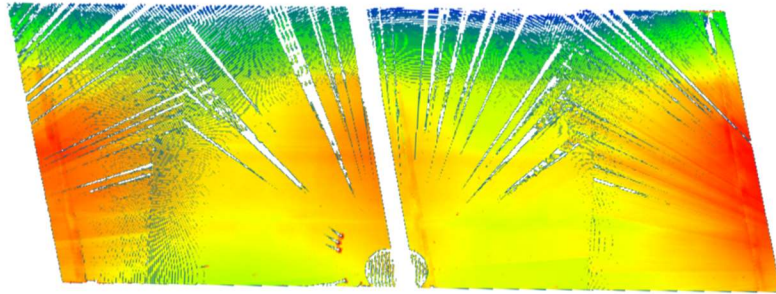
Figure 69. Sectioning the Bridge Deck based on Slopes variation.

It is still also visible from Figure 69 that further sectioning was needed, as both the right and the left spans showed dipping, and it was more evident on the right span. Figure 70 shows the results of further sectioning, where finally, the deck was sectioned into five different sections. Each was individually projected on a horizontal plane and prepared for the (Mplane) plane fitting procedure.
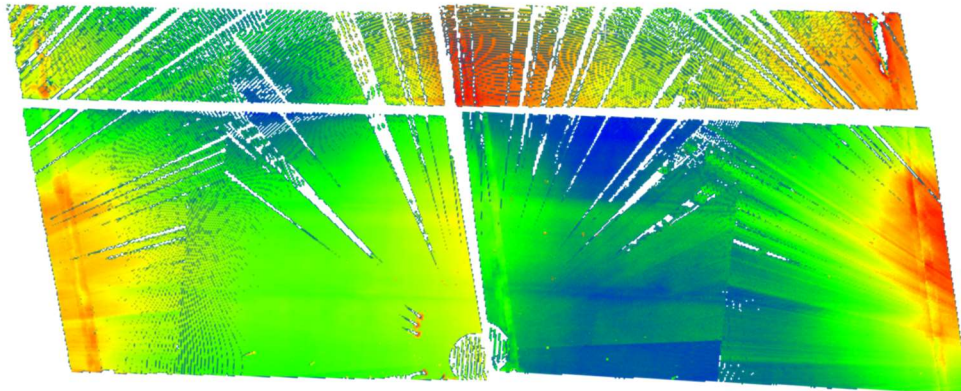
Figure 70. Further Sectioning of Bridge Deck

Plane fitting on the parameter for each generated section was performed, as demonstrated in Figure 71. Finally, the distance between the points in the section and its associated plane was computed, and the result can be seen in Figure 72.
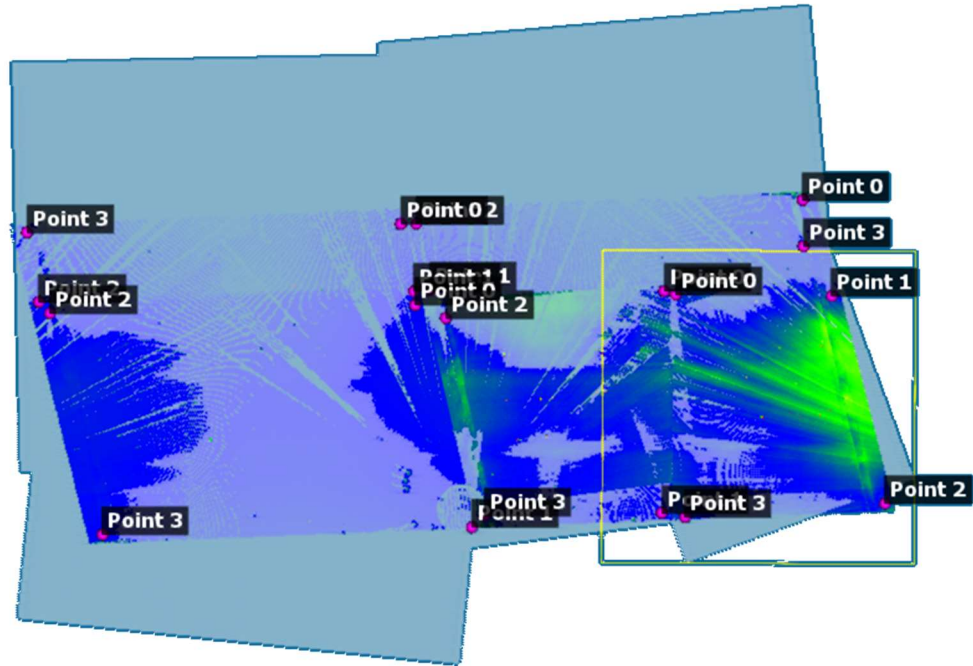
Figure 71. (MPlane) Plane Fitting of the generated Cross Sections
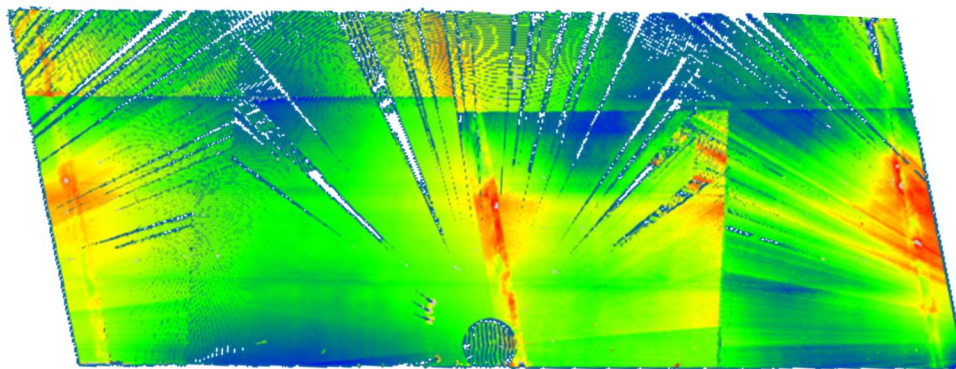
Figure 72. Heat Map after Plane Fitting

Each section shows a local points elevation where high and low points can be visible on each generated section individually. The plane-fitted sections were merged into a one point cloud, leaving the scalar field for each separate but combining all the scalar fields to include all points in all sections. The obtained results can be visualized in Figure 73.
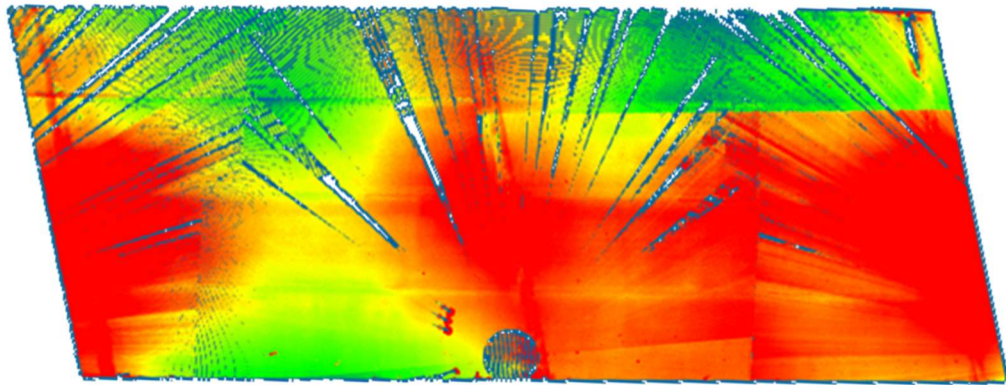
Figure 73. Fitted Planes Heat Map

Moreover, hiding the higher flat regions to be able to study damage even in dipped areas as the study is interested in the areas of damage that were spalling larger than 0.75"-1" to match the criteria for condition rating of our data validation model, the BEAST.

For this particular Bridge Deck, and based on the distances of points from the planes after plane fitting results. Figure 74 Shows the Bridge Deck of structure 1816154, where points up to 0.005 meters (5 mm) and up to -0.035 m (35 mm) are only visible, while the flat regions that showed a distance greater than 5 mm from the fitted planes were eliminated, note that the process here isn't explained to the deepest extinct of analysis as

the process required more and more detailed horizontal projection and plane fitting Figure 74 demonstrates the process on a bigger scale for visualization purposes.

(a)

(b)
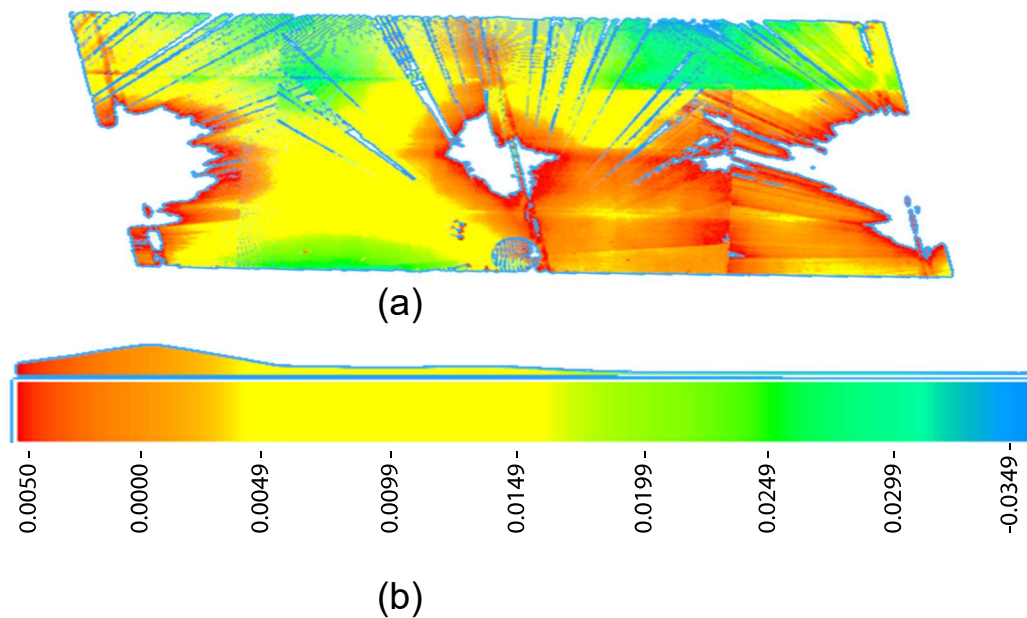
Figure 74. (a) Plane Fitted Bridge Deck of Structure 1816154, (b) Elevation scale after choosing the representative Elevation ranging from 0.005 to -0.035

As our study was interested in spalling greater than 1" in depth, the points with a distance of 0.02 and more below the fitted planes were isolated and identified as damaged points in the point cloud, and the results can be seen in Figure 75 which represent an exaggeration of the plane fitting and isolation process for visual demonstration purposes .

The resultant Isolated damaged points data was obtained. The number of overall damaged points in the Point cloud was used to describe the Damaged area percentage assuming ideal scanning conditions, and the Bridge Deck was fully scanned in detail.

(a)

(b)

-0.0200　-0.0218　-0.0237　-0.0255　-0.0274　-0.0293　-0.0311　-0.0330　-0.0394
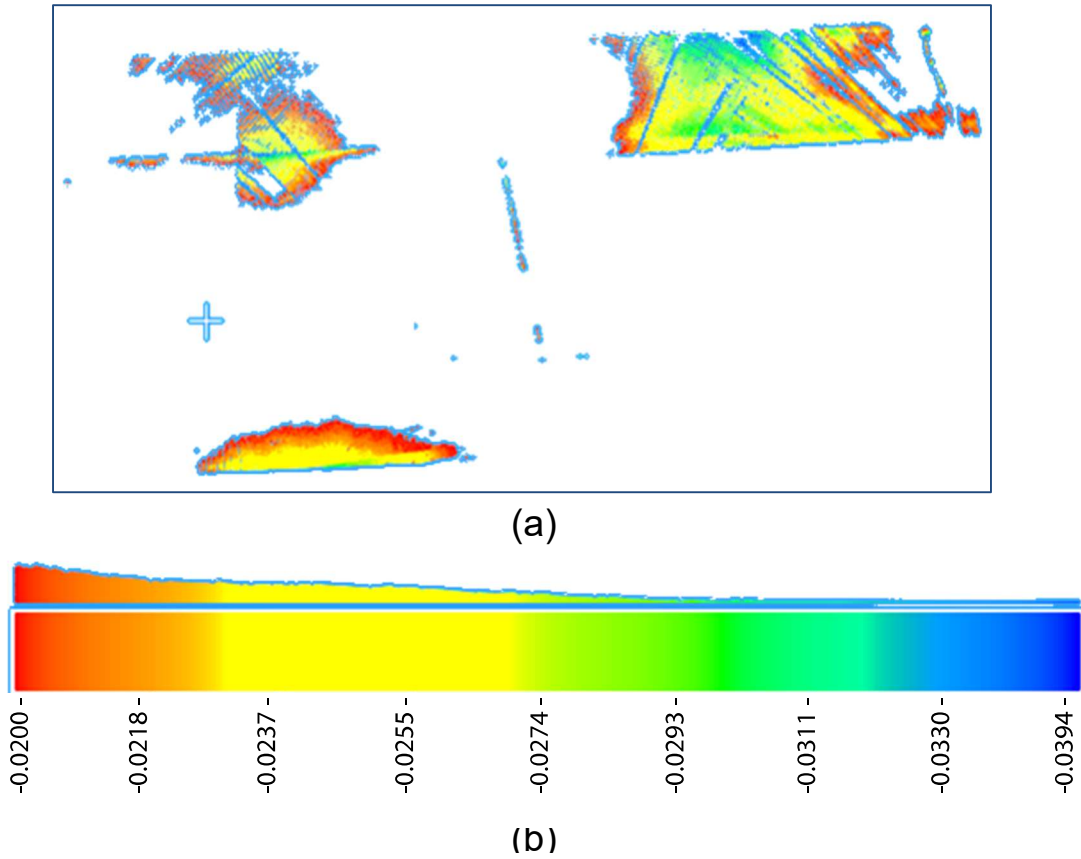
Figure 75. (a) Isolated Damaged Points, (b) Elevation Scale representing damaged points ranging from -0.02 to -0.035.

The same procedure was implemented on all Bridge Decks in the study, and the following results were obtained.

5.8 Second Approach Results

5.8.1 Structure 0416151

After multiple cross-sectioning, Horizontal projections and planes fitting Bridge 0416151 showed areas of interest where distances from the fitted planes were 0.0054 m above to -.07 m below the fitted planes, and the isolated points that represent damaged points below -.02 m can be seen in Figure 76.

(a)

(b)

(c)

(d)
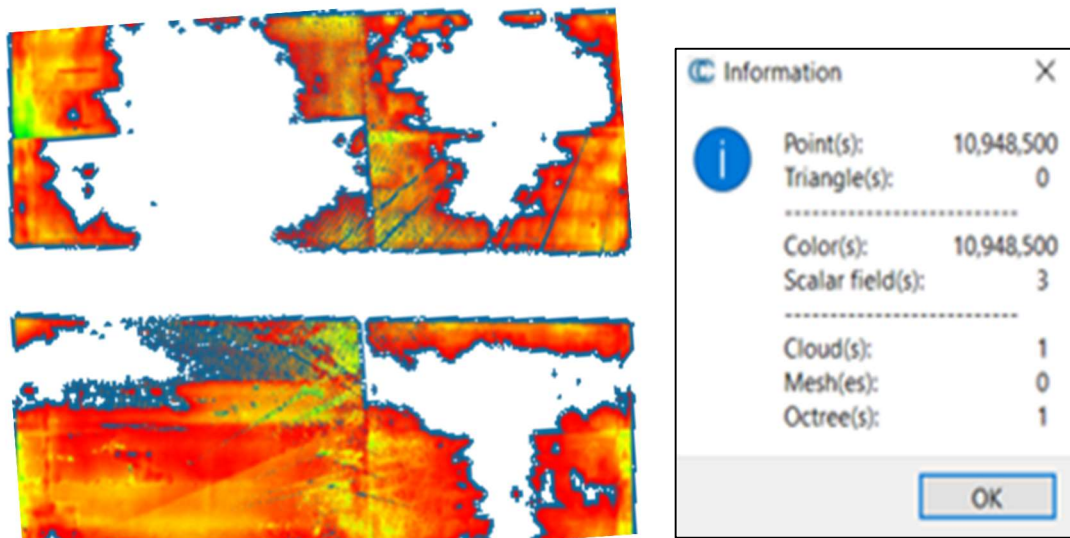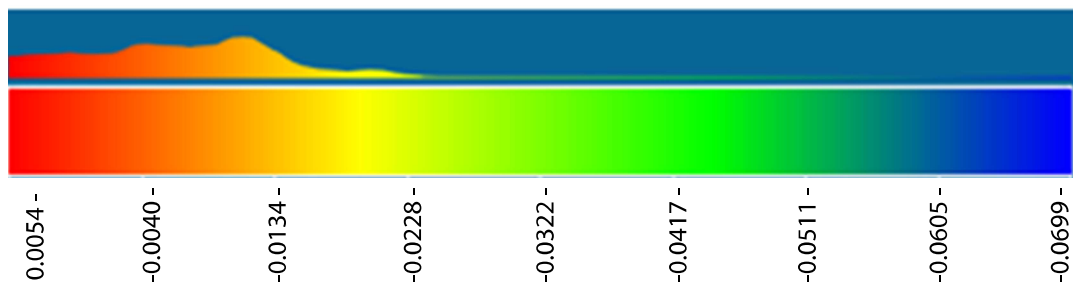
Figure 76. Analysis of Structure 0416151Bridge Deck (a) Heat map of the plane fitted bridge deck (b) Elevation scale showing Elevations from 5.4 to - 70 mm (c) Isolated damaged points along with the number of points in the isolated cloud that represent damage, (d) Elevation scale showing elevations from -20 to -70 mm

Table 7 shows the information on Bridge 0416151 and the result of the damage percentage analysis.

Table 7

Results of Damage Analysis for Structure 0416151

Bridge #	County	ADT	ADTT	Deck Condition	Damage Percentage
0833150	Camden	54495	4	4	3.93%

5.8.2 Structure 0821155

After multiple cross-sectioning, Horizontal projections and planes fitting Bridge 0821155 showed areas of interest where distances from the fitted planes were 0.01 m above to -.08 m below the fitted planes, and the isolated points that represent damaged points below -.02 m can be seen in Figure 77.

(a)

(b)

(c)

(d)
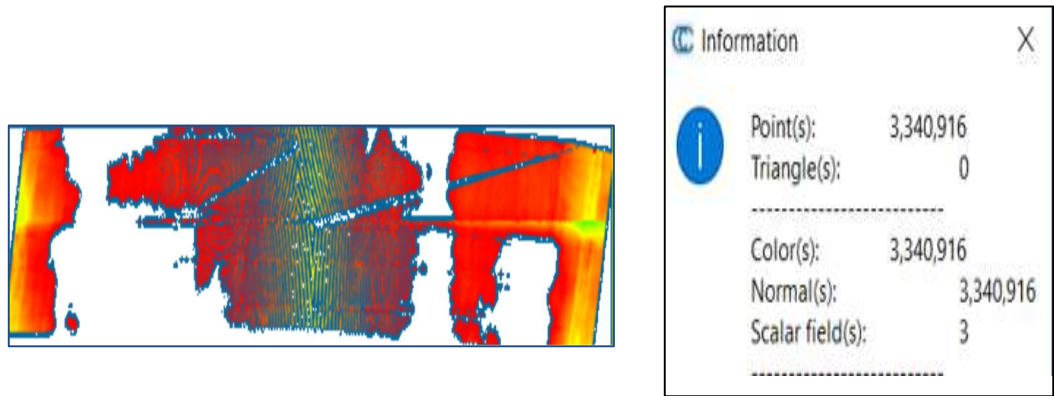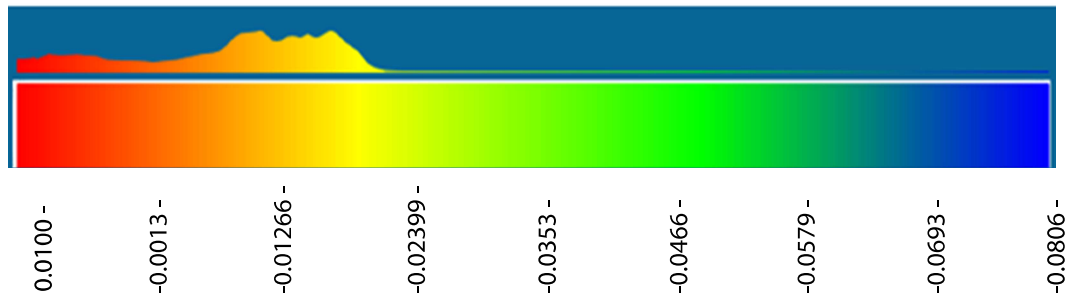
Figure 77. Analysis of Structure 0821155 Bridge Deck (a) Heat map of the plane fitted bridge deck (b) Elevation scale showing Elevations from 10 to - 80 mm(c) Isolated damaged points along with the number of points in the isolated cloud that represent damage,(d) Elevation scale showing elevations from -20 to – 80 mm.

Table 8 shows the information on Bridge 0821155 and the result of the damage percentage analysis.

Table 8

Results of Damage Analysis for Structure 0821155

Bridge #	County	ADT	ADTT	Deck Condition	Damage Percentage
0821155	Gloucester	1086	3	9	1.08%

5.8.3 Structure 18G0701

After multiple cross-sectioning, Horizontal projections and planes fitting Bridge 18G0701 showed areas of interest where distances from the fitted planes were 0.015 m above to -.015 m below the fitted planes, and the isolated points that represent damaged points below -.01 m can be seen in Figure 78.
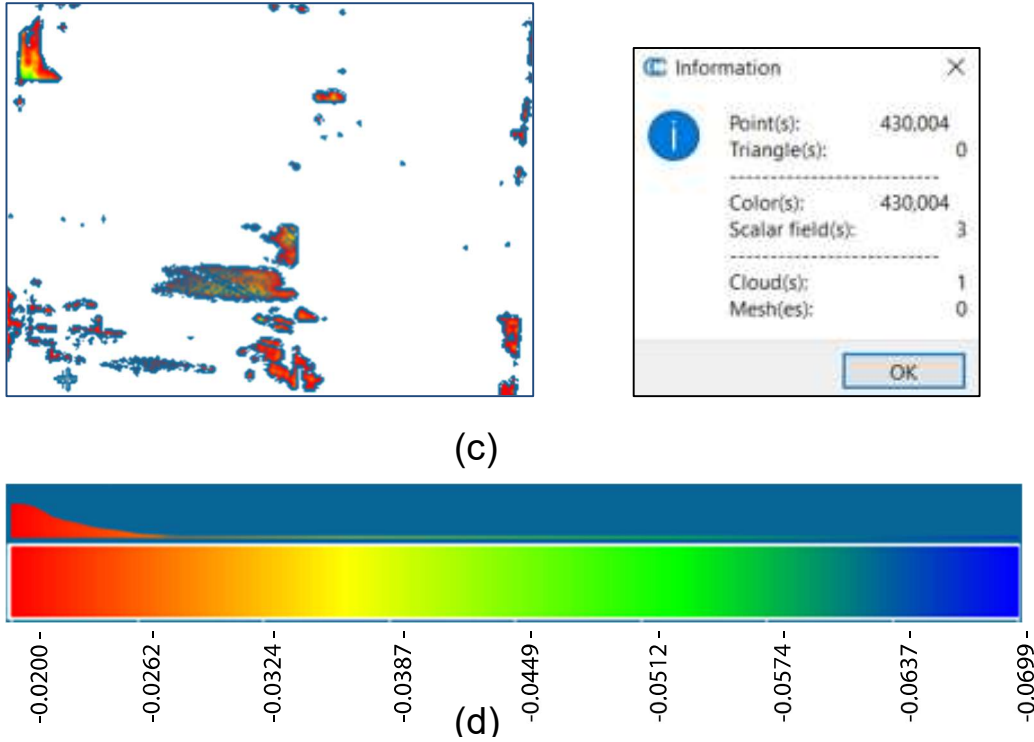

(a)

(b)

(c)

(d)

Figure 78. Analysis of Structure 18G0701 Bridge Deck (a) Heat map of the plane fitted bridge deck (b) Elevation scale showing Elevations from 15 to - 15 mm (c) Isolated damaged points along with the number of points in the isolated cloud that represent damage,(d) Elevation scale showing elevations from -10 to -15 mm

Table 9, shows the information on Bridge 18G0701 and the result of the damage percentage analysis.

Table 9

Results of Damage Analysis for Structure 18G0701

Bridge #	County	ADT	ADTT	Deck Condition	Damage Percentage
18G0701	Somerset	24478	4	9	1.16%

5.8.4 Structure 0954163

After multiple cross-sectioning, Horizontal projections and planes fitting Bridge 0954163 showed areas of interest where distances from the fitted planes were 0.0054 m above to -.076 m below the fitted planes, and the isolated points that represent damaged points below -.019 m can be seen in *Figure 80*.

.

(a)

(b)
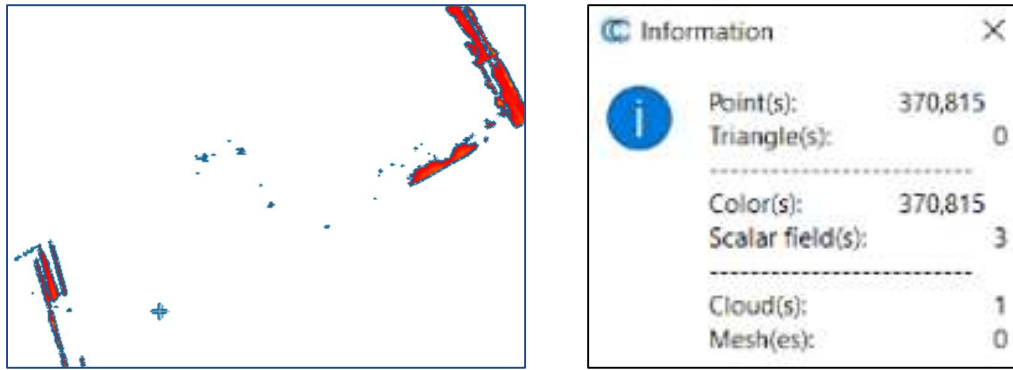
(c)
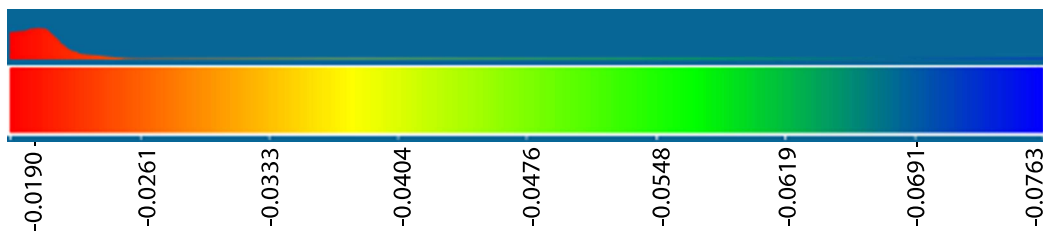
(d)

Figure 79. Analysis of Structure 0954163 Bridge Deck(a) Heat map of the plane fitted bridge deck (b) Elevation scale showing Elevations from 5.4 to - 76 mm (c) Isolated damaged points along with the number of points in the isolated cloud that represent damage,(d) Elevation scale showing elevations from -19 to -76 mm.

Table 10 shows the information on Bridge 0954163 and the result of the damage percentage analysis.

Table 10

Results of Damage Analysis for Structure 0954163

Bridge #	County	ADT	ADTT	Deck Condition	Damage Percentage
0954163	Hudson	37940	4	4	3.83%

5.8.5 Structure 1816155

After multiple cross-sectioning, Horizontal projections and planes fitting Bridge 1816155 showed areas of interest where distances from the fitted planes were 0.015 m above to -.093 m below the fitted planes, and the isolated points that represent damaged points below -.01 m can be seen in Figure 80.
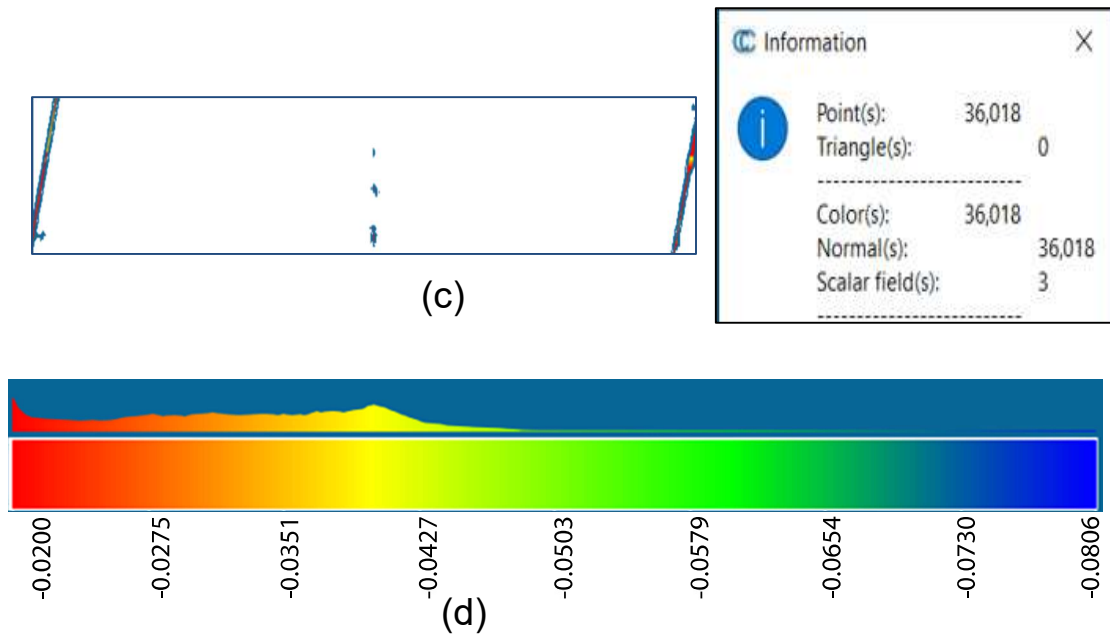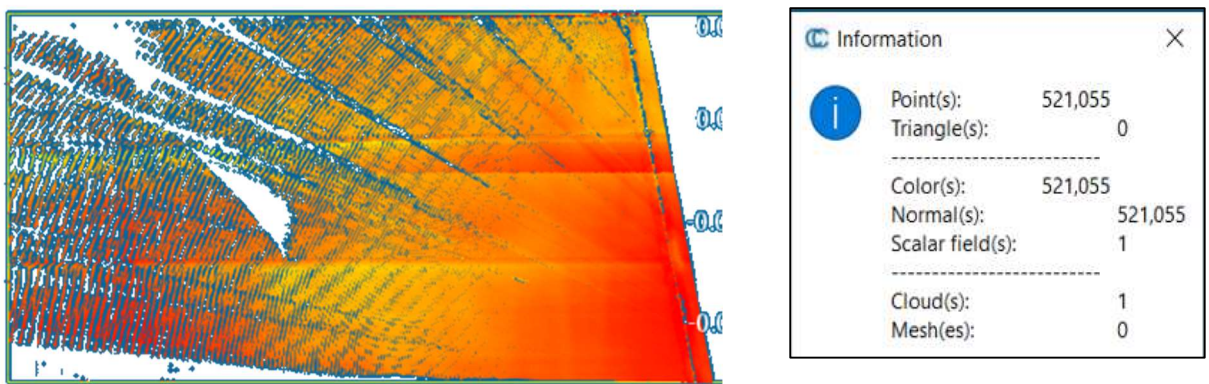

(a)
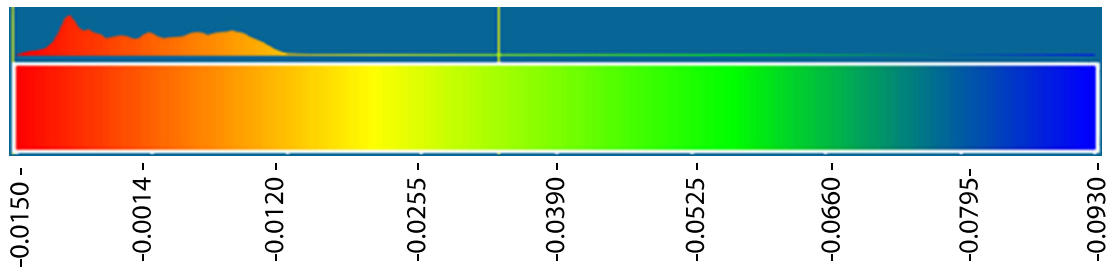
(b)

(c)

(d)

Figure 80. Analysis of Structure 1816155 Bridge Deck. (a) Heat map of the plane fitted bridge deck (b) Elevation scale showing Elevations from 15 to - 93 mm (c) Isolated damaged points along with the number of points in the isolated cloud that represent damage,(d) Elevation scale showing elevations from -10 to – 93 mm.

Table 11, shows the information on Bridge 1816155 and the result of the damage percentage analysis.
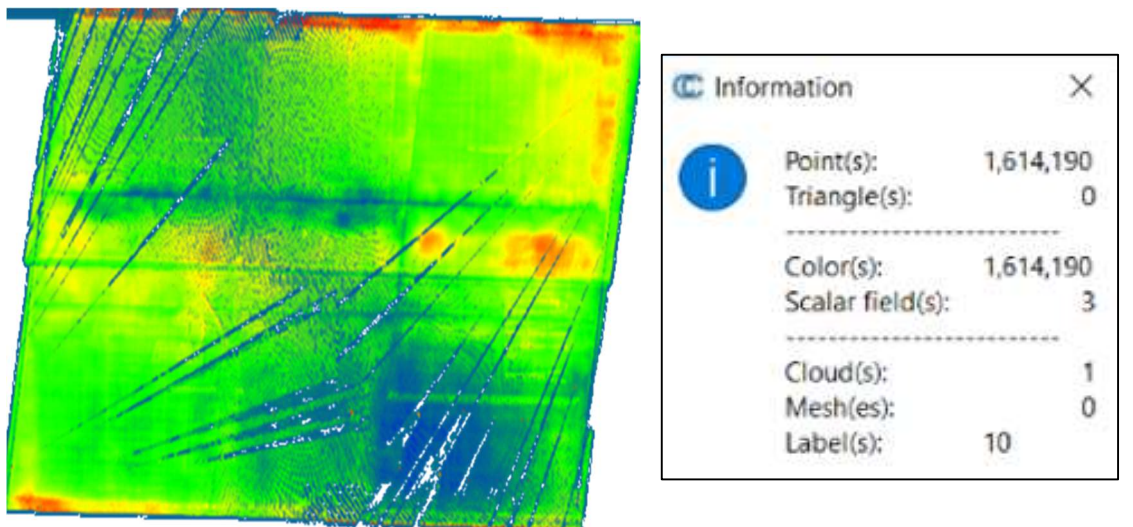
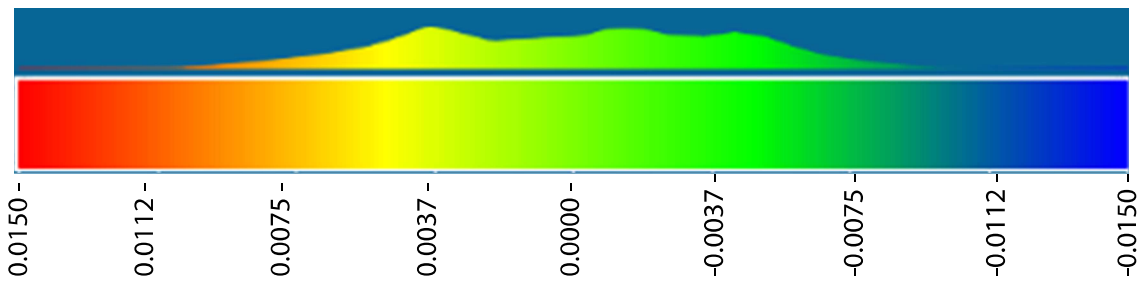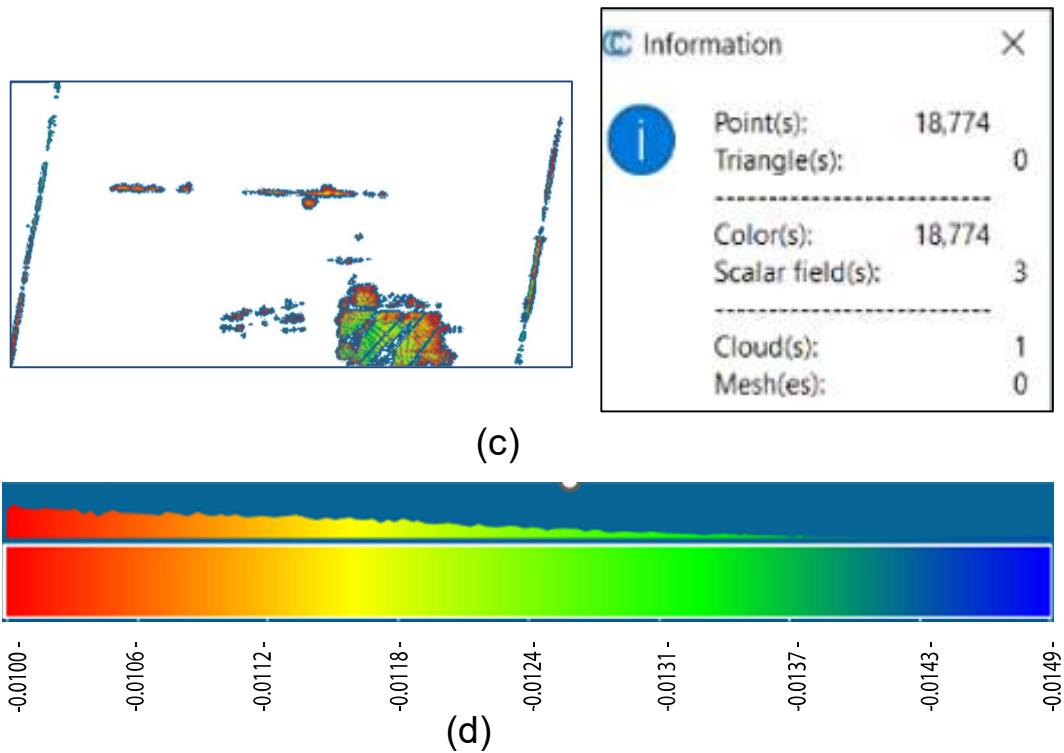**Table 11**

Results of Damage Analysis for Structure 1816155

Bridge #	County	ADT	ADTT	Deck Condition	Damage Percentage
1816155	Somerset	54406	14	3	5.07%

5.8.6 Structure 1816154

After multiple cross-sectioning, Horizontal projections and planes fitting Bridge 1816154 showed areas of interest where distances from the fitted planes were 0.0 m above to -.06 m below the fitted planes, and the isolated points representing damaged points below -.026 m can be seen in Figure 81.

(a)

(b)

(c)

(d)
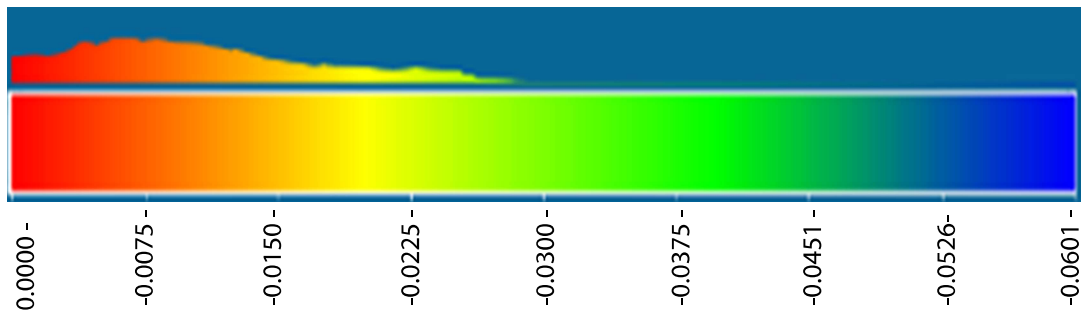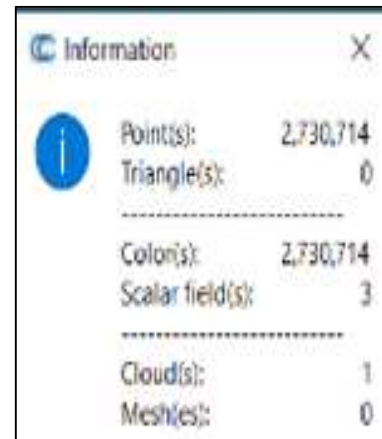
Figure 81. Analysis of Structure 1816154 Bridge Deck. (a) Heat map of the plane fitted bridge deck (b) Elevation scale showing Elevations from 0.0 to – 60 mm (c) Isolated damaged points along with the number of points in the isolated cloud that represent damage,(d) Elevation scale showing elevations from -26 to – 60 mm.

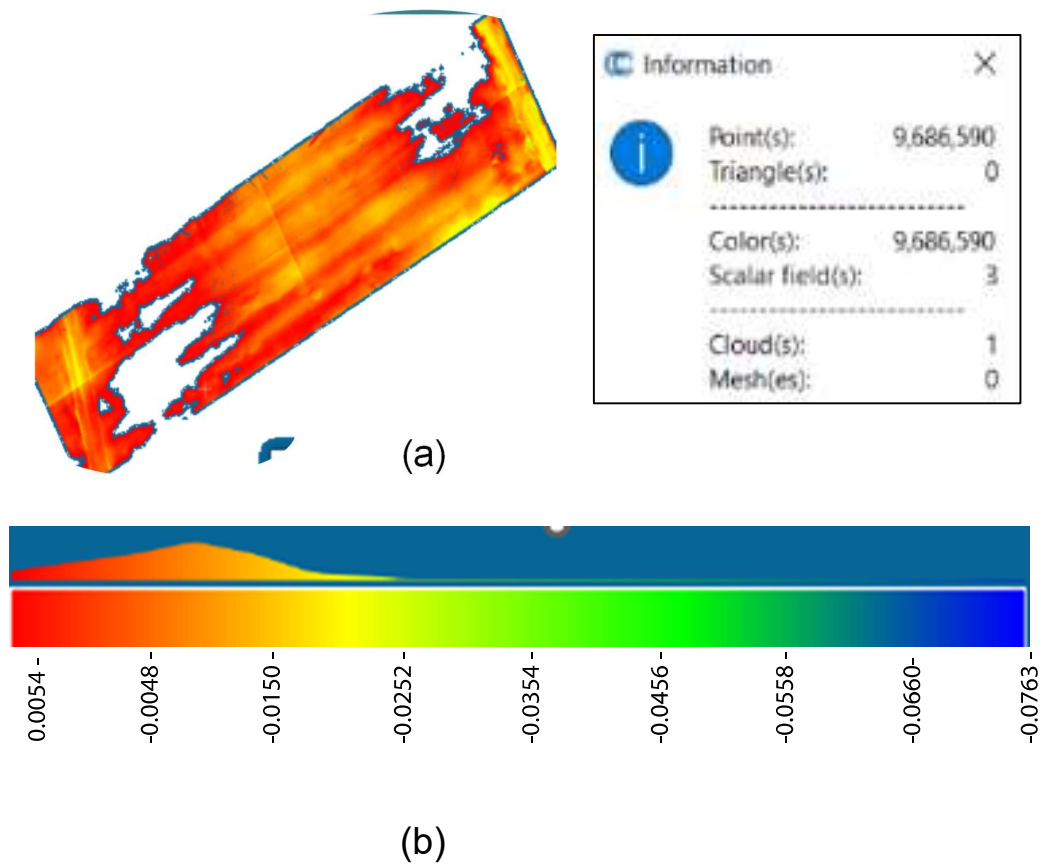Table **12**, shows the information on Bridge 1816154 and the result of the damage percentage analysis.

Table 12

Results of Damage Analysis for Structure 1816154

| Bridge #	County	ADT	ADTT	Deck Condition	Damage Percentage
1816154	Somerset	54406	14	6	2.52%

5.8.7 Structure 361632N

After multiple cross-sectioning, Horizontal projections and planes fitting Bridge 361632N showed areas of interest where distances from the fitted planes were 0.013 m above to -.05 m below the fitted planes, and the isolated points that represent damaged points below -.012 m can be seen in Figure 82.

(a)

(b)

(c)

(d)

Figure 82. Analysis of Structure 361632N Bridge Deck (a) Heat map of the plane fitted bridge deck (b) Elevation scale showing Elevations from 13 to – 50 (c) Isolated damaged points along with the number of points in the isolated cloud that represent damage,(d) Elevation scale showing elevations from -12 to – 50

Table **13** shows the information on Bridge 361632N and the result of the damage percentage analysis.

**Table 13**

Results of Damage Analysis for Structure 361632N

Bridge #	County	ADT	ADTT	Deck Condition	Damage Percentage
361632N	Bergen	36400	1	8	1.31 %

5.8.8 Structure 1317154

After multiple cross-sectioning, Horizontal projections and planes fitting Bridge 1317154 showed areas of interest where distances from the fitted planes were 0.0174 m above to -.041 m below the fitted planes, and the isolated points that represent damaged points below -.008 m can be seen in Figure 83.
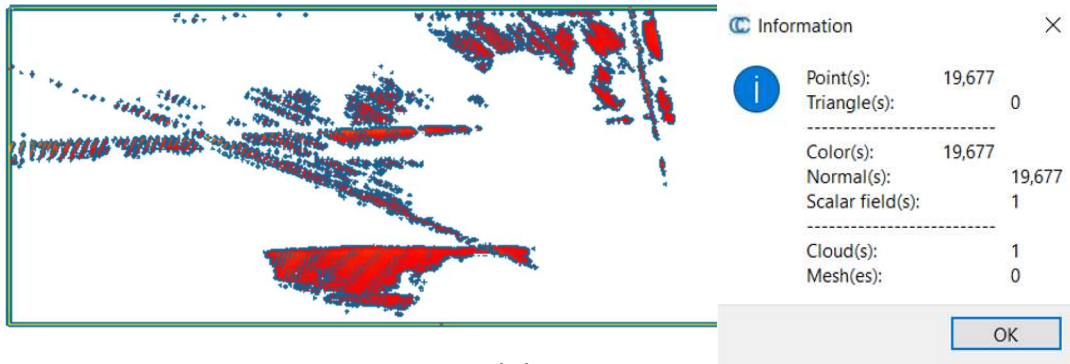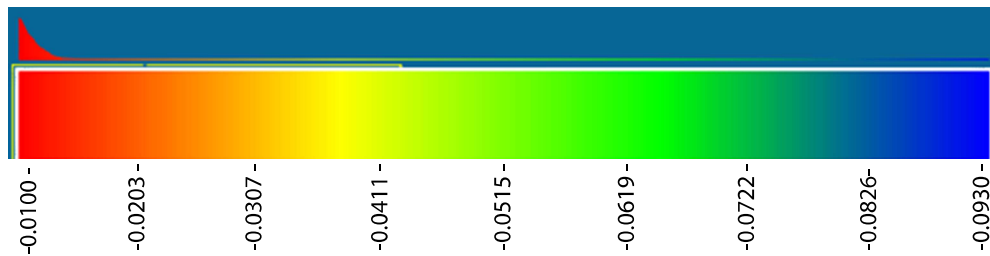

(a)

(b)

(c)

(d)
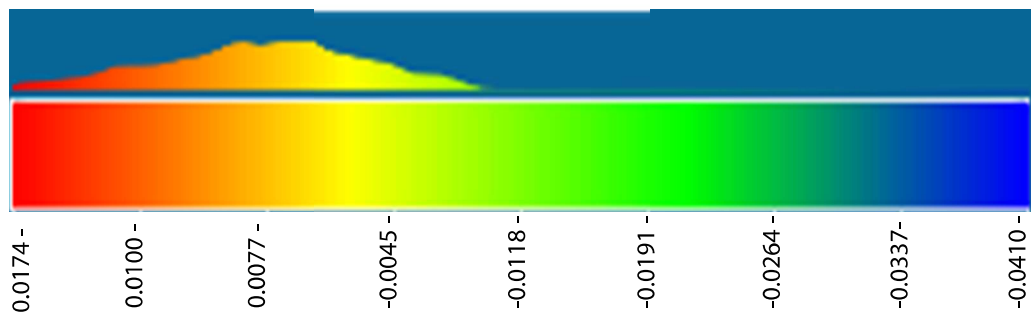
Figure 83. Analysis of Structure 1317154 Bridge Deck. (a) Heat map of the plane fitted bridge deck (b) Elevation scale showing Elevations from 17.4 to – 41 mm (c) Isolated damaged points along with the number of points in the isolated cloud that represent damage,(d) Elevation scale showing elevations from -8 to – 41 mm.

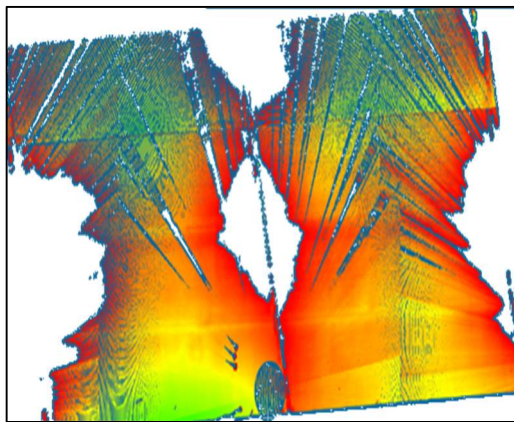Table 14 shows the information on Bridge 1317154 and the result of the damage percentage analysis.

Table 14

*Results of Damage Analysis for Structure 1317154*

Bridge #	County	ADT	ADTT	Deck Condition	Damage Percentage
1317154	Monmouth	30130	5	7	2.2%

5.8.9 Structure 0411163

After multiple cross-sectioning, Horizontal projections and planes fitting Bridge 0411163 showed areas of interest where distances from the fitted planes were 0.0129 m above to -.027 m below the fitted planes, and the isolated points that represent damaged points below -.0125 m can be seen in Figure 84.
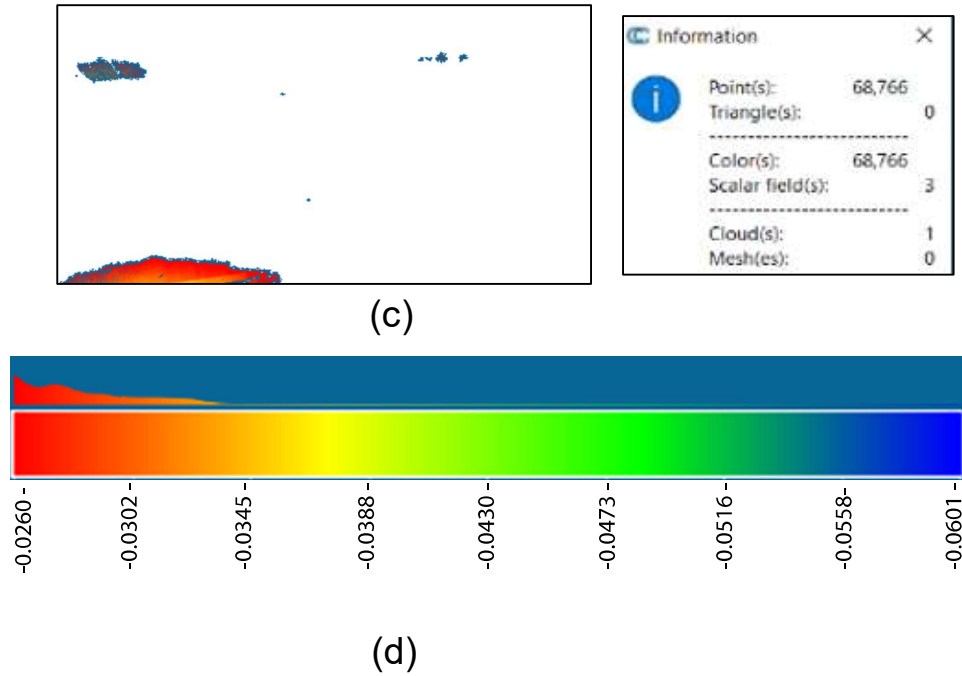

(a)

(b)

(c)

(d)
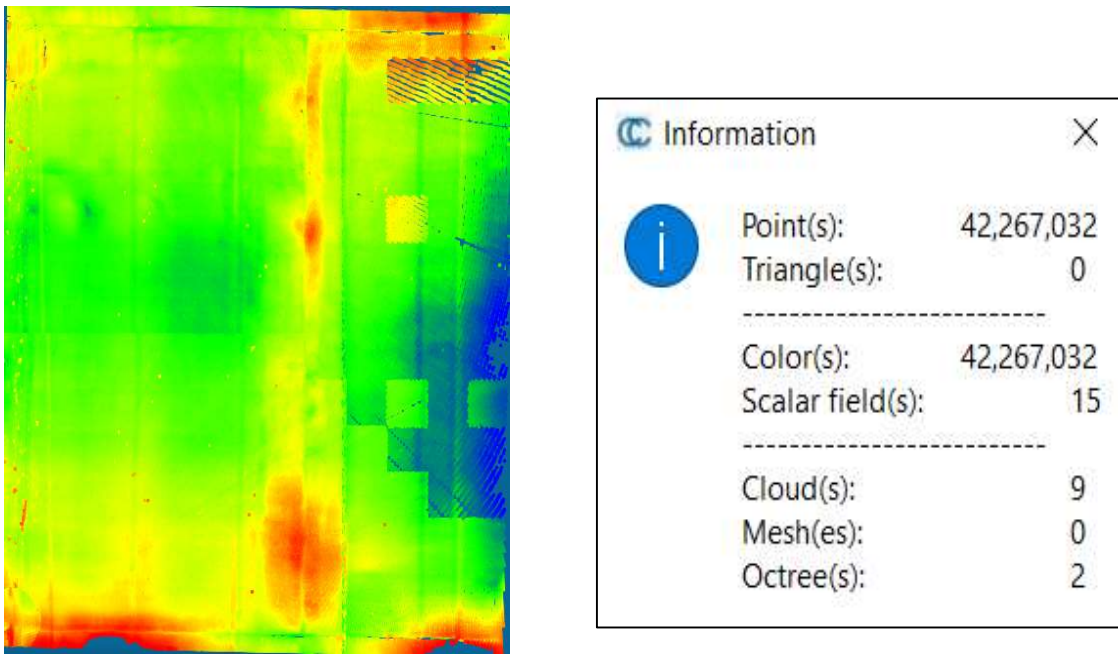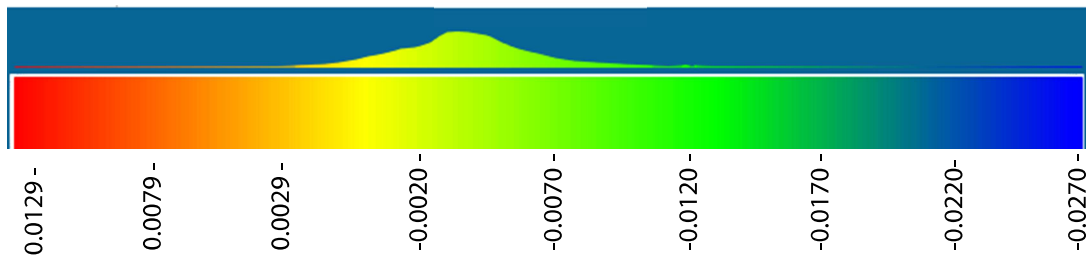
Figure 84. Analysis of Structure 0411163 Bridge Deck. (a) Heat map of the plane fitted bridge deck (b) Elevation scale showing Elevations from 12.9 to – 27 mm (c) Isolated damaged points along with the number of points in the isolated cloud that represent damage,(d) Elevation scale showing elevations from -12.5 to – 27 mm.

Table 15 shows the information on Bridge 0411163 and the result of the damage percentage analysis.

Table 15

Results of Damage Analysis for Structure 0411163

Bridge #	County	ADT	ADTT	Deck Condition	Damage Percentage
0411163	Camden	65984	5	5	2.72%

5.8.10 Structure 0411164

After multiple cross-sectioning, Horizontal projections and planes fitting Bridge 0411164 showed areas of interest where distances from the fitted planes were 0.015 m above to -.067 m below the fitted planes, and the isolated points that represent damaged points below -.01 m can be seen in Figure 85.

(a)

(b)

(c)

(d)
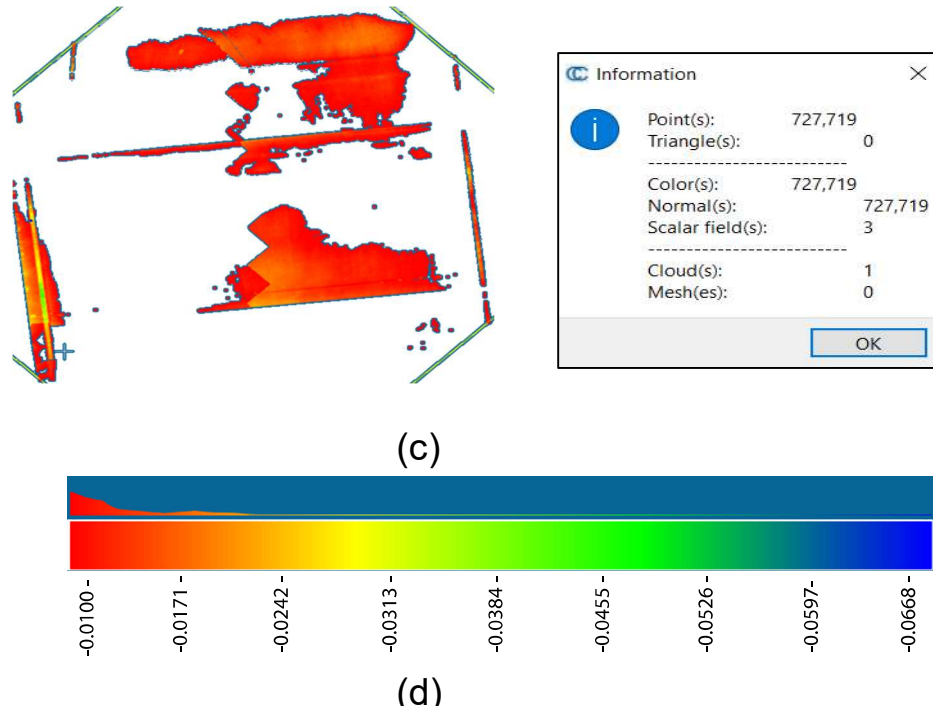
Figure 85. Analysis of Structure 0411164 Bridge Deck. (a) Heat map of the plane fitted bridge deck (b) Elevation scale showing Elevations from 15 to – 67 mm (c) Isolated damaged points along with the number of points in the isolated cloud that represent damage,(d) Elevation scale showing elevations from -10 to – 67 mm.

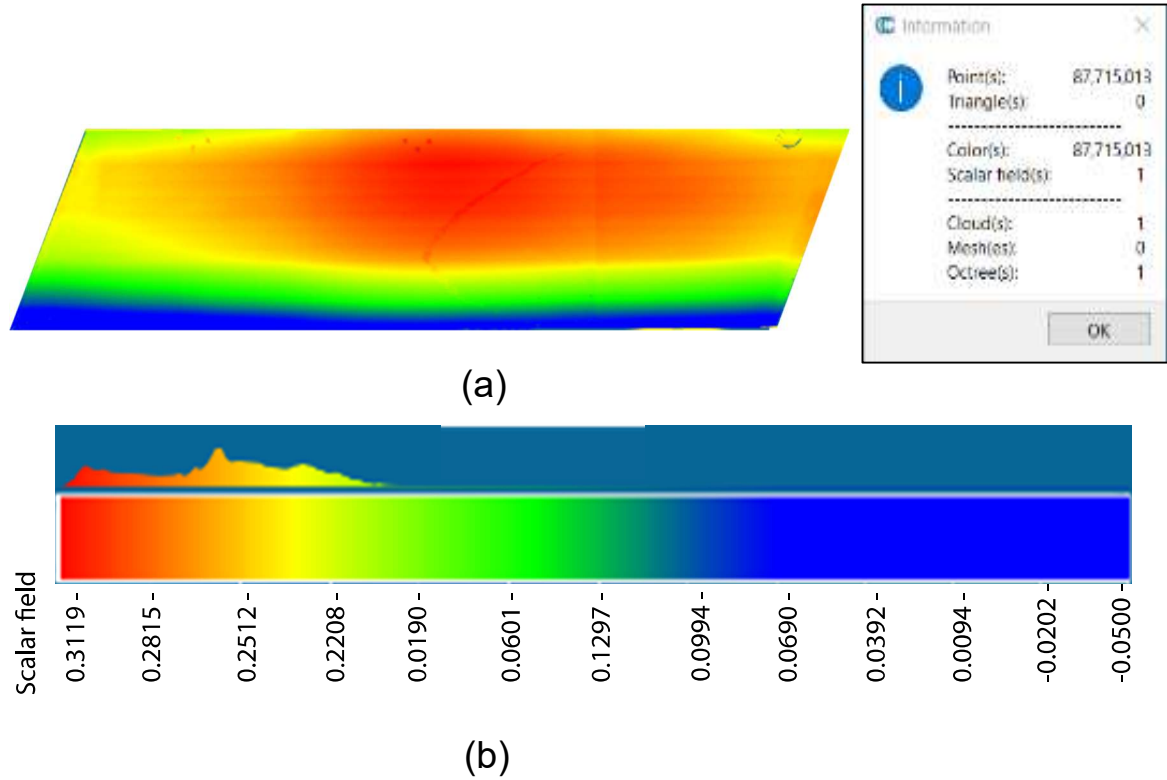Table 16 shows the information on Bridge 0411164 and the result of the damage percentage analysis.

Table 16

Results of Damage Analysis for Structure 0411164

Bridge #	County	ADT	ADTT	Deck Condition	Damage Percentage
0411164	Camden	65349	5	8	2.00%

5.8.11 Structure 0805F03

After multiple cross-sectioning, Horizontal projections and planes fitting Bridge 0805F03 showed areas of interest where distances from the fitted planes were 0.015 m above to -.042 m below the fitted planes, and the isolated points that represent damaged points below -.0135 m can be seen in Figure 86.
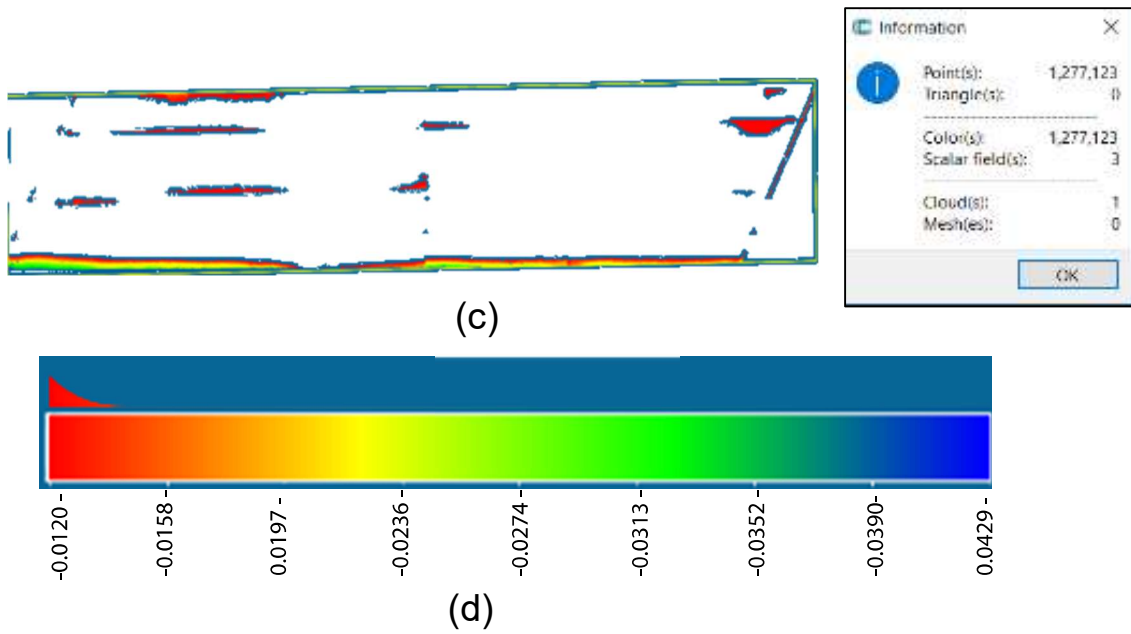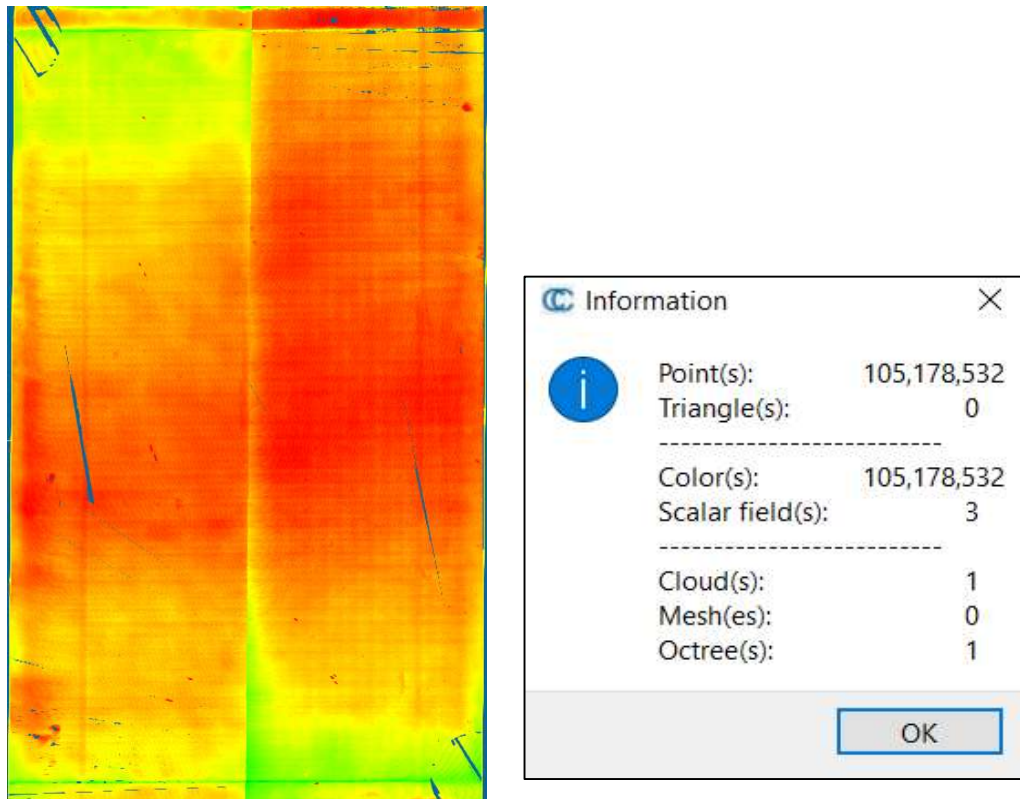

(a)
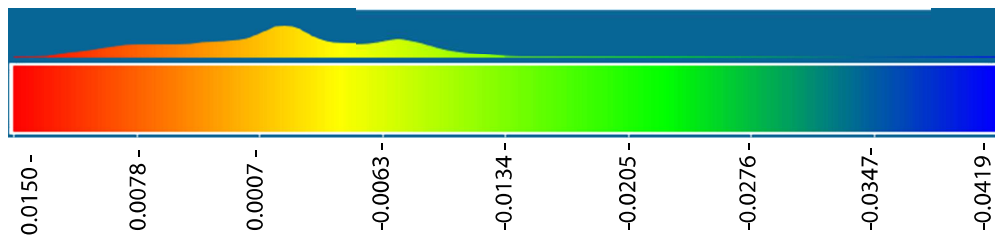
(b)
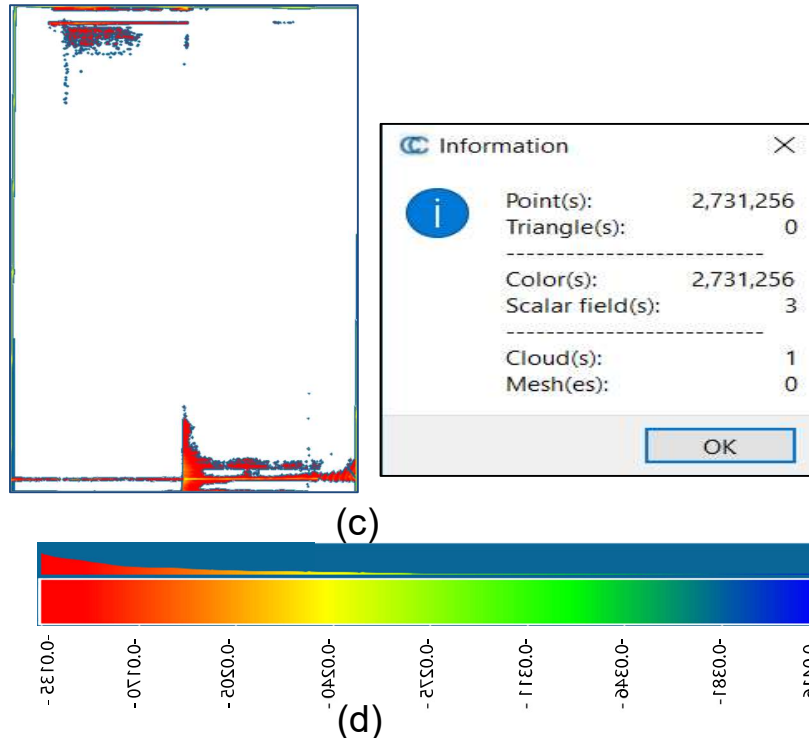
Figure 86. Analysis of Structure 0805F03 Bridge Deck. (a) Heat map of the plane fitted bridge deck (b) Elevation scale showing Elevations from 15 to – 42 mm (c) Isolated damaged points along with the number of points in the isolated cloud that represent damage,(d) Elevation scale showing elevations from -13.5vto – 42 mm.

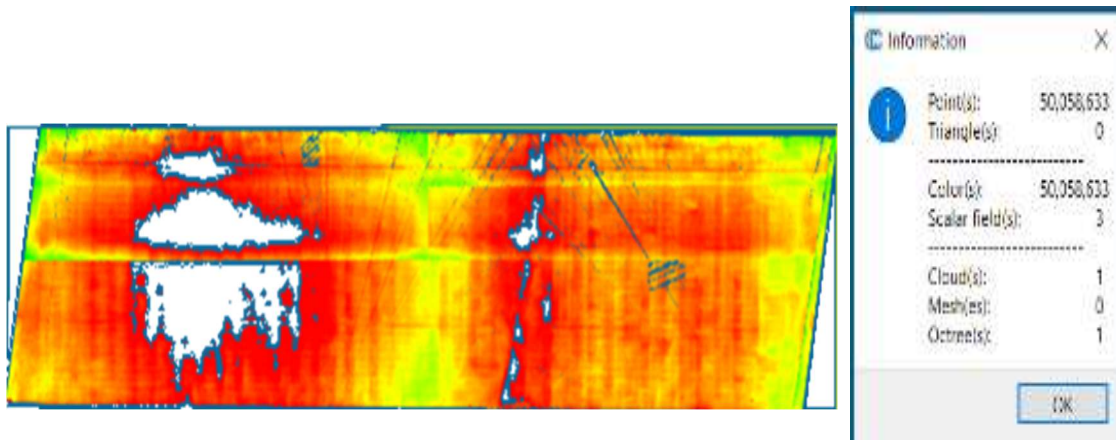Table 17 shows the information on Bridge 0805F03 and the result of the damage percentage analysis.

Table 17

Results of Damage Analysis for Structure 0805F03

Bridge #	County	ADT	ADTT	Deck Condition	Damage Percentage
0805F03	Gloucester	3626	3	6	2.6%

5.8.12 Structure 0807P01

After multiple cross-sectioning, Horizontal projections and planes fitting Bridge 0807P01 showed areas of interest where distances from the fitted planes were 0.0m above to -.038 m below the fitted planes, and the isolated points that represent damaged points below -.028 m can be seen in Figure 87.
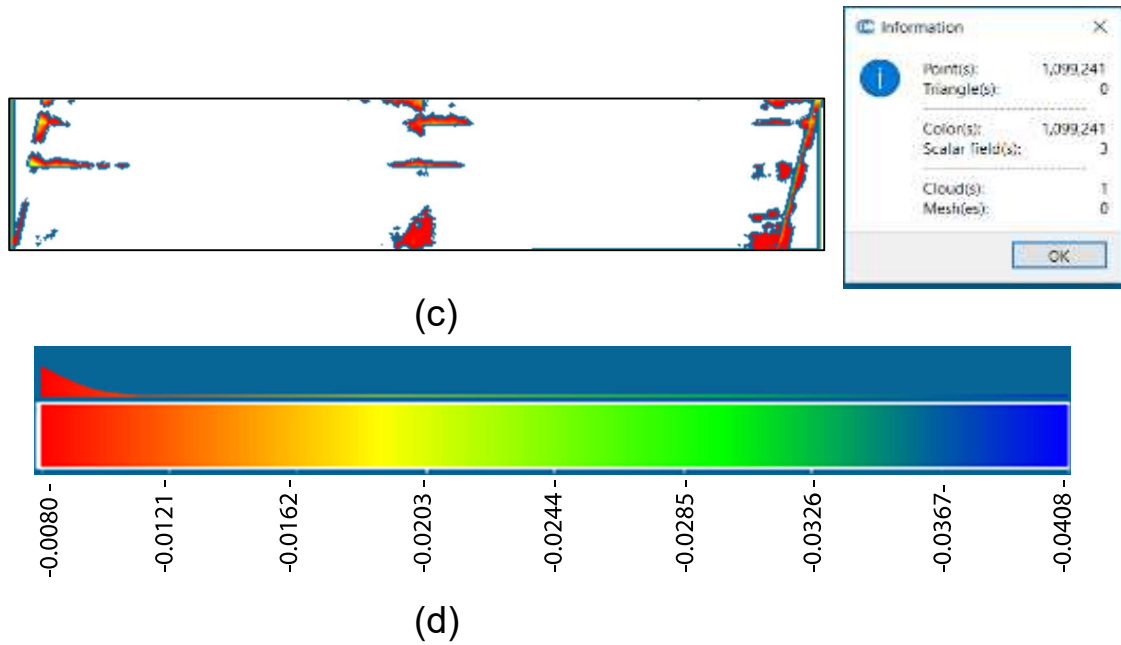

(a)

(b)
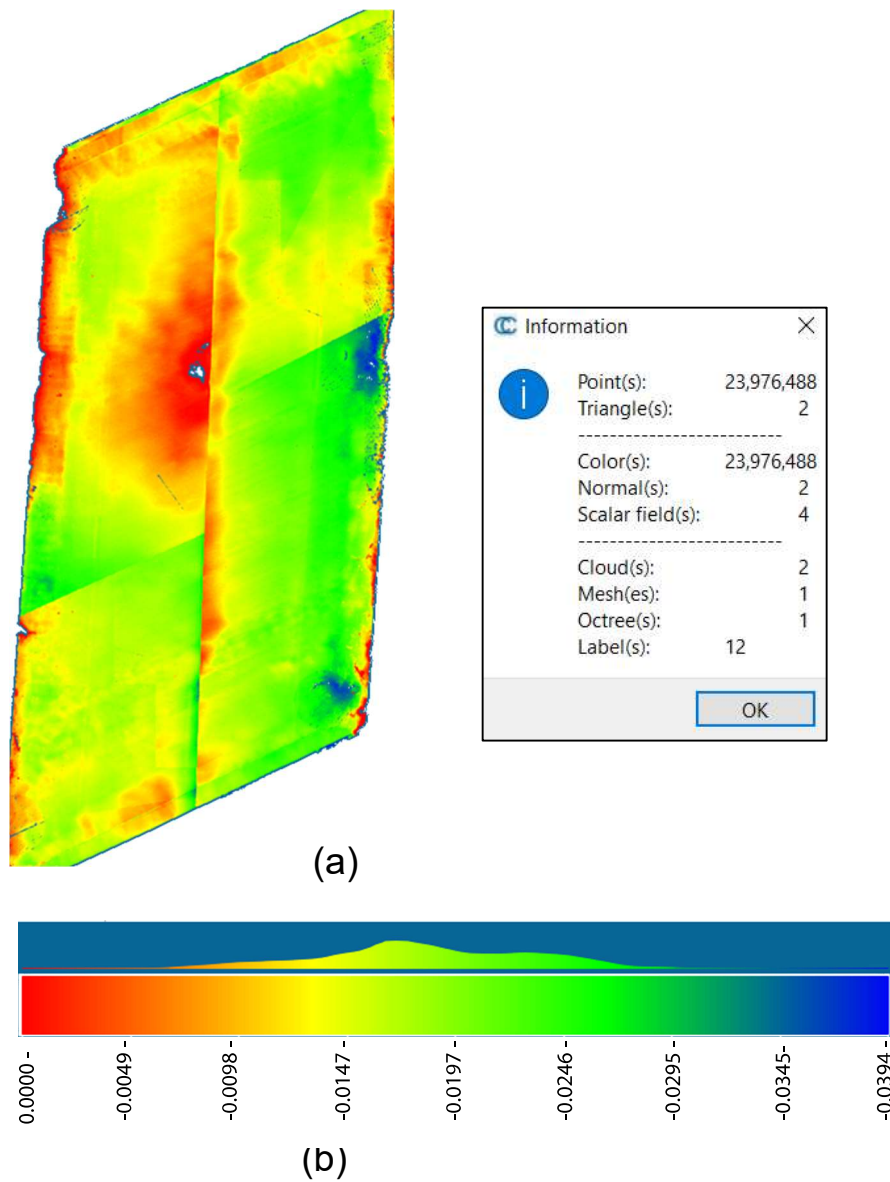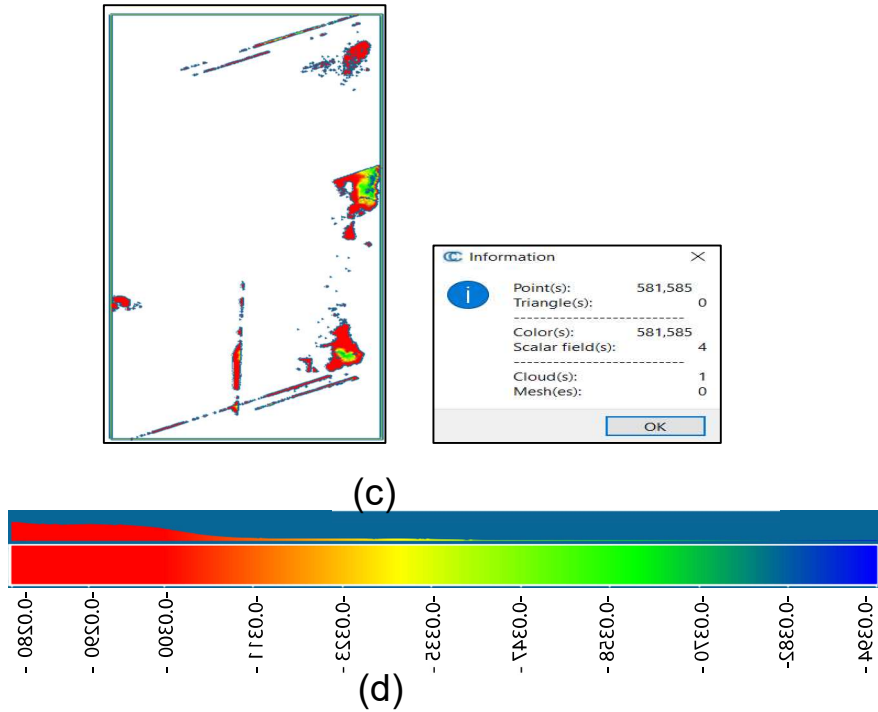
Figure 87. Analysis of Structure 0807P01 Bridge Deck.(a) Heat map of the plane fitted bridge deck (b) Elevation scale showing Elevations from 0.0 to – 38 mm (c) Isolated damaged points along with the number of points in the isolated cloud that represent damage,(d) Elevation scale showing elevations from -28 to – 38 mm.

Table **18** shows the information on Bridge 0807P01 and the result of the damage percentage analysis.

Table 18

Results of Damage Analysis for Structure 0807P01

Bridge #	County	ADT	ADTT	Deck Condition	Damage Percentage
0807P01	Gloucester	2600	3	7	2.43%

5.8.13 Structure 0833150

After multiple cross-sectioning, Horizontal projections and planes fitting Bridge 0833150 showed areas of interest where distances from the fitted planes were 0.008 m above to -.036 m below the fitted planes, and the isolated points that represent damaged points below -.0155 m can be seen in Figure 88.
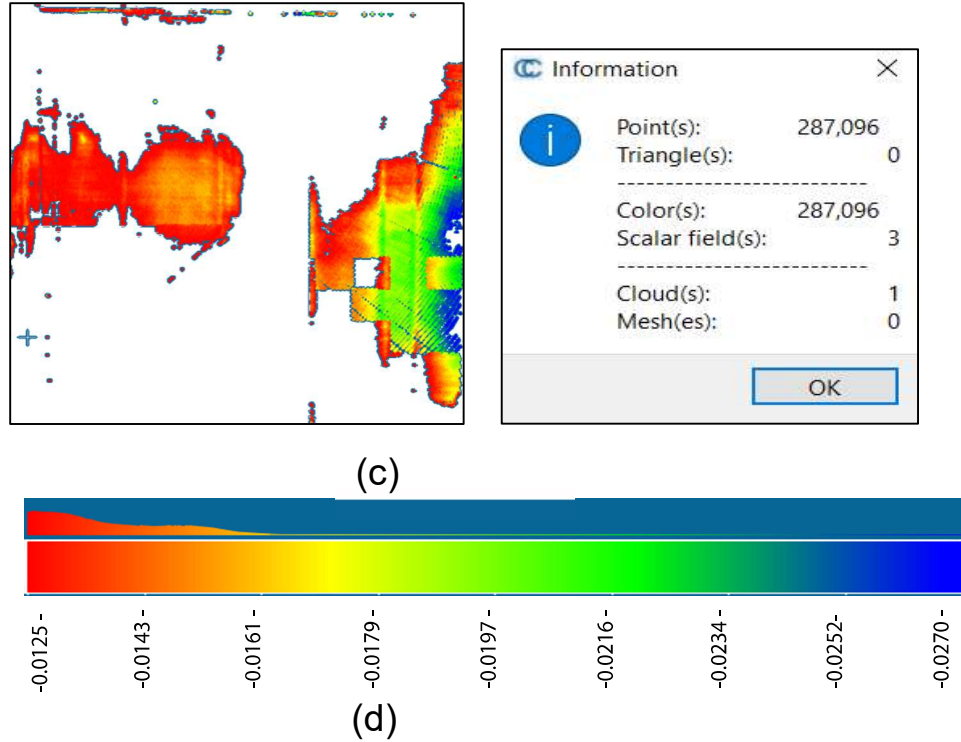

(a)

(b)

(c)

(d)
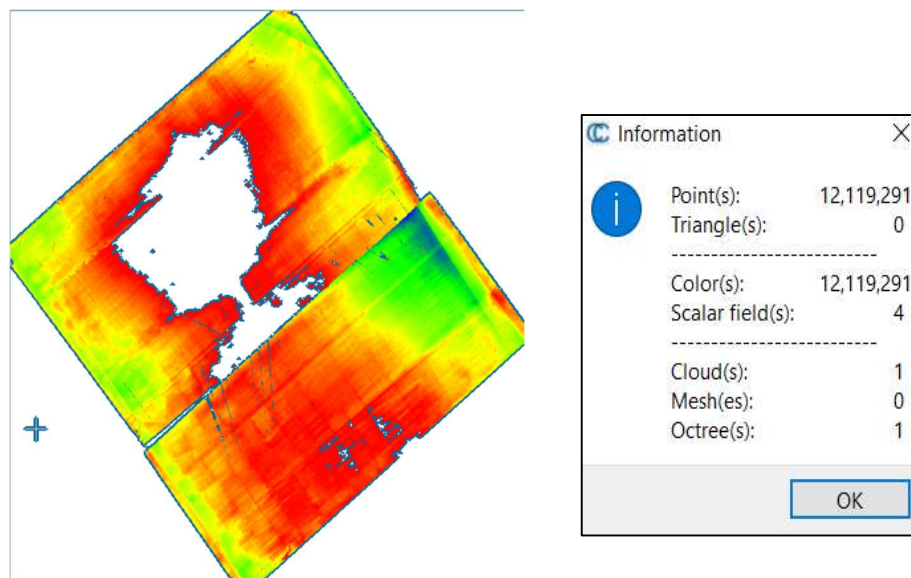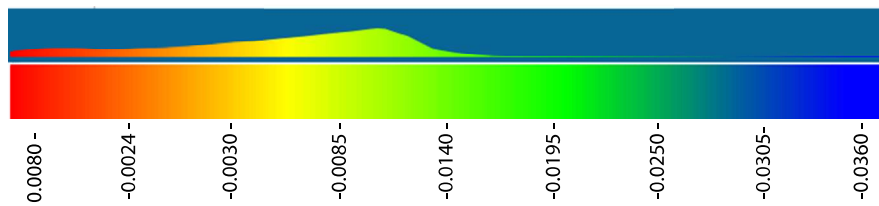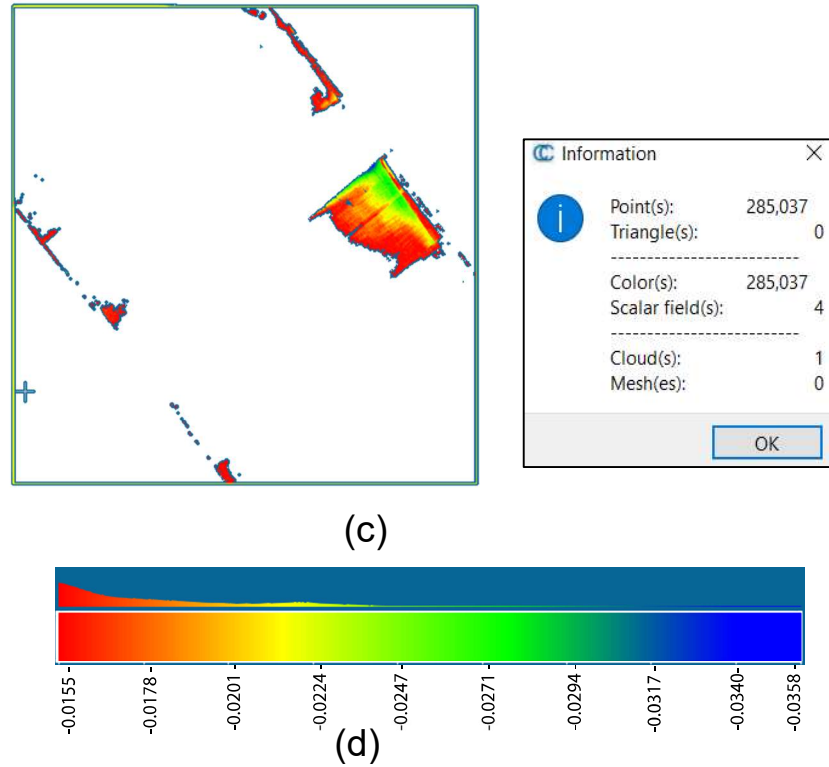
Figure 88. Analysis of Structure 0807P01 Bridge Deck. (a) Heat map of the plane fitted bridge deck (b) Elevation scale showing Elevations from 8 to –36 mm (c) Isolated damaged points along with the number of points in the isolated cloud that represent damage,(d) Elevation scale showing elevations from -15.5 to – 36 mm.

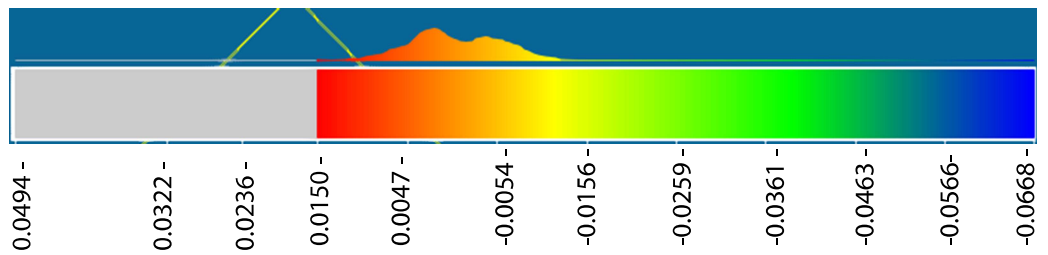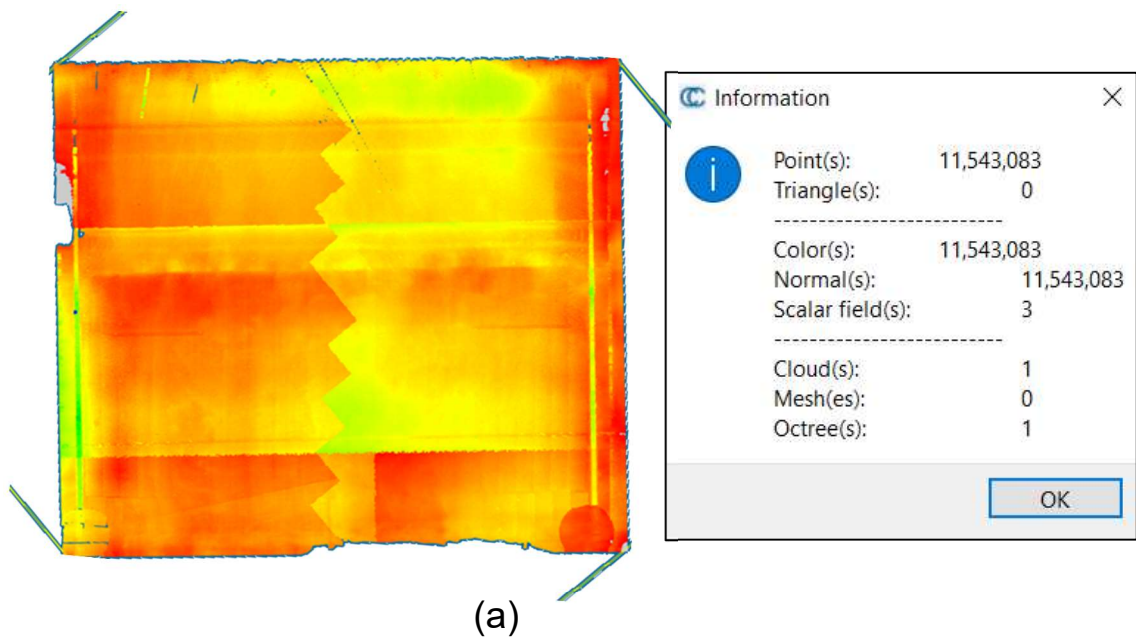Table 19 shows the information on Bridge 0833150 and the result of the damage percentage analysis.

Table 19

Results of Damage Analysis for Structure 0833150

Bridge #	County	ADT	ADTT	Deck Condition	Damage Percentage
0833150	Gloucester	11740	4	7	2.35%

In this chapter, objective number 3 was successfully achieved, which involved quantifying the information gained from deploying LiDAR on operating bridges in New Jersey to estimate the condition rating based on the level of damage found on the decks' top surface. The information from Chapter 4, where the BEAST deck was analyzed, and Chapter 5, where the operating bridges in New Jersey were analyzed, was utilized to analyze and establish a deterioration trend further validated by the information obtained from analyzing the BEAST deck. Valuable insights into the condition of bridges in New Jersey and the impact of LiDAR technology in assessing bridge health were provided in this chapter.

The results of this study demonstrate a clear correlation between the Bridge Deck Condition rating and the percentage of damaged points identified as spalls deeper than 1" in depth and more significant than 6" in diameter. After analyzing LiDAR data for 14 bridge decks and validating these findings through the analysis of the BEAST bridge specimen and comparison with visual inspection reports, a trend was developed that ties these variables together. This trend provides valuable insights into the condition of bridge decks and can inform decision-making processes related to bridge maintenance and repair. The findings of this study highlight the importance of regular monitoring and timely repairs to prevent further deterioration of the bridge deck and ensure the safety and longevity of the bridge. The Analysis results can be found in Table 20 and *Figure 89*:

Table 20

Damage Percentage Analysis through Least Square Plane Fitting Results

Bridge #	Deck Condition	points in damaged area spall>1."	points in Point Cloud	Damage Percentage
416151	4	430004	10948500	3.93%
821155	9	36018	3340916	1.08%
18G0701	9	18774	1614190	1.16%
954163	4	370815	9676590	3.83%
1816155	3	26396	521055	5.07%
1816154	6	68766	2730714	2.52%
361632N	8	1277123	97715013	1.31%
1317154	7	1099241	50058036	2.20%
411163	5	287096	10566997	2.72%
411164	8	230851	11543083	2.00%
0805F03	6	2731256	1.05E+08	2.60%
0807P01	7	581585	23976488	2.43%
833150	7	285037	12119792	2.35%
BEAST	5	1022188	36085551	2.83%
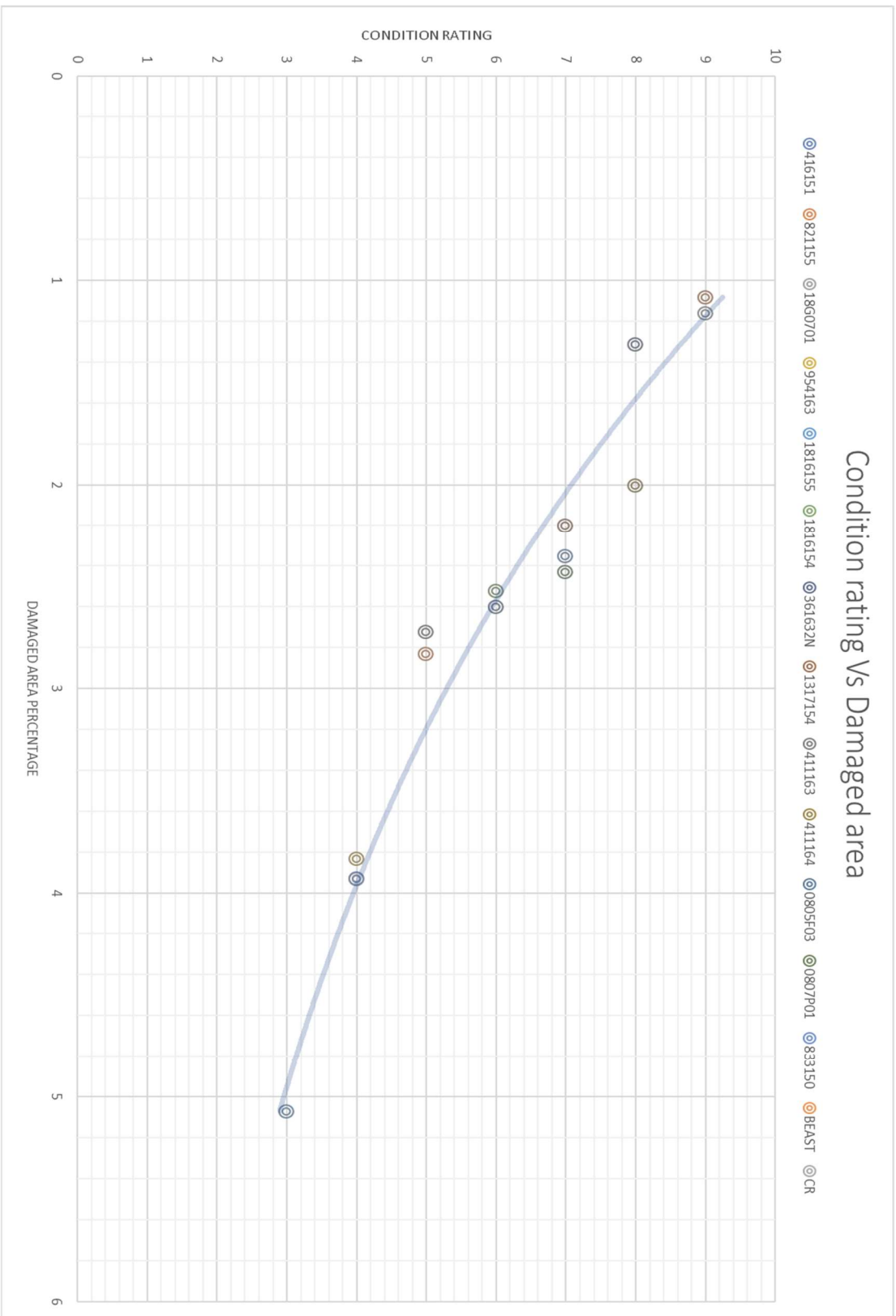
Figure 89. Condition Rating Vs Damaged area Analysis Trend

Chapter 6

Comparing Strain Gauges to LiDAR for Structural Health Monitoring: A Cost and Benefits Analysis

Structural health monitoring is crucial for maintaining the safety and integrity of buildings, bridges, and other structures. Traditional methods of structural health monitoring, such as strain gauges, have been used for many years. However, the emergence of LiDAR technology has provided a new, efficient, and accurate way to monitor the health of structures. This chapter compares the cost and benefits of using strain gauges versus LiDAR for structural health monitoring, based on the data provided.

By interviewing companies in charge of the instrumentation of bridges subjected to structural health monitoring and long-term evaluation, the following information was collected: the short-term structural monitoring system for the steel girder bridge using 64 strain gauges cost a total of $116,686. The breakdown of the costs included project preparation and management at $5,700, site visit at $3,500, instrumentation design and build-out at $13,000, system installation at $35,970, analysis and reporting at $19,000, system removal at $7,750, supplies at $22,016, and equipment rental at $9,750.

In comparison, the cost of a LiDAR system for structural health monitoring varies depending on factors such as the size and complexity of the structure, the frequency of scans, and the data processing and analysis requirements. However, the FARO Focus S 150 Laser Scanner, a popular LiDAR system used for structural health monitoring, is priced at around $50,000 USD. By adding a similar breakdown to the short-term strain gauges monitoring system, the cost of a LiDAR system for structural health monitoring would

include a site visit at $3,500 and a similar analysis and reporting at $19,000 due to the computational expensive data processing required for point cloud data. However, it would not include instrumentation design and build-out at $13,000, system installation at $35,970, system removal at $7,750, supplies at $22,016, and equipment rental at $9,750.

While the upfront cost of a LiDAR system may be higher than that of a traditional strain gauge system, the efficiency, accuracy, and frequency of data collection provided by LiDAR can result in significant cost savings over the long term. Traditional strain gauges require physical measurements and inspections, which can be time-consuming and costly. LiDAR, on the other hand, can quickly capture a large amount of data points in 3D, allowing for a more comprehensive and accurate assessment of structural health. This can reduce the need for physical measurements and inspections, resulting in significant cost savings. Additionally, LiDAR scans can be conducted remotely, reducing the need for on-site personnel and equipment, and improving safety.

In comparison, the FARO Focus S 150 Laser Scanner, a popular LiDAR system used for structural health monitoring, is priced at around $50,000 USD. However, the cost of a LiDAR system for structural health monitoring varies depending on factors such as the size and complexity of the structure, the frequency of scans, and the data processing and analysis requirements. Therefore, a comprehensive cost-benefit analysis should be conducted to determine the most appropriate monitoring system for a given structure. Based on the data provided, incorporating LiDAR for structural health monitoring can have several cost benefits over traditional methods.

Chapter 7

Conclusions and Recommendations

7.1 Conclusions

The goals of this research were successfully met through LiDAR scanning on operating bridges in New Jersey, analyzing the results using two different techniques, and validating the findings using the BEAST bridge specimen as a reference. The main objective of correlating the deck condition rating with the percentage of damaged surface area was achieved, providing valuable insights into the deterioration trend of bridge decks.

Based on the analysis of the NDE and LiDAR data, it was found that the condition rating of bridge decks can be correlated with the percentage of damaged surface area. This correlation was established by comparing the results obtained from scanning operating bridges in New Jersey with the BEAST bridge specimen, which served as a reliable validator. By establishing this correlation, it was possible to develop a deterioration trend that can be used to prioritize bridge inspections and maintenance efforts.

The findings of this research have significant implications for bridge maintenance and repair operations. By utilizing LiDAR technology as a non-destructive evaluation technique, it is possible to accurately assess the health of bridge decks and predict their future deterioration rates. This information can be used to develop strategies to extend the service life of bridges, prioritize repair and maintenance efforts, and effectively manage limited resources.

In conclusion, this research has demonstrated the effectiveness of LiDAR scanning for evaluating the condition of operating bridges in New Jersey and establishing a

correlation between deck condition rating and the percentage of damaged surface area. The results obtained from this study provide valuable insights into the deterioration trend of bridge decks and highlight the potential of LiDAR technology as a reliable tool for bridge assessment and maintenance planning. Further research and scanning of more bridges can enhance the accuracy and reliability of the established deterioration trend, contributing to the development of robust strategies for preserving the structural health of bridge decks and ensuring the safety and longevity of bridge infrastructure.

For future research, the research team will expand the scanning to include more bridges in New Jersey to help in coming out with deterioration patterns and a better understanding of the main factors causing the rapid deterioration of bridge decks; other factors affecting the deck will be taken into consideration for future research including the Average Daily Traffic (ADT), the Average Daily Truck Traffic (ADTT) and the wearing surface material.

LiDAR proved its efficiency as a geometry-capturing tool for bridges' decks. The future goal through further studies and analysis is to deploy Terrestrial Lidar Scanning TLS as a screening technique to add to the suite of non-destructive evaluation (NDE) techniques to address early bridge deck deterioration efficiently and accurately.

7.2 Recommendations

One potential area of research that could be explored is the use of LiDAR technology for monitoring the condition of other critical infrastructure, such as buildings or dams. Research could investigate how LiDAR data can be integrated into existing assessment protocols to provide more comprehensive data on the condition of these

structures. Additionally, research could explore how LiDAR data can be used for structural health monitoring, such as detecting early signs of damage or wear, and predicting future maintenance needs.

Another area of research that could be explored is the development of automated analysis tools that can process and interpret LiDAR data to identify areas of concern or track changes in condition over time. This could involve developing machine learning algorithms that can detect subtle changes in bridge morphology, such as cracking or warping, or identify patterns in the data that indicate potential issues.

Furthermore, additional research could focus on the development of LiDAR technology itself, such as the improvement of sensors, algorithms, and data processing techniques. This could involve exploring new types of LiDAR sensors that are more accurate, have greater range, or can be deployed in more challenging environments. Additionally, research could focus on improving the speed and accuracy of data processing algorithms, allowing for real-time condition assessments and more efficient data analysis. Overall, the integration of LiDAR technology into SOPs for bridge condition assessment represents a promising area of research with many potential benefits. By continuing to investigate and refine the use of LiDAR technology in this context, we can improve the safety, reliability, and longevity of critical infrastructure across the country.

References

1. Abdelkhalek, S. I. F. M. (n.d.). *Managing the inspection process of concrete bridge decks*. PolyU Electronic Theses: Home. Retrieved April 21, 2023, from https://theses.lib.polyu.edu.hk/handle/200/11748

2. Abdelkhalek, S., & Zayed, T. (2020). Comprehensive inspection system for Concrete Bridge Deck Application: Current situation and future needs. *Journal of Performance of Constructed Facilities*, *34*(5). https://doi.org/10.1061/(asce)cf.1943-5509.0001484

3. Abu Dabous, S., Yaghi, S., Alkass, S., & Moselhi, O. (2017). Concrete bridge deck condition assessment using IR thermography and ground penetrating radar technologies. *Automation in Construction*, *81*, 340–354. https://doi.org/10.1016/j.autcon.2017.04.006

4. Alla, S., & Asadi, S. S. (2020). Integrated methodology of structural health monitoring for civil structures. *Materials Today: Proceedings*, *27*, 1066–1072. https://doi.org/10.1016/j.matpr.2020.01.435

5. Alsharqawi, M., Zayed, T., & Abu Dabous, S. (2018). Integrated condition rating and forecasting method for bridge decks using visual inspection and ground penetrating radar. *Automation in Construction*, *89*, 135–145. https://doi.org/10.1016/j.autcon.2018.01.016

6. Alsharqawi, M., Zayed, T., & Abu Dabous, S. (2018). Integrated condition rating and forecasting method for bridge decks using visual inspection and ground penetrating radar. *Automation in Construction*, *89*, 135–145. https://doi.org/10.1016/j.autcon.2018.01.016

7. Amiri, A. S., Erdogmus, E., & Richter-Egger, D. (2021). A comparison between ultrasonic guided wave leakage and half-cell potential methods in detection of corrosion in reinforced concrete decks. *Signals*, *2*(3), 413–433. https://doi.org/10.3390/signals2030026

8. ASCE. (2021). *ASCE's 2021 infrastructure report card*. ASCE Infrastructure Report. Retrieved December 13, 2022, from https://www.infrastructurereportcard.org/wp-content/uploads/2020/12/Bridges-2021.pdf

9. Basheer, P. A. M., Chidiact, S. E., & Long, A. E. (1996). Predictive models for deterioration of concrete structures. *Construction and Building Materials*, *10*(1), 27–37. https://doi.org/10.1016/0950-0618(95)00092-5

10. Bolourian, N., & Hammad, A. (2020). Lidar-equipped UAV path planning considering potential locations of defects for Bridge Inspection. *Automation in Construction*, *117*, 103250. https://doi.org/10.1016/j.autcon.2020.103250

11. Bolourian, N., & Hammad, A. (2020). Lidar-equipped UAV path planning considering potential locations of defects for Bridge Inspection. *Automation in Construction*, *117*, 103250. https://doi.org/10.1016/j.autcon.2020.103250

12. Cha, G., Park, S., & Oh, T. (2019). A terrestrial LIDAR-based detection of shape deformation for maintenance of bridge structures. *Journal of Construction Engineering and Management*, *145*(12). https://doi.org/10.1061/(asce)co.1943-7862.0001701

13. Cha, G., Sim, S.-H., Park, S., & Oh, T. (2020). Lidar-based bridge displacement estimation using 3D spatial optimization. *Sensors*, *20*(24), 7117. https://doi.org/10.3390/s20247117

14. Chen, S., Laefer, D. F., Mangina, E., Zolanvari, S. M., & Byrne, J. (2019). UAV bridge inspection through evaluated 3D reconstructions. *Journal of Bridge Engineering*, *24*(4). https://doi.org/10.1061/(asce)be.1943-5592.0001343

15. Chen, S., Laefer, D. F., Mangina, E., Zolanvari, S. M., & Byrne, J. (2019). UAV bridge inspection through evaluated 3D reconstructions. *Journal of Bridge Engineering*, *24*(4). https://doi.org/10.1061/(asce)be.1943-5592.0001343

16. Cheng, L., Chen, S., Liu, X., Xu, H., Wu, Y., Li, M., & Chen, Y. (2018). Registration of Laser Scanning Point Clouds: A Review. *Sensors*, *18*(5), 1641. https://doi.org/10.3390/s18051641

17. Dai, K., Boyajian, D., Liu, W., Chen, S.-E., Scott, J., & Schmieder, M. (2014). Laser-based field measurement for a bridge finite-element model validation. *Journal of Performance of Constructed Facilities*, *28*(5). https://doi.org/10.1061/(asce)cf.1943-5509.0000484

18. Delatte, N. (2009). Failure, distress and repair of concrete structures. https://doi.org/10.1533/9781845697037

19. Dong, P., & Chen, Q. (2017). Basics of Lidar Data Processing. *LiDAR Remote Sensing and Applications*, 41–62. https://doi.org/10.4324/9781351233354-3

20. Dorafshan, S., & Maguire, M. (2018). Bridge inspection: Human performance, unmanned aerial systems and automation. *Journal of Civil Structural Health Monitoring*, *8*(3), 443–476. https://doi.org/10.1007/s13349-018-0285-4

21. Erdélyi, J., Kopáčik, A., & Kyrinovič, P. (2020). Spatial data analysis for deformation monitoring of bridge structures. *Applied Sciences*, *10*(23), 8731. https://doi.org/10.3390/app10238731

22. Faro. (2021). *3D measurement, imaging & realization solutions*. FARO.com. Retrieved from https://www.faro.com/

23. FHWA. (1995). (rep.). *The Recording and Coding Guide for the Structure Inventory and Appraisal of the Nation's Bridges*. Washington, DC: Office of Engineering, Office of Engineering.

24. Graybeal, B. A., Phares, B. M., Rolander, D. D., Moore, M., & Washer, G. (2002). *Journal of Nondestructive Evaluation*, *21*(3), 67–83. https://doi.org/10.1023/a:1022508121821

25. Gucunski, N., & Nazarian, S. (2010). Material characterization and condition assessment of reinforced concrete bridge decks by complementary NDE Technologies. *Structures Congress 2010*. https://doi.org/10.1061/41130(369)40

26. Gucunski, N., Imani, A., Romero, F., Nazarian, S., Yuan, D., Wiggenhauser, H., Shokouhi, P., Taffe, A., & Kutrubes, D. (2012). Nondestructive testing to identify concrete bridge deck deterioration. https://doi.org/10.17226/22771

27. Gucunski, N., Romero, F., Kruschwitz, S., Feldmann, R., Abu-Hawash, A., & Dunn, M. (2010). Multiple Complementary Nondestructive Evaluation Technologies for condition assessment of concrete bridge decks. *Transportation Research Record: Journal of the Transportation Research Board*, *2201*(1), 34–44. https://doi.org/10.3141/2201-05

28. Henderson, M. E., Dion, G. N., & Costley, R. D. (1999). *SPIE Proceedings*. https://doi.org/10.1117/12.339927

29. Hendricks, L. J., Baxter, J. S., Chou, Y., Thomas, M., Boekweg, E., Guthrie, W. S., & Mazzeo, B. A. (2020). High-speed acoustic impact-echo sounding of concrete bridge decks. *Journal of Nondestructive Evaluation*, *39*(3). https://doi.org/10.1007/s10921-020-00695-0

30. Hohenthal, J., Alho, P., Hyyppä, J., & Hyyppä, H. (2011). Laser scanning applications in fluvial studies. *Progress in Physical Geography: Earth and Environment*, *35*(6), 782–809. https://doi.org/10.1177/0309133311414605

31. Huang, Z., Fu, H., Chen, W., Zhang, J., & Huang, H. (2018). Damage detection and quantitative analysis of Shield Tunnel Structure. *Automation in Construction*, *94*, 303–316. https://doi.org/10.1016/j.autcon.2018.07.006

32. Hugenschmidt, J., & Mastrangelo, R. (2006). GPR inspection of Concrete Bridges. *Cement and Concrete Composites*, *28*(4), 384–392. https://doi.org/10.1016/j.cemconcomp.2006.02.016

33. Kaartinen, E., Dunphy, K., & Sadhu, A. (2022). LIDAR-based Structural Health Monitoring: Applications in Civil Infrastructure Systems. *Sensors*, *22*(12), 4610. https://doi.org/10.3390/s22124610

34. Kashif Ur Rehman, S., Ibrahim, Z., Memon, S. A., & Jameel, M. (2016). Nondestructive test methods for Concrete Bridges: A Review. *Construction and Building Materials*, *107*, 58–86. https://doi.org/10.1016/j.conbuildmat.2015.12.011

35. Kee, S.-H., Oh, T., Popovics, J. S., Arndt, R. W., & Zhu, J. (2012). Nondestructive bridge deck testing with air-coupled impact-echo and infrared thermography. *Journal of Bridge Engineering*, *17*(6), 928–939. https://doi.org/10.1061/(asce)be.1943-5592.0000350

36. Kermarrec, G., Kargoll, B., & Alkhatib, H. (2020). Deformation analysis using B-spline surface with correlated terrestrial laser scanner observations—a bridge under load. *Remote Sensing*, *12*(5), 829. https://doi.org/10.3390/rs12050829

37. Kim, I.-H., Jeon, H., Baek, S.-C., Hong, W.-H., & Jung, H.-J. (2018). Application of crack identification techniques for an aging concrete bridge inspection using an unmanned aerial vehicle. *Sensors*, *18*(6), 1881. https://doi.org/10.3390/s18061881

38. Kim, M.-K., Thedja, J. P., & Wang, Q. (2020). Automated Dimensional Quality Assessment for formwork and rebar of reinforced concrete components using 3D point cloud data. *Automation in Construction*, *112*, 103077. https://doi.org/10.1016/j.autcon.2020.103077

39. Kim, M.-K., Wang, Q., & Li, H. (2019). Non-contact sensing based geometric quality assessment of buildings and Civil Structures: A Review. *Automation in Construction*, *100*, 163–179. https://doi.org/10.1016/j.autcon.2019.01.002

40. Kwiatkowski, J., Anigacz, W., & Beben, D. (2020). A case study on the noncontact inventory of the oldest European cast-iron bridge using terrestrial laser scanning and photogrammetric techniques. *Remote Sensing*, *12*(17), 2745. https://doi.org/10.3390/rs12172745

41. Le, T., Gibb, S., Pham, N., La, H. M., Falk, L., & Berendsen, T. (2017). Autonomous robotic system using non-destructive evaluation methods for Bridge Deck Inspection. *2017 IEEE International Conference on Robotics and Automation (ICRA)*. https://doi.org/10.1109/icra.2017.7989421

42. Lee, J., Lee, K. C., Lee, S., Lee, Y. J., & Sim, S. H. (2019). Long-term displacement measurement of bridges using a lidar system. *Structural Control and Health Monitoring*, *26*(10). https://doi.org/10.1002/stc.2428

43. Liu, W., & Chen, S.-en. (2013). Reliability Analysis of bridge evaluations based on 3D Light Detection and Ranging Data. *Structural Control and Health Monitoring*, *20*(12), 1397–1409. https://doi.org/10.1002/stc.1533

44. Liu, W., Chen, S., & Hauser, E. (2010). Lidar-based bridge structure defect detection. *Experimental Techniques*, *35*(6), 27–34. https://doi.org/10.1111/j.1747-1567.2010.00644.x

45. Liu, W., Chen, S.-en, & Hasuer, E. (2012). Bridge Clearance Evaluation based on terrestrial LIDAR SCAN. *Journal of Performance of Constructed Facilities*, *26*(4), 469–477. https://doi.org/10.1061/(asce)cf.1943-5509.0000208

46. Liu, X., Wang, P., Lu, Z., Gao, K., Wang, H., Jiao, C., & Zhang, X. (2019). Damage detection and analysis of urban bridges using Terrestrial Laser Scanning (TLS), ground-based microwave interferometry, and permanent scatterer interferometry synthetic aperture radar (PS-Insar). *Remote Sensing*, *11*(5), 580. https://doi.org/10.3390/rs11050580

47. McManamon, P. F. (2019). Lidar Technologies and Systems. https://doi.org/10.1117/3.2518254

48. Mijić, N. (2018). Application of the Airborne Lidar technology on the quarry using autocad Civil 3D software. *Advanced Technologies, Systems, and Applications III*, 43–51. https://doi.org/10.1007/978-3-030-02577-9_6

49. Mohammadi, M. E., Wood, R. L., & Wittich, C. E. (2019). Non-temporal Point Cloud Analysis for surface damage in civil structures. *ISPRS International Journal of Geo-Information*, *8*(12), 527. https://doi.org/10.3390/ijgi8120527

50. Moore, M., Washer , G., Rolander, D., Graybeal, B., & Phares, Brent M. (2001). (rep.). *Reliiability of Visual Inspection for Highway Bridges, Volume I: Final Report*. FHWA https://rosap.ntl.bts.gov/view/dot/33883.

51. Mukupa, W., Roberts, G. W., Hancock, C. M., & Al-Manasir, K. (2016). A review of the use of terrestrial laser scanning application for change detection and deformation monitoring of structures. *Survey Review*, 1–18. https://doi.org/10.1080/00396265.2015.1133039

52. Mukupa, W., Roberts, G. W., Hancock, C. M., & Al-Manasir, K. (2016). A review of the use of terrestrial laser scanning application for change detection and deformation monitoring of structures. *Survey Review*, 1–18. https://doi.org/10.1080/00396265.2015.1133039

53. Penttala, V. (2009). Causes and mechanisms of deterioration in reinforced concrete. *Failure, Distress and Repair of Concrete Structures*, 3–31. https://doi.org/10.1533/9781845697037.1.3

54. Penttala, V., & Al-Neshawy, F. (2002). Stress and strain state of concrete during freezing and thawing cycles. *Cement and Concrete Research*, *32*(9), 1407–1420. https://doi.org/10.1016/s0008-8846(02)00785-8

55. Pereira, Á., Cabaleiro, M., Conde, B., & Sánchez-Rodríguez, A. (2021). Automatic identification and geometrical modeling of steel rivets of historical structures from Lidar Data. *Remote Sensing*, *13*(11), 2108. https://doi.org/10.3390/rs13112108

56. Pérez, J., de Sanjosé Blasco, J., Atkinson, A., & del Río Pérez, L. (2018). Assessment of the structural integrity of the Roman Bridge of Alcántara (Spain) using TLS and GPR. *Remote Sensing*, *10*(3), 387. https://doi.org/10.3390/rs10030387

57. Ranyal, E., Sadhu, A., & Jain, K. (2022). Road condition monitoring using Smart Sensing and Artificial Intelligence: A Review. *Sensors*, *22*(8), 3044. https://doi.org/10.3390/s22083044

58. Rashidi, M., Mohammadi, M., Sadeghlou Kivi, S., Abdolvand, M. M., Truong-Hong, L., & Samali, B. (2020). A decade of modern bridge monitoring using Terrestrial Laser Scanning: Review and Future Directions. *Remote Sensing*, *12*(22), 3796. https://doi.org/10.3390/rs12223796

59. Rashidi, M., Mohammadi, M., Sadeghlou Kivi, S., Abdolvand, M. M., Truong-Hong, L., & Samali, B. (2020). A decade of modern bridge monitoring using Terrestrial Laser Scanning: Review and Future Directions. *Remote Sensing*, *12*(22), 3796. https://doi.org/10.3390/rs12223796

60. *Research and technology program*. Research and Technology Program | FHWA. (n.d.). Retrieved from https://highways.dot.gov/research/long-term-infra-structure-performance/ltbp/long-term-bridge-perfor-mance

61. Riveiro, B., DeJong, M. J., & Conde, B. (2016). Automated processing of large point clouds for structural health monitoring of Masonry Arch Bridges. *Automation in Construction*, *72*, 258–268. https://doi.org/10.1016/j.autcon.2016.02.009

62. Riveiro, B., González-Jorge, H., Varela, M., & Jauregui, D. V. (2013). Validation of Terrestrial Laser Scanning and photogrammetry techniques for the measurement of vertical underclearance and beam geometry in structural inspection of Bridges. *Measurement*, *46*(1), 784–794. https://doi.org/10.1016/j.measurement.2012.09.018

63. Rönnholm, P., & Haggrén, H. (2012). Registration of Laser Scanning Point Clouds and aerial images using either artificial or natural tie features. *ISPRS Annals of the Photogrammetry, Remote Sensing and Spatial Information Sciences*, *I-3*, 63–68. https://doi.org/10.5194/isprsannals-i-3-63-2012

64. Schlögl, M., Dorninger, P., Kwapisz, M., Ralbovsky, M., & Spielhofer, R. (2022). Remote sensing techniques for bridge deformation monitoring at Millimetric Scale: Investigating the potential of satellite radar interferometry, airborne laser scanning and ground-based mobile laser scanning. *PFG – Journal of Photogrammetry, Remote Sensing and Geoinformation Science*, *90*(4), 391–411. https://doi.org/10.1007/s41064-022-00210-2

65. Scott, M., Rezaizadeh, A., Delahaza, A., Santos, C. G., Moore, M., Graybeal, B., & Washer, G. (2003). A comparison of Nondestructive Evaluation Methods for Bridge Deck Assessment. *NDT & E International*, *36*(4), 245–255. https://doi.org/10.1016/s0963-8695(02)00061-0

66. Su, J. K., Yang, C. C., Wu, W. B., & Huang, R. (2002). Effect of moisture content on concrete resistivity measurement. *Journal of the Chinese Institute of Engineers*, *25*(1), 117–122. https://doi.org/10.1080/02533839.2002.9670686

67. Suchocki, C., & Katzer, J. (2018). Terrestrial laser scanning harnessed for moisture detection in building materials – problems and limitations. *Automation in Construction*, *94*, 127–134. https://doi.org/10.1016/j.autcon.2018.06.010

68. Sánchez-Rodríguez, A., Riveiro, B., Conde, B., & Soilán, M. (2017). Detection of structural faults in piers of masonry arch bridges through automated processing of Laser Scanning Data. *Structural Control and Health Monitoring*, *25*(3). https://doi.org/10.1002/stc.2126

69. Teza, G., Galgaro, A., & Moro, F. (2009). Contactless recognition of concrete surface damage from laser scanning and curvature computation. *NDT & E International*, *42*(4), 240–249. https://doi.org/10.1016/j.ndteint.2008.10.009

70. Trias Blanco, A. C. (2020). *Quantify lidar's geometry capturing capability for structural and construction assessment*. Welcome to RUcore - Rutgers University Community Repository. Retrieved from https://rucore.libraries.rutgers.edu/rutgers-lib/64897/.

71. Trias-Blanco, A. (2022). Bridge Deck Surface Profile Evaluation for Rapid Screening and Deterioration Monitoring (No. CAIT-UTC-REG52). Rutgers University. Center for Advanced Infrastructure and Transportation.

72. Trias, A., Yu, Y., Gong, J., & Moon, F. L. (2021). Supporting quantitative structural assessment of highway bridges through the use of Lidar scanning. *Structure and Infrastructure Engineering*, *18*(6), 824–835. https://doi.org/10.1080/15732479.2021.1880446

73. Wang, Chen, Zhu, Liu, Li, & Zheng. (2019). A survey of mobile laser scanning applications and key techniques over urban areas. *Remote Sensing*, *11*(13), 1540. https://doi.org/10.3390/rs11131540

74. Wang, Q., Cheng, J. C., & Sohn, H. (2017). Automated estimation of reinforced precast concrete rebar positions using colored laser scan data. *Computer-Aided Civil and Infrastructure Engineering*, *32*(9), 787–802. https://doi.org/10.1111/mice.12293

75. Watson, C., Chen, S.-E., Bian, H., & Hauser, E. (2012). Three-dimensional terrestrial LIDAR for Operational Bridge Clearance Measurements. *Journal of Performance of Constructed Facilities*, *26*(6), 803–811. https://doi.org/10.1061/(asce)cf.1943-5509.0000277

76. You, K., Jeong, H., & Hyung, W. (2014). Effects of accelerated carbonation on physical properties of mortar. *Journal of Asian Architecture and Building Engineering*, *13*(1), 217–221. https://doi.org/10.3130/jaabe.13.217

77. You, K., Jeong, H., & Hyung, W. (2014). Effects of accelerated carbonation on physical properties of mortar. *Journal of Asian Architecture and Building Engineering*, *13*(1), 217–221. https://doi.org/10.3130/jaabe.13.217

78. Zhang, T., & Gjørv, O. E. (1994). An electrochemical method for accelerated testing of chloride diffusivity in concrete. *Cement and Concrete Research*, *24*(8), 1534–1548. https://doi.org/10.1016/0008-8846(94)90168-6

79. Ziolkowski, P., Szulwic, J., & Miskiewicz, M. (2018). Deformation analysis of a composite bridge during proof loading using Point Cloud Processing. *Sensors*, *18*(12), 4332. https://doi.org/10.3390/s18124332

80. Šavija, B., Luković, M., Pacheco, J., & Schlangen, E. (2013). Cracking of the concrete cover due to reinforcement corrosion: A two-dimensional lattice model study. *Construction and Building Materials*, *44*, 626–638. https://doi.org/10.1016/j.conbuildmat.2013.03.063

81. Rebolledo, C., & Garcia-Diaz, A. (2014). Computerized Methodology for Selecting Projects in Multi-Period Bridge Management Systems. IIE Annual Conference. Proceedings, 2060.

82. Panesar, D. K. (2019). Supplementary cementing materials. Developments in the Formulation and Reinforcement of Concrete (Second Edition), 55-85. https://doi.org/10.1016/B978-0-08-102616-8.00003-4